Journal
of
The Franklin Institute
Devoted to Science and the Mechanic Arts

Vol. 236 NOVEMBER, 1943 No. 5

# VELOCITY AND MASS DISTRIBUTIONS RESULTING FROM THE LATERAL DIFFUSION OF A CURRENT IN A STRATIFIED MEDIUM ON A ROTATING EARTH.[1]

BY

G. GRIMMINGER.

David W. Taylor Model Basin, Navy Dept., Washington, D. C.

## INTRODUCTION.

The effects of the lateral diffusion of a rectilinear current upon the distribution of mass and velocity when the motion takes place on a rotating earth have been investigated by C. G.-Rossby (1) for the case of a fluid consisting of a single, homogeneous and incompressible layer.

In this paper these methods are extended so as to treat the case of rectilinear flow in a stratified medium which for simplicity in treatment and understanding will be supposed to consist of two homogeneous and incompressible fluid layers, each of a different temperature and density. The diffusion of a circular vortex (curvilinear flow) in a stratified medium is also treated. In applications to meteorology this medium can be considered as approximating the case in which there is a colder or polar air mass below, underlying a warmer or tropical air mass above.

## DIFFUSION IN THE SINGLE LAYER.

Rossby has treated the single fluid layer under the assumption that the diffusion process takes place so slowly that the motion can be considered as passing through an infinite number of equilibrium stages. The motion is thus assumed to be quasi-static. Initially there is assumed to be a strong, but very narrow current flowing in the $x$-direction, that is, from West to East, and extending to the top of the fluid.

[1] Presented at the Washington meeting of the American Meteorological Society, April, 1938.

(Note—The Franklin Institute is not responsible for the statements and opinions advanced by contributors in the JOURNAL.)

The main motion will, therefore, be parallel to the $x$-axis where this latter is perfectly arbitrary and can be chosen as having any desired direction. For definiteness, this is assumed to be from West to East. The $x$-axis is, therefore, the axis of a very narrow current or fluid sheet, as it may be more properly called. The fluid extends to infinity on each side of the $x$-axis and is at rest relative to the motion in the narrow current. Under these conditions and neglecting surface friction, the equation of motion of a fluid column becomes:

$$0 = fv + \frac{1}{\rho H}\frac{\partial}{\partial y}(\tau H) \tag{1}$$

for the $x$-direction, and

$$u = -\frac{1}{\rho f}\frac{\partial p}{\partial y} \tag{2}$$

for the $y$-direction, while the equation of continuity is

$$\frac{\partial H}{\partial t} = -\frac{\partial (vH)}{\partial y}, \tag{3}$$

where $p$ = pressure; $H$ = vertical extent of a fluid column measured from the ground; $\tau$ = shearing stress; $\rho$ = density; $f$ = coriolis parameter; $t$ = time; $u$ = velocity component in $x$ direction (axial component); $v$ = velocity component in $y$ direction (transversal component).

Rossby has shown further that, with the aid of the three equations above and with a suitable assumption concerning the eddy viscosity [2] the motion can be expressed in terms of the single equation

$$\frac{\partial H}{\partial s} + \frac{\partial^4 H}{\partial \eta^4} = 0, \tag{4}$$

where $s = (\nu_0 t/\lambda^2)$ is a non-dimensional time variable, $\eta = (y/\lambda)$ is a non-dimensional distance variable, and $\nu_0$ is the kinematic coefficient of eddy viscosity.

Since the solution of equation (4) was only stated in (1) and not derived, the solution is developed here in detail in Appendix 1.

## PART I.

### LATERAL DIFFUSION OF A RECTILINEAR CURRENT IN A STRATIFIED MEDIUM COMPOSED OF TWO LAYERS.

#### A. Initial Current of Zero Width.

We now proceed to the case of a stratified medium composed of two layers; and it will be shown how the solution of this case can be made to

[2] This assumption is that $\nu H = \nu_0 H_0$, where $H_0$ is the mean depth of the fluid and $\nu_0$ the corresponding value of the coefficient of eddy viscosity. In meteorological applications $H_0$ would be the height of the homogeneous atmosphere.

depend on the solution of equation (4) for the single layer problem which is derived in Appendix 1.

If now, $D_1$ denote the thickness of the upper layer measured from the internal boundary, $D_2$ the thickness of the lower layer measured from the ground, and the subscripts 1 and 2 refer to the upper and lower layer respectively, we have, since equations (1), (2) and (3) must hold separately for each layer, that

$$(13)\quad \begin{cases} 0 = fv_1D_1 + \dfrac{\partial}{\partial y}\left(\dfrac{\tau_1}{\rho_1}D_1\right), & 0 = fv_2D_2 + \dfrac{\partial}{\partial y}\left(\dfrac{\tau_2}{\rho_2}D_2\right), \\ 0 = -fu_1 - \dfrac{1}{\rho_1}\dfrac{\partial p_1}{\partial y}, & 0 = -fu_2 - \dfrac{1}{\rho_2}\dfrac{\partial p_2}{\partial y}, \\ 0 = \dfrac{\partial D_1}{\partial t} + \dfrac{\partial}{\partial y}(v_1D_1), & 0 = \dfrac{\partial D_2}{\partial t} + \dfrac{\partial}{\partial y}(v_2D_2), \end{cases}$$

where ground friction and friction at the internal boundary between the two layers are neglected. As in the single layer we now use

$$\frac{\tau_1}{\rho_1} = \nu_1\frac{\partial u_1}{\partial y}, \qquad \frac{\tau_2}{\rho_2} = \nu_2\frac{\partial u_2}{\partial y},$$

with the further condition that

$$\nu_1 = \nu_0\frac{H_0}{D_1} \quad \text{and} \quad \nu_2 = \nu_0\frac{H_0}{D_2}.$$

This agrees with the idea expressed by Parr (2) that the lateral turbulence is greatest when the vertical stability is greatest.

Using these relations and the following expressions for the pressure gradients in the two layers

$$\frac{1}{\rho_1}\frac{\partial p_1}{\partial y} = g\left(\frac{\partial D_1}{\partial y} + \frac{\partial D_2}{\partial y}\right), \qquad \frac{1}{\rho_2}\frac{\partial p_2}{\partial y} = g\left(\frac{\rho_1}{\rho_2}\frac{\partial D_1}{\partial y} + \frac{\partial D_2}{\partial y}\right),$$

equations (13) reduce to the two simultaneous partial differential equations

$$(14)\quad \begin{cases} \dfrac{\partial D_1}{\partial s} = \dfrac{-g}{\lambda^2}\left(\dfrac{\partial^4 D_1}{\partial \eta^4} + \dfrac{\partial^4 D_2}{\partial \eta^4}\right), \\ \dfrac{\partial D_2}{\partial s} = \dfrac{-g}{\lambda^2}\left(\dfrac{\rho_1}{\rho_2}\dfrac{\partial^4 D_1}{\partial \eta^4} + \dfrac{\partial^4 D_2}{\partial \eta^4}\right), \end{cases}$$

where $\eta = (y/\lambda)$, $\lambda = (\sqrt{gH_0}/f)$ and $s = (\nu_0 t/\lambda^2)$. These equations can be reduced to two having the same form as (4). Multiplying the

second of equations (14) by a parameter $\sigma$ and adding to the first, one obtains

$$\frac{\partial}{\partial s}(D_1 + \sigma D_2) + \frac{\nu_0}{\lambda^2}\left(1 + \sigma\frac{\rho_1}{\rho_2}\right)\frac{\partial^4}{\partial \eta^4}\left[D_1 + \frac{1+\sigma}{1+\sigma\dfrac{\rho_1}{\rho_2}} D_2\right] = 0.$$

Letting $\sigma = (1+\sigma)/[1+\sigma(\rho_1/\rho_2)]$, one finds that $\sigma = \pm\sqrt{(\rho_2/\rho_1)}$, and with the further substitutions

$$(15)\qquad \begin{cases} K_1 = D_1 + \sqrt{\dfrac{\rho_2}{\rho_1}}\, D_2, & K_2 = D_1 - \sqrt{\dfrac{\rho_2}{\rho_1}}\, D_2, \\ s_1 = s\left(1 + \sqrt{\dfrac{\rho_1}{\rho_2}}\right), & s_2 = s\left(1 - \sqrt{\dfrac{\rho_1}{\rho_2}}\right), \end{cases}$$

the equations (14) are finally reduced to the form

$$(16)\qquad \frac{\partial K_1}{\partial s_1} + \frac{\partial^4 K_1}{\partial \eta^4} = 0, \qquad \frac{\partial K_2}{\partial s_2} + \frac{\partial^4 K_2}{\partial \eta^4} = 0,$$

for which the solutions are known from that of equation (4). See Appendix 1.

Assuming the same type initial condition as in the case of the single layer, that is, a discontinuity in the height of the free surface and internal boundary at the center of the current, we have the solutions in the same form as (12); namely,

$$(17)\qquad K_1 - K_{10} = -\frac{\Delta_1}{\pi}\Phi(\xi_1), \qquad K_2 - K_{20} = -\frac{\Delta_2}{\pi}\Phi(\xi_2),$$

where

$$\xi_1 = \frac{\eta}{\sqrt[4]{4s_1}} = \frac{\eta}{\sqrt[4]{4s\left(1 + \sqrt{\dfrac{\rho_1}{\rho_2}}\right)}} = \frac{\xi}{\sqrt[4]{1 + \sqrt{\dfrac{\rho_1}{\rho_2}}}},$$

$$\xi_2 = \frac{\eta}{\sqrt[4]{4s_2}} = \frac{\eta}{\sqrt[4]{4s\left(1 - \sqrt{\dfrac{\rho_1}{\rho_2}}\right)}} = \frac{\xi}{\sqrt[4]{1 - \sqrt{\dfrac{\rho_1}{\rho_2}}}}$$

and the subscript zero refers to the center of the current.

By analogy with the solution for the single layer and from equations (15), it is easily seen that $\Delta_1$ and $\Delta_2$ are defined by the relations

$$(18)\qquad \begin{cases} \Delta_1 = K_{1r} - K_{1l} = D_{1r} - D_{1l} + \sqrt{\dfrac{\rho_2}{\rho_1}}\,(D_{2r} - D_{2l}), \\ \Delta_2 = K_{2r} - K_{2l} = D_{1r} - D_{1l} - \sqrt{\dfrac{\rho_2}{\rho_1}}\,(D_{2r} - D_{2l}), \end{cases}$$

where the subscripts $r$ and $l$ refer to the right hand and left hand side, respectively, of the axis of the current.

$\Delta_1$ and $\Delta_2$ will now be chosen so as to satisfy prescribed initial conditions. Initially, it is assumed that a current from West to East exists in the upper layer, the current being in the form of a fluid sheet. This approximates the case in which the momentum of an atmospheric current is confined within very narrow limits. The lower layer will be assumed to be at rest initially; hence, the North-South pressure gradient must be zero at the ground, and this condition determines the initial

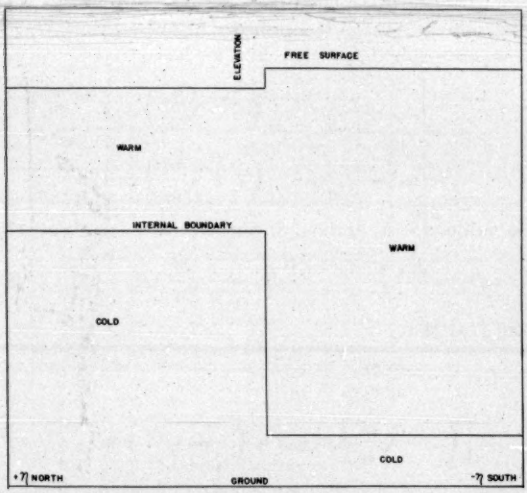


FIG. 1. Initial elevation profile for free surface and internal boundary. Double layer, initial current of zero width. Schematic.

profile of the internal boundary. The initial profile for the free surface and the internal boundary is shown schematically in Fig. 1. The condition for zero pressure gradient at the ground is that $\rho_1 D_{1l} + \rho_2 D_{2l} = \rho_1 D_{1r} + \rho_2 D_{2r}$, from which it follows that

$$D_{2r} - D_{2l} = -\frac{\rho_1}{\rho_2}\Delta', \quad \text{where} \quad \Delta' = D_{1r} - D_{1l}.$$

Hence,

$$\Delta_1 = \Delta'\left(1 - \sqrt{\frac{\rho_1}{\rho_2}}\right), \qquad \Delta_2 = \Delta'\left(1 + \sqrt{\frac{\rho_1}{\rho_2}}\right).$$

In order to compare the effects of diffusion in a stratified medium with those which result in a single homogeneous fluid layer, we shall choose $\Delta'$ so that the initial discontinuity of pressure in the upper layer is exactly the same as that for the single layer treated by Rossby (1). To satisfy this condition we must have

$$(19)\quad \rho_0\Delta_s g = \rho_1 g[D_{1r} + D_{2r} - (D_{1l} + D_{2l})] = \Delta' \frac{\rho_2 - \rho_1}{\rho_2}\rho_1 g = \rho_1 g\Delta_u$$

or $\Delta' = \rho_2/(\rho_2 - \rho_1)(\rho_0/\rho_1)\Delta_s$, where $\rho_0$ is the density of the single layer or homogeneous atmosphere, and where $\Delta_u$ is the discontinuity in height of the free surface of the double layer.

Assuming now that the lower layer has the same density as the homogeneous atmosphere, $\rho_2 = \rho_0$, and we have that

$$(20)\quad \begin{cases} \Delta_1 = \dfrac{\rho_2}{\rho_1}\dfrac{\rho_2}{\rho_2 - \rho_1}\left(1 - \sqrt{\dfrac{\rho_1}{\rho_2}}\right)\Delta_s, \\ \Delta_2 = \dfrac{\rho_2}{\rho_1}\dfrac{\rho_2}{\rho_2 - \rho_1}\left(1 + \sqrt{\dfrac{\rho_1}{\rho_2}}\right)\Delta_s. \end{cases}$$

Using these values for $\Delta_1$ and $\Delta_2$, and also noting from (15) that

$$D_1 = \frac{K_1 + K_2}{2}, \qquad D_2 = \frac{1}{2}\sqrt{\frac{\rho_1}{\rho_2}}(K_1 - K_2),$$

we find from (17) that

$$(21)\quad D_1 - D_{10} = -\frac{\Delta_s}{2\pi}\frac{\rho_2}{\rho_1}\frac{\rho_2}{\rho_2 - \rho_1} \times\left[\left(1 - \sqrt{\frac{\rho_1}{\rho_2}}\right)\Phi(\xi_1) + \left(1 + \sqrt{\frac{\rho_1}{\rho_2}}\right)\Phi(\xi_2)\right]$$

and

$$(22)\quad D_2 - D_{20} = -\frac{\Delta_s}{2\pi}\frac{\rho_2}{\rho_1}\sqrt{\frac{\rho_1}{\rho_2}}\frac{\rho_2}{\rho_2 - \rho_1} \times\left[\left(1 - \sqrt{\frac{\rho_1}{\rho_2}}\right)\Phi(\xi_1) - \left(1 + \sqrt{\frac{\rho_1}{\rho_2}}\right)\Phi(\xi_2)\right].$$

We now use $H_1$ and $H_{10}$ to denote actual elevation for the free surface and $H_2$ and $H_{20}$ for the internal boundary, where, as before, the subscript zero refers to the center of the current. Since $H_1 = D_1 + D_2$ and $H_{10} = D_{10} + D_{20}$, we have, after a few reductions, that

$$(23)\quad \frac{H_1 - H_{10}}{\Delta_s} = -\frac{1}{2\pi}\frac{\rho_2}{\rho_1}[\Phi(\xi_1) + \Phi(\xi_2)],$$

which gives the elevation profile for the free surface in non-dimensional

form. Since $H_2 = D_2$, the non-dimensional form for the elevation profile of the internal boundary is given by

$$(24)\quad \frac{H_2 - H_{20}}{\Delta_s} = -\frac{1}{2\pi}\frac{\rho_2}{\rho_2 - \rho_1} \times \left[\left(\sqrt{\frac{\rho_2}{\rho_1}} - 1\right)\Phi(\xi_1) - \left(\sqrt{\frac{\rho_2}{\rho_1}} + 1\right)\Phi(\xi_2)\right].$$

These profiles are shown in Fig. 2 for three different values of the time parameter $s$ which are the same values which have been used by Rossby (1) in the discussion of the single layer; namely, $s = .055 \times 10^{-4}$, $.880 \times 10^{-4}$ and $.141 \times 10^{-2}$. These same values have, in fact, been

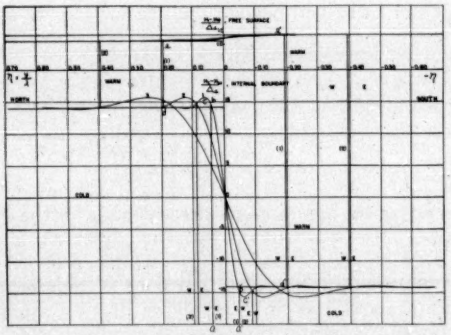

FIG. 2. Elevation profiles for the double layer, initial current of zero width.
Curves 1: $s = .055 \times 10^{-4}$.
Curves 2: $s = .880 \times 10^{-4}$.
Curves 3: $s = .141 \times 10^{-2}$.

used for all the various profiles given in this section. This fact, plus the fact that we have chosen the same initial pressure difference as in the single layer, permits a strict comparison of the results of diffusion in a stratified medium and in one which is not stratified.

Throughout this paper a temperature discontinuity of 10° C. has been assumed to exist between the two layers; the lower layer is taken to have a temperature of 0° C. and the upper layer 10° C. Since variations in the internal boundary are proportional to $\rho_2/(\rho_2 - \rho_1)$, they will be about 28 times as great as those in the free surface; and the smaller the temperature discontinuity, the greater will be this effect. It should also be noticed that the elevation profiles are referred to $H_{10}$ and $H_{20}$, the mean elevations above the ground of the free surface and internal boundary, respectively. Since $H_{10}$ and $H_{20}$ can

be chosen arbitrarily, these profiles bear no fixed relation to elevation above the ground until $H_{10}$ and $H_{20}$ are chosen. The only restriction on $H_{10}$ and $H_{20}$ is that they must represent an atmosphere approximately equivalent in mass to the homogeneous atmosphere.

There does, however, appear to be a restriction on the value of $\Delta_u$, which can be used to represent the initial pressure discontinuity in the upper layer. If $\Delta_l$ denote the initial discontinuity in height of the internal boundary, then, from the initial condition of zero pressure gradient at the ground, we must have

$$\Delta_l = \frac{\rho_1}{\rho_2 - \rho_1} \Delta_u.$$

$\Delta_l$ represents the actual range in elevation of the internal boundary and since this cannot extend beyond the free surface, we must have

$$\Delta_l = \frac{\rho_1}{\rho_2 - \rho_1} \Delta_u < H_0,$$

where $H_0$ is the height of the homogeneous atmosphere. Therefore, we must have

$$\Delta_u < \frac{\rho_2 - \rho_1}{\rho_1} H_0.$$

As a consequence of the assumptions already made for the discontinuity of temperature, $\rho_1/(\rho_2 - \rho_1)$ has a value of about 28, and hence we must have $\Delta_u < (H_0/28)$. Since $\Delta_u$ is directly proportional to the initial discontinuity of pressure aloft and since $H_0$ represents a pressure at the ground of about 1000 mb., it follows that we cannot assume a pressure discontinuity greater than 1000/28 or about 36 mb. In order to use larger discontinuities of pressure than this, one would have to increase the temperature discontinuity between the two layers in the proper proportion.

The velocity profiles are easily obtained from the elevation profiles by use of the gradient wind relation. For the upper layer this is

$$u_1 = -\frac{1}{\rho_1 f} \frac{\partial p_1}{\partial y}.$$

Since

$$\frac{\partial p_1}{\partial y} = \frac{-g}{f} \frac{1}{\lambda} \frac{1}{\sqrt[4]{4s}} \frac{\partial H_1}{\partial \xi},$$

we find by differentiation of equation (23), giving the elevation of the free surface, and after a few reductions that

$$(25) \quad \frac{1}{\Delta_u} \sqrt{\frac{H_0}{g}}\, u_1 = \frac{1}{2\pi} \frac{\rho_2}{\rho_1} \frac{1}{\sqrt[4]{4s}} \left[ \frac{1}{\sqrt[4]{1 + \sqrt{\frac{\rho_1}{\rho_2}}}} F(\xi_1) + \frac{1}{\sqrt[4]{1 + \sqrt{\frac{\rho_1}{\rho_2}}}} F(\xi_2) \right],$$

which is the non-dimensional expression for the velocity profiles of the upper layer.

The velocity in the lower layer is obtained in a similar manner. In the lower layer we have

$$u_2 = -\frac{1}{\rho_2 f}\frac{\partial p_2}{\partial y} = -\frac{1}{\rho_2 f}\frac{1}{\lambda}\frac{1}{\sqrt[4]{4s}}\frac{\partial p_2}{\partial \xi},$$

where

$$\frac{\partial p_2}{\partial y} = g\left(\rho_1\frac{\partial D_1}{\partial y} + \rho_2\frac{\partial D_2}{\partial y}\right).$$

Hence,

$$u_2 = -\frac{g}{f\lambda}\frac{1}{\sqrt[4]{4s}}\left(\frac{\rho_1}{\rho_2}\frac{\partial D_1}{\partial \xi} + \frac{\partial D_2}{\partial \xi}\right).$$

Using equations (21) and (22) to evaluate $\partial D_1/\partial\xi$ and $\partial D_2/\partial\xi$, the above equation reduces to the following non-dimensional expression for the velocity in the lower layer.

$$(26)\quad \frac{1}{\Delta_s}\sqrt{\frac{H_0}{g}}\,u_2 = \frac{1}{2\pi}\frac{1}{\sqrt[4]{4s}}\sqrt{\frac{\rho_2}{\rho_1}}\left[\frac{1}{\sqrt[4]{1+\sqrt{\frac{\rho_1}{\rho_2}}}}F(\xi_1) - \frac{1}{\sqrt[4]{1-\sqrt{\frac{\rho_1}{\rho_2}}}}F(\xi_2)\right].$$

The velocity profiles for the upper and lower layers for the same three values of the time parameter $s$, as given above, are given in Fig. 3. Since ground friction has been neglected, the velocity at the ground is the same as that in the lower layer.

The most significant result, perhaps, of the mixing of the upper layer current is the fact that an induced current is set up in the opposite direction in the lower layer which is of the same order of magnitude as the upper layer current. We, therefore, have a west wind aloft and an induced east wind below.

As Rossby has already indicated, in his discussion of the single layer, the effect of the diffusion process is to produce regions of convergence and divergence upon which the Coriolis forces act so as to produce a counter current. The velocity profiles for the single layer, taken from (1), are shown in Fig. 4. It is seen that, on either side of the main westerly current, there are weak easterly counter currents and beyond this still weaker west winds. As the diffusion progresses the current spreads to both sides of the axis.

By comparing Figs. 3 and 4, it is seen that, in comparison with the single layer, the effect of stratification is to maintain for a longer time a narrower and stronger portion of the central current; that is, in the upper layer, for instance, the central part of the westerly current does not spread so fast as the single layer current, and the velocity at the center is about twice that in the case of the single layer in the

same stage of decay or diffusion. In the lower layer, the main easterly current is somewhat narrower than the main current in the upper layer, and the velocity in this portion is almost the same as in the single layer. Another effect of stratification is to produce a secondary maximum in the velocity of the upper layer current which occurs before the velocity goes to zero and changes sign. The counter current in the upper layer is slightly broader and about one-half as strong as in the single layer. In the lower layer, on the other hand, the counter current is twice as large as in the single layer and is of the same order

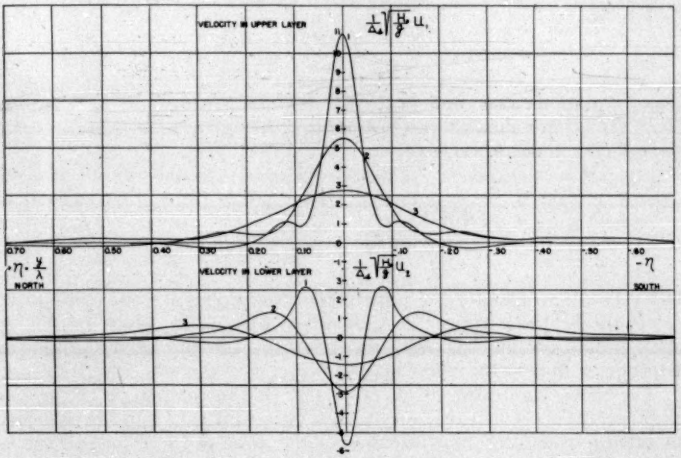


FIG. 3. Velocity profiles in the double layer: initial current of zero width.
Curves 1: $s = .055 \times 10^{-4}$.
Curves 2: $s = .880 \times 10^{-4}$.
Curves 3: $s = .141 \times 10^{-2}$.

of magnitude as the main easterly current itself. We thus see that one of the principal effects of stratification is to produce an induced easterly current at the ground, which is attended by a relatively strong and well marked westerly counter current. There is thus a well marked wind shift at the ground which is especially well shown by profile (1) for the lower layer in Fig. 3. Thus, if we consider this profile, we find that the change from the maximum velocity, at the center of the current, to the maximum velocity in the counter current occurs within a range in $\eta$ of .08. Since $\lambda$ is about 2800 km., this range is about 224 km.

Upon consulting the profiles in Fig. 2, one sees that, owing to

mixing of the upper layer current, there is a gradual reduction in the horizontal pressure gradient in the upper layer; this can be seen on a larger scale in the upper curves of Fig. 5. This reduction of pressure gradient is necessarily accompanied by a net northward transport of the warm air. These changes in the upper layer will destroy the initially assumed zero pressure gradient at the ground and create a pressure gradient southward. This must necessarily mean a net

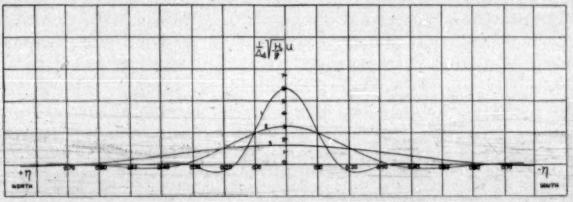

FIG. 4. Velocity profiles for single layer. Initial current of zero width.

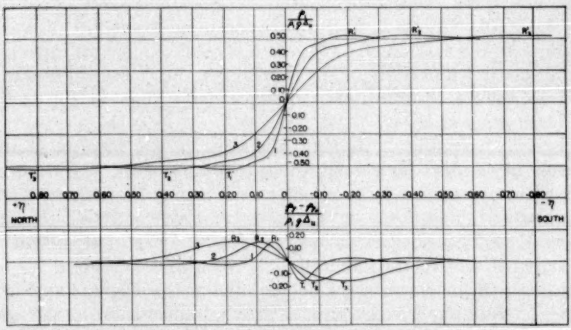

FIG. 5. Pressure profiles for the double layer. Initial current of zero width.

Curves 1: $s = .055 \times 10^{-4}$.
Curves 2: $s = .880 \times 10^{-4}$.
Curves 3: $s = .141 \times 10^{-3}$.

southward transport of the cold air and a decrease in the slope of the internal boundary. Since, owing to the rotation of the earth, the mass distribution is continually striving for perfect dynamic equilibrium, these cross stream transports will be indicated as East-West velocity components. Thus, it is seen that the cold air which was originally at rest will acquire certain East-West velocity components.

The order of events brought about by the mixing process can be described more precisely, perhaps, as follows: Since momentum can be

transmitted more easily than mass, the first effect of mixing in the upper warm layer is to produce in that current certain unbalanced wind components. This is followed by a readjustment of mass in the upper layer which is necessarily accompanied by a net transport of mass northward. The effect of this is to destroy the equilibrium of the lower layer by creating a pressure gradient southward. This must be followed by a net transport southward of the cold air which, as dynamic equilibrium is again approached, must appear in the form of East-West wind components.

Thus it is seen that, whereas an unbalanced wind component is the first effect of mixing in the upper layer, it is the last effect to appear in the lower layer. It is therefore seen how, in the atmosphere, it is possible to have the pressure distribution as the result of the wind distribution as in the upper layer, and also to have the wind distribution as the result of the pressure distribution as in the lower layer. Thus, both points of view regarding the relation of wind to pressure gradient seem to be equally logical and equally correct.

As is indicated in Fig. 2 by the always decreasing slope of the internal boundary, there is a continuous transport of cold air southward below the level marked $L$, and a corresponding transport of warm air northward above this level. Owing to stratification and especially to the small density difference of the two layers, the redistribution of mass needed to restore equilibrium is much greater than in the case of a single homogeneous layer.

It is seen from Fig. 2 that, as the slope of the internal boundary decreases, there must be a northward transport of the warm air above $L$ and a southward movement of the cold air below this point; the circulation will, therefore, be somewhat as indicated by the curved arrows. From considerations of continuity, this circulation must necessarily contain vertical as well as horizontal components.

The vertical lines, shown in Fig. 2, refer to profiles (1) and (2) and separate, in each layer, the main or central current from the counter current. These regions of east and west winds are indicated by E and W, respectively. These wind shift lines for profiles (1) are indicated by $ab$, $a'b'$ for the lower layer and $de$, $d'e'$ for the upper layer. Since these two layers represent individual isentropic layers, it is seen how lateral mixing necessarily leads to wind shift lines within individual isentropic layers. It will be noted that these wind shift lines are transient, that is, they move relative to the surrounding air. The real boundary between the air masses is the internal boundary (isentropic surface). As a result of mixing, however, it is seen that wind shift lines are set up in the individual layers which, in no way, represent air mass boundaries. Moreover, the wind shift lines in the lower layer extend down to the ground; whereas, the air mass boundary, as it has been considered in this problem, does not. This would seem to detract

from the importance of wind shift alone as an indicator of an air mass boundary.

One of the most interesting effects of the lateral diffusion and mixing of an atmospheric current is the resulting distribution of pressure. This effect, in fact, appears to be of fundamental meteorological importance.

The pressure distribution in the upper layer when referred to the pressure at the center of the current, that is, at the height $H_{10}$, is proportional to the elevation profile for the free surface and is given in non-dimensional form by

$$\frac{p_1}{\rho_1 g \Delta_u} = -\frac{1}{2\pi}[\Phi(\xi_1) + \Phi(\xi_2)], \tag{27}$$

where $p_1 = \rho_1 g(H_1 - H_{10})$.

If $p_g$ denote the pressure at the ground, then $p_g = \rho_1 g D_1 + \rho_2 g D_2$, and the pressure at the ground at the center of the current will be given by $p_{g0} = \rho_1 g D_{10} + \rho_2 g D_{20}$. Since there is initially no pressure gradient at the ground and since $D_{10}$ and $D_{20}$ are constants, it is seen that $p_{g0}$ is simply an expression for the initial pressure at the ground. If one now evaluates $p_g$ by using equations (21) and (22), and also uses the above expression for $p_{g0}$ it is found that the non-dimensional expression for the pressure distribution at the ground is given by

$$\frac{p_g - p_{g0}}{\rho_1 g \Delta_u} = -\frac{1}{2\pi}\sqrt{\frac{\rho_2}{\rho_1}}[\Phi(\xi_1) - \Phi(\xi_2)]. \tag{28}$$

The pressure profiles are shown in Fig. 5 and are expressed in units of $\rho_1 g \Delta_u$, which is the initial discontinuity of pressure in the free surface of the double layer. In this connection it is seen from equation (19) that $\rho_2 g \Delta_s = \rho_1 g \Delta_u$.

These pressure profiles exhibit some interesting properties. It is seen that, as a result of the diffusion process, a characteristic pressure distribution is set up at the ground in such a way that a low pressure trough is formed to the right of the axis of the lower layer current and a high pressure ridge to the left. At first, the distance between the trough and ridge is quite small, and the isobars will be closely packed in this region and a steep pressure gradient will exist. As the currents in the two layers spread, owing to lateral mixing, the distance between the trough and the ridge constantly increases in such a way that the low pressure trough is found farther and farther to the right. At the same time, the isobars become more and more widely separated and the pressure gradients become less. Finally, as is seen from Fig. 5, the high and low pressure areas become of wide extent.

We thus have the important result that the lateral mixing and diffusion of a current existing initially only in the upper atmosphere

can lead, at the ground, to trough formation or cyclogenesis to the right of the current axis and high pressure or anticyclogenesis to the left of the axis. Let us assume, for instance, that the initial discontinuity of pressure in the upper layer is 25 mb. Pressure changes of this order of magnitude can be found on the high level pressure charts. Then both the cyclogenesis and anticyclogenesis are about 15 per cent. of this, or about 3.7 mb., which is about 0.11 inch. The total pressure difference between $T$ and $R$ is therefore about 0.22 inch.

On this basis the pressure gradients at the ground from $R$ to $T$ can be evaluated from the lower profiles in Fig. 5 and corresponding to profiles 1, 2, and 3, these are found to be 1.50, 0.75, and 0.38 inches per 1000 miles, respectively. These gradients are of about the same order of magnitude as some of those found on the synoptic charts in the case of migratory anticyclones.

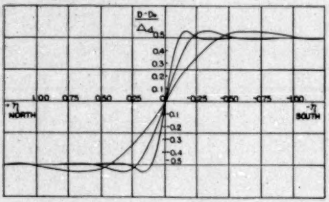


FIG. 6. Elevation profiles for the single layer.
Curve 1: $s = .055 \times 10^{-4}$.
Curve 2: $s = .880 \times 10^{-4}$.
Curve 3: $s = .141 \times 10^{-2}$.

We see from the upper profiles of Fig. 5 that, in the upper layer, the trough and ridge formation are smaller than at the ground, are not nearly so well pronounced, and their positions with respect to the current axis are reversed; that is, the low pressure is formed to the left and the high pressure to the right. These are indicated by $T'$ and $R'$, respectively. Also, $T'$ is always to the north of $R$ and $R'$ always to the south of $T$. The secondary pressure trough at the ground to the north of the axis is identical in extent, position, and magnitude with the pressure trough aloft, and similarly for the pressure ridges to the south of the axis. This similarity holds, in fact, for the entire portion of the ground profile beyond that point where the pressure first becomes equal to the initial ground pressure, that is, where the ground profile first crosses the axis. This indicates that the pressure distribution at the ground beyond this point is the direct result of the deformations in the free surface. The pressure distribution at the ground between this point and the origin (axis of current) is the combined result of the mass distribution in both the upper and lower layers.

In the case of an atmosphere composed of a single homogeneous layer, the pressure variations at the ground are simply the result of the deformations in the free surface. The free surface profiles, taken from (1), for an atmosphere composed of a single homogeneous layer are shown in Fig. 6. The deviations in these profiles from 0.5 give the deviations in the pressure at the ground from its initial value. Comparing these with the pressure distributions at the ground for the double layer, it is seen that trough and ridge formation is only about one-third as great as for the double layer and are reversed in position. This is because in a stratified medium the mass transports necessary for the existence of a quasi-equilibrium state are much larger than in a single layer and also take place in the opposite direction so that they not only counteract the effect at the ground of mass transports in the upper layer, but also produce a larger pressure variation in the opposite sense.

### B. Initial Current of Finite Width.

We shall now make the previous discussion more general by treating the case in which the current in the upper layer is initially of finite width. Before doing this, however, it is necessary to have the solution for a single layer when the initial current is of finite width. This solution is developed in Appendix 2.

In developing the solution for the double layer we can use the same general procedure and methods as in the former case for the double layer when the initial current was of zero width. The equations of motion are, as before,

$$\frac{\partial K_1}{\partial s_1} + \frac{\partial^4 K_1}{\partial \eta^4} = 0, \qquad \frac{\partial K_2}{\partial s_2} + \frac{\partial^4 K_2}{\partial \eta^4} = 0, \tag{37}$$

where

$$K_1 = D_1 + \sqrt{\frac{\rho_2}{\rho_1}}\, D_2, \qquad K_2 = D_1 - \sqrt{\frac{\rho_2}{\rho_1}}\, D_2,$$

$$s_1 = s\left(1 + \sqrt{\frac{\rho_1}{\rho_2}}\right), \qquad s_2 = s\left(1 - \sqrt{\frac{\rho_1}{\rho_2}}\right),$$

Since the initial condition for the $K$'s is the same as that for $H$ in the single layer case in Appendix 2, the solution of (37) is of the same form as for the single layer. We therefore have from equation (35) that

$$K_1 = K_{10} + \frac{\Delta_1}{2\pi}\sqrt[4]{\frac{4s_1}{a^4}}\left[\psi\left(\frac{1-\zeta}{\sqrt[4]{\frac{4s_1}{a^4}}}\right) - \psi\left(\frac{1+\zeta}{\sqrt[4]{\frac{4s_1}{a^4}}}\right)\right], \tag{38}$$

$$K_2 = K_{20} + \frac{\Delta_2}{2\pi}\sqrt[4]{\frac{4s_2}{a^4}}\left[\psi\left(\frac{1-\zeta}{\sqrt[4]{\frac{4s_2}{a^4}}}\right) - \psi\left(\frac{1+\zeta}{\sqrt[4]{\frac{4s_2}{a^4}}}\right)\right]. \tag{39}$$

It is assumed, as in Appendix 2, that the initial velocity distribution consists of a current of uniform velocity $u_i$ over a distance $2a$, and zero elsewhere.

As in Case A, we have

$$\Delta_1 = K_{1r} - K_{1l} = D_{1r} - D_{1l} + \sqrt{\frac{\rho_2}{\rho_1}}(D_{2r} - D_{2l}),$$

$$\Delta_2 = K_{2r} - K_{2l} = D_{1r} - D_{1l} - \sqrt{\frac{\rho_2}{\rho_1}}(D_{2r} - D_{2l}),$$

where $D_{1r}$ and $D_{1l}$, for instance, are the values of $D$, at the right and left hand edges of the current. We now choose $\Delta_1$ and $\Delta_2$ so as to have initially a zero pressure gradient at the ground, and hence the lower layer at rest. This assumption of an initially zero pressure gradient at the ground is used because it enables the pressure changes at the ground and motion of the lower layer to be more easily studied. We thus find as before that

$$\Delta_1 = \Delta'\left(1 - \sqrt{\frac{\rho_1}{\rho_2}}\right), \quad \Delta_2 = \Delta'\left(1 + \sqrt{\frac{\rho_1}{\rho_2}}\right), \quad \text{where} \quad \Delta' = D_{1r} - D_{1l}.$$

If we now, as previously, choose $\Delta'$ so that the initial pressure difference in the upper layer is the same as in the case of the homogeneous atmosphere, we find that

$$\Delta_1 = \frac{\rho_2}{\rho_2 - \rho_1}\frac{\rho_0}{\rho_1}\left(1 - \sqrt{\frac{\rho_1}{\rho_2}}\right)\Delta_u = \frac{\rho_2}{\rho_2 - \rho_1}\left(1 - \sqrt{\frac{\rho_1}{\rho_2}}\right)\Delta_u,$$

$$\Delta_2 = \frac{\rho_2}{\rho_2 - \rho_1}\frac{\rho_0}{\rho_1}\left(1 + \sqrt{\frac{\rho_1}{\rho_2}}\right)\Delta_u = \frac{\rho_2}{\rho_2 - \rho_1}\left(1 + \sqrt{\frac{\rho_1}{\rho_2}}\right)\Delta_u,$$

where $\Delta_u$ is the initial difference in elevation in the upper layer of the stratified medium and $\rho_0$ is the density of the homogeneous atmosphere.

Using the above values of $\Delta_1$ and $\Delta_2$, one finds after some reduction that

$$(40)\quad \frac{D_1 - D_{10}}{\Delta_u} = \frac{1}{4\pi}\sqrt{\frac{4s}{a^4}}\frac{\rho_2}{\rho_2 - \rho_1}\left[\left(1 - \sqrt{\frac{\rho_1}{\rho_2}}\right)\sqrt[4]{1 + \sqrt{\frac{\rho_1}{\rho_2}}}\,\psi(\beta_1)\right.$$
$$- \left(1 - \sqrt{\frac{\rho_1}{\rho_2}}\right)\sqrt[4]{1 + \sqrt{\frac{\rho_1}{\rho_2}}}\,\psi(\beta_2)$$
$$+ \left(1 + \sqrt{\frac{\rho_1}{\rho_2}}\right)\sqrt[4]{1 - \sqrt{\frac{\rho_1}{\rho_2}}}\,\psi(\beta_3)$$
$$\left. - \left(1 + \sqrt{\frac{\rho_1}{\rho_2}}\right)\sqrt[4]{1 - \sqrt{\frac{\rho_1}{\rho_2}}}\,\psi(\beta_4)\right]$$

and

$$(41)\quad \frac{D_2 - D_{20}}{\Delta_u} = \frac{1}{4\pi}\sqrt[4]{\frac{4s}{a^4}}\frac{\rho_2}{\rho_2 - \rho_1}\sqrt{\frac{\rho_1}{\rho_2}}\left[\left(1 - \sqrt{\frac{\rho_1}{\rho_2}}\right)\sqrt[4]{1 + \sqrt{\frac{\rho_1}{\rho_2}}}\,\psi(\beta_1)\right.$$
$$- \left(1 - \sqrt{\frac{\rho_1}{\rho_2}}\right)\sqrt[4]{1 + \sqrt{\frac{\rho_1}{\rho_2}}}\,\psi(\beta_2)$$
$$- \left(1 + \sqrt{\frac{\rho_1}{\rho_2}}\right)\sqrt[4]{1 - \sqrt{\frac{\rho_1}{\rho_2}}}\,\psi(\beta_3)$$
$$\left. + \left(1 + \sqrt{\frac{\rho_1}{\rho_2}}\right)\sqrt[4]{1 - \sqrt{\frac{\rho_1}{\rho_2}}}\,\psi(\beta_4)\right],$$

where $\zeta = (\eta/a)$ and

$$\beta_1 = \frac{a - \eta}{\sqrt[4]{4s\left(1 + \sqrt{\frac{\rho_1}{\rho_2}}\right)}} = \frac{1 - \zeta}{\sqrt[4]{\frac{4s}{a^4}\left(1 + \sqrt{\frac{\rho_1}{\rho_2}}\right)}},$$

$$\beta_2 = \frac{a + \eta}{\sqrt[4]{4s\left(1 + \sqrt{\frac{\rho_1}{\rho_2}}\right)}} = \frac{1 + \zeta}{\sqrt[4]{\frac{4s}{a^4}\left(1 + \sqrt{\frac{\rho_1}{\rho_2}}\right)}},$$

$$\beta_3 = \frac{a - \eta}{\sqrt[4]{4s\left(1 - \sqrt{\frac{\rho_1}{\rho_2}}\right)}} = \frac{1 - \zeta}{\sqrt[4]{\frac{4s}{a^4}\left(1 - \sqrt{\frac{\rho_1}{\rho_2}}\right)}},$$

$$\beta_4 = \frac{a + \eta}{\sqrt[4]{4s\left(1 - \sqrt{\frac{\rho_1}{\rho_2}}\right)}} = \frac{1 + \zeta}{\sqrt[4]{\frac{4s}{a^4}\left(1 - \sqrt{\frac{\rho_1}{\rho_2}}\right)}}.$$

The elevation of the free surface is then given in non-dimensional form by

$$(42)\quad \frac{H_1 - H_{10}}{\Delta_u} = \frac{1}{4\pi}\sqrt[4]{\frac{4s}{a^4}}\left\{\sqrt[4]{1 + \sqrt{\frac{\rho_1}{\rho_2}}}\,[\psi(\beta_1) - \psi(\beta_2)]\right.$$
$$\left. + \sqrt[4]{1 - \sqrt{\frac{\rho_1}{\rho_2}}}\,[\psi(\beta_3) - \psi(\beta_4)]\right\}$$

and the elevation of the internal boundary is given by (41).

In the computations, a temperature discontinuity of 10° C. was assumed to exist between the two layers; the upper layer was taken to have a temperature of 10° C. and the lower layer that of 0° C. This

gives $(\rho_2/\rho_1) = 1.0367$. The initial width, $2a$, has been given the value 0.4; this corresponds to a current 1120 km. wide. On the basis of these values, the elevation profiles are as shown in Fig. 7.

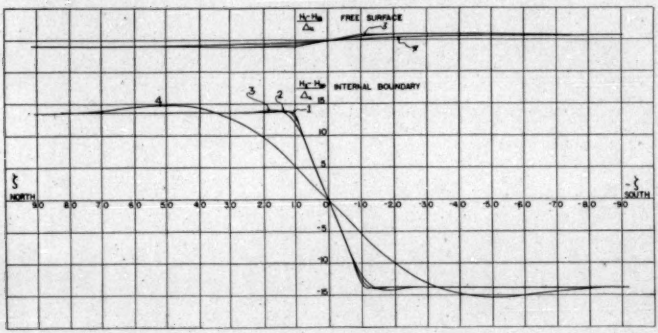


FIG. 7. Elevation profiles for double layer, initial current of finite width.
Curves 1: $s = .055 \times 10^{-4}$.
Curves 2: $s = .880 \times 10^{-4}$.
Curves 3: $s = .141 \times 10^{-2}$.
Curves 4: $s = .360$.

From the gradient wind relation, the velocity in the upper layer is given by

$$u_1 = -\sqrt{\frac{g}{H_0}}\frac{1}{a}\frac{\partial H_1}{\partial \zeta}$$

and for the lower layer by

$$u_2 = -\sqrt{\frac{g}{H_0}}\frac{1}{a}\left(\frac{\rho_1}{\rho_2}\frac{\partial D_1}{\partial \zeta} + \frac{\partial D_2}{\partial \zeta}\right).$$

Since $(\partial\psi/\partial\zeta) = \Phi$, it follows that the non-dimensional expressions for the velocities are

$$\frac{1}{\Delta_u}\sqrt{\frac{H_0}{g}}\,u_1 = \frac{1}{4\pi a}\left[\Phi(\beta_1) + \Phi(\beta_2) + \Phi(\beta_3) + \Phi(\beta_4)\right] \tag{43}$$

for the upper layer, and

$$\frac{1}{\Delta_u}\sqrt{\frac{H_0}{g}}\,u_2 = \frac{1}{4\pi a}\sqrt{\frac{\rho_1}{\rho_2}}\left\{\left[\Phi(\beta_1) + \Phi(\beta_2)\right] - \left[\Phi(\beta_3) + \Phi(\beta_4)\right]\right\} \tag{44}$$

for the lower layer. The velocity profiles are shown in Fig. 8.

The pressure profiles for the upper layer and at the ground are obtained by precisely the same method as used above for the case when

the current is initially of zero width. The pressure $p_1$ in the upper layer is therefore referred to the pressure at the height $H_{10}$ and is given by

$$(45)\quad \frac{p_1}{\rho_1 g \Delta_u} = \frac{1}{4\pi}\sqrt{\frac{4s}{a^4}}\left\{\sqrt[4]{1+\sqrt{\frac{\rho_1}{\rho_2}}}\,[\psi(\beta_1)-\psi(\beta_2)] + \sqrt[4]{1-\sqrt{\frac{\rho_1}{\rho_2}}}\,[\psi(\beta_3)-\psi(\beta_4)]\right\}.$$

The pressure distribution at the ground is easily found to be

$$(46)\quad \frac{p_g - p_{g0}}{\rho_1 g \Delta_u} = \frac{1}{4\pi}\sqrt{\frac{4s}{a^4}}\sqrt{\frac{\rho_2}{\rho_1}}\left\{\sqrt[4]{1+\sqrt{\frac{\rho_1}{\rho_2}}}\,[\psi(\beta_1)-\psi(\beta_2)] - \sqrt[4]{1-\sqrt{\frac{\rho_1}{\rho_2}}}\,[\psi(\beta_3)-\psi(\beta_4)]\right\}.$$

The pressure profiles are therefore expressed in units of $\rho_1 g \Delta_u$, which is the initial pressure difference across the current in the upper layer. These profiles are given in Fig. 9.

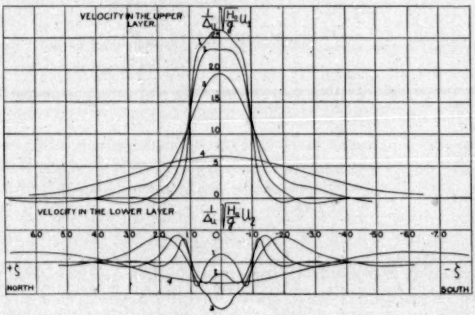


FIG. 8. Velocity profiles for the double layer; initial current of finite width.

Curves 1: $s = .055 \times 10^{-4}$.
Curves 2: $s = .880 \times 10^{-4}$.
Curves 3: $s = .141 \times 10^{-3}$.
Curves 4: $s = .360$.

In their main features the results for a current of finite width are somewhat the same as those for the case when the current is assumed to start originally in the form of a fluid sheet. The case of finite width, however, is much more acceptable as a representation of actual atmospheric conditions and the solution in this case is more satisfactory

since it gives the time change in the intensity of certain of the phenomena, a result which was lacking in the previous case owing to the restriction imposed by the somewhat artificial initial conditions. An example of the time change in intensity mentioned above can be seen by comparing Figs. 5 and 9 for the pressure distribution at the ground. The profiles for both case A and case B show the characteristic region of convergence to the left of the current and region of divergence to the right, producing a high pressure ridge and low pressure trough respectively. The solution for case B, however, shows how the intensity of the ridge and trough formation must vary with time, being zero at first and then gradually increasing.

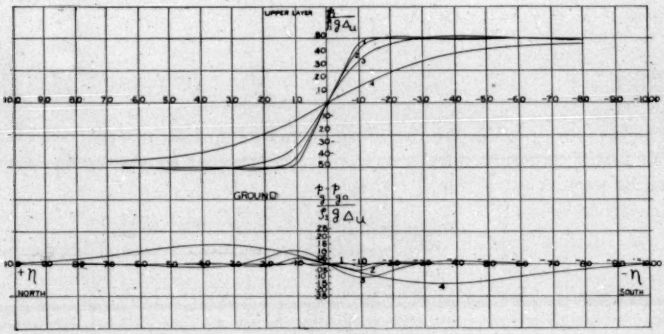


FIG. 9. Pressure profiles in the double layer; initial current of finite width.

Curves 1: $s = .055 \times 10^{-4}$.
Curves 2: $s = .880 \times 10^{-4}$.
Curves 3: $s = .141 \times 10^{-3}$.
Curves 4: $s = .360$.

From Fig. 8 it is seen that for small values of time, the velocity at the center of the upper layer current actually undergoes a slight increase as a result of the diffusion process, corresponding to a slight increase in the pressure gradient; i.e., a slight increase in the slope of the internal boundary. The explanation of this effect must lie in the fact that initially the velocity distribution is such that the rate of shear $\partial u/\partial y$ is infinite at the boundaries of the current. This effect soon dies out, however, and the velocity in the main portion of the upper current then begins to decrease, as weak counter currents are set up on both sides.

The profiles for the lower layer are more complicated. Profile 1, which is for a small value of time, shows a weak west wind at the center, a maximum east wind at $\zeta = 0.8$, a maximum west wind at

$\zeta = 1.2$, and another weak westerly counter current at $\zeta = 2.0$. For succeeding times as shown by profiles 2, 3, and 4, the velocity in the center of the current changes direction, reaches a maximum from the east and then gradually dies out.

The elevation profiles in Fig. 7 can be considered as a simple representation of a warm or tropical air mass above overlying a cold or polar air mass below, with the internal boundary as the sloping air mass boundary separating the two air masses; the internal boundary must therefore be regarded as a front. Initially there is assumed to be a broad uniform current from west to east in the upper warm layer while the lower cold layer is at rest. The effect of the diffusion of the upper layer current produces changes and deformations in the internal boundary or front as shown in the figure. During the early stages of the diffusion process, the slope of the internal boundary at the center undergoes a slight increase; but this effect soon disappears and the slope then decreases steadily, attended by a net southward transport of the cold air below and northward transport of the warm air above.

Let us now suppose that the internal boundary represents an initially stationary frontal surface. We then see how mixing through turbulence of a current in the upper atmosphere could be the agency by which the stationary property is destroyed, since, as we have seen above, a low pressure trough is formed to the south of the current axis and anticyclogenesis takes place to the north and this is attended by a net southward transport of cold air. At any rate the results presented here would seem to indicate that frictional forces resulting from lateral turbulence in the atmosphere are of fundamental importance to the understanding of many meteorological phenomena. These forces appear to be exactly what are needed for any adequate discussion of deepening and filling since they not only permit, but necessarily demand, flow across the isobars at all levels and not at the ground alone.

It will be noticed that the boundary conditions of this problem have been chosen in such a way that the internal boundary must never intersect the ground; this has been done in order to facilitate the mathematical work and make the solution reasonably simple. Even though the internal boundary must not intersect the ground, it can, depending upon the conditions assumed, be brought down quite close to it as will be shown below.

From the initial condition of zero pressure gradient at the ground it is easily found that

$$\Delta_l = \frac{\rho_1}{\rho_2 - \rho_1} \Delta_u = 27.2\Delta_u,$$

corresponding to the values used for $\rho_1$ and $\rho_2$. Moreover, for the horizontal portions of the initial distribution of the internal boundary,

we have

$$H_{2l} = H_{20} + \frac{27.2}{2}\Delta_u, \qquad H_{2r} = H_{20} - \frac{27.2}{2}\Delta_u.$$

Since our atmospheric model is to give a pressure at the ground of 1000 mb., $H_{10}$ will be about the same as $H_0$ the height of the homogeneous atmosphere, or about 8 km. If we further specify that $\Delta_u$ is to correspond to a pressure drop across the upper layer of 25 mb., then $\Delta_u = (H_0/40)$ very nearly. Since the internal boundary must not intersect the ground, it is necessary to consider now the magnitude of the largest deformation in this surface. This will not be larger than that for case A shown in Fig. 3, or about $1.7\Delta_u$. Therefore, in order that the minimum elevation of the internal boundary to the right shall just reach the ground, we must have

$$H_{20} - \frac{27.2}{2}\Delta_u - 1.7\Delta_u = 0,$$

or, using $\Delta_u = (H_0/40)$,

$$H_{20} = 0.382H_0 = 3.06 \text{ km.},$$

which is the smallest value that can be assigned to $H_{20}$ consistent with the above assumptions. On this basis one then finds that

$$H_{2l} = H_{20} + 0.34H_0 = 0.722H_0 = 5.77 \text{ km.},$$
$$H_{2r} = H_{20} - 0.34H_0 = 0.042H_0 = 0.336 \text{ km.}$$

Hence, corresponding to the above assumptions concerning the densities $\rho_1$ and $\rho_2$, we find that the cold air to the North comprises about 0.7 of the total atmosphere while that to the South only a negligible proportion. The value 0.7, although admittedly large, is probably not too far removed from the case of large polar air masses which would comprise about 0.5 or more of the total atmospheric mass. It is evident that the cold air can be made to comprise any portion of the total mass of the atmosphere by a suitable choice of $\Delta_u$, $\rho_1$, and $\rho_2$, but that the choice of these quantities is not mutually independent.

As is evident from the expression for $s$, the time scale of the diffusion process depends upon the value assigned to the coefficient of eddy viscosity $\nu_0$, and in Table 1 this is given for 3 different values of $\nu_0$; namely, $10^9$, $10^{10}$, and $10^{11}$ cm.$^2$ sec.$^{-1}$. The author has previously described a method for evaluating the coefficient of eddy diffusion from isentropic charts (3), where it was found that the values for this lay mostly in the range from $10^9$ to $10^{10}$ cm.$^2$ sec.$^{-1}$. Assuming the coefficient of eddy diffusion and eddy viscosity to be the same, the appropriate time scale would lie somewhere between the values in columns 5 and 6 in Table 1, and values of $s$ having the greatest meteorological importance would lie between $.880 \times 10^{-4}$ and .0225.

From the large values of the coefficient of eddy diffusion evaluated in (3) and from the developments above, it would appear that, strictly speaking, the gradient wind (as defined by the geostrophic and cyclostrophic equations) is something which hardly, if ever, occurs in the atmosphere. The deviations from the gradient wind, that is, the cross-stream components of velocity, $v$, can be computed by integrating the equation of continuity and placing one of the limits of integration at infinity.

TABLE 1.

*Time Scale for the Diffusion of Straight Parallel Flow.*

| (1) | (2) | (3) | (4) | (5) | (6) |
|---|---|---|---|---|---|
| $\frac{1}{\sqrt[4]{45}}$ | $\sqrt[4]{45}$ | $s = \frac{\nu_0 t}{\lambda^2}$ | $\nu_0 = 10^9$ | $\nu_0 = 10^{10}$ | $\nu_0 = 10^{11}$ |
| | | | $t$ in hours | $t$ in hours | $t$ in hours |
| 14.60 | .06849 | $.055 \times 10^{-4}$ | 0.12 | 0.012 | .0012 |
| 7.30 | .1370 | $.880 \times 10^{-4}$ | 1.92 | 0.192 | .0192 |
| 3.65 | .2740 | $.141 \times 10^{-2}$ | 30.7 | 3.07 | .307 |
| 1.825 | .5479 | .0225 | 491 | 49.1 | 4.91 |
| 0.9125 | 1.0959 | .360 | 7860 | 786 | 78.6 |

$\nu_0$ is the kinematic coefficient of eddy viscosity having the dimensions cm.$^2$ sec.$^{-1}$.

## APPENDIX 1.

### SOLUTION OF THE EQUATION $\frac{\partial H}{\partial s} + \frac{\partial^4 H}{\partial \eta^4} = 0$ (4)

If $H_i(\eta)$ denote the initial distribution of $H$, we may write

$$H_i(\eta) = \operatorname*{Lim}_{\beta \to 0} \epsilon^{-\beta|\eta|} H_i(\eta).$$

The exponential is used here as a convergence factor and is introduced to satisfy the conditions of the Fourier Integral Theorem. Particular integrals of (4) are $\epsilon^{-\sigma^4 s} \cos \sigma\eta$ and $\epsilon^{-\sigma^4 s} \sin \sigma\eta$, and since (4) is linear, a solution is

$$(5) \qquad H = \int_0^\infty (A \cos \sigma\eta + B \sin \sigma\eta) \epsilon^{-\sigma^4 s} d\sigma.$$

Also, since $\int_{-\infty}^{\infty} \epsilon^{-\beta|\eta|} H_i(\eta) d\eta$ is an absolutely convergent integral under the conditions which we shall use for $H_i(\eta)$, we can represent $H_i(\eta)$ by a Fourier Integral as follows.

$$(6) \qquad H_i(\eta) = \operatorname*{Lim}_{\beta \to 0} \frac{1}{\pi} \int_0^\infty d\alpha \int_{-\infty}^{\infty} \epsilon^{-\beta|\alpha|} H_i(\alpha) \cos \sigma(\alpha - \eta) d\sigma.$$

Since, when $s = 0$, (7) must be identical with (8), it follows that

$$A = \operatorname{Lim}_{\beta \to 0} \frac{1}{\pi} \int_{-\infty}^{\infty} \epsilon^{-\beta|\alpha|} H_i(\alpha) \cos \sigma\alpha d\alpha,$$

$$B = \operatorname{Lim}_{\beta \to 0} \frac{1}{\pi} \int_{-\infty}^{\infty} \epsilon^{-\beta|\alpha|} H_i(\alpha) \sin \sigma\alpha d\alpha.$$

Hence

$$(7) \qquad H = \operatorname{Lim}_{\beta \to 0} \frac{1}{\pi} \int_{-\infty}^{\infty} \epsilon^{-\beta|\alpha|} H_i(\alpha) d\alpha \int_0^{\infty} \epsilon^{-\sigma^4 s} \cos \sigma(\alpha - \eta) d\sigma.$$

If we now let $\sigma^4 s = (m^4/4)$, we then have

$$\sigma = \frac{m}{\sqrt[4]{4s}}, \qquad d\sigma = \frac{dm}{\sqrt[4]{4s}},$$

and

$$(8) \qquad H = \operatorname{Lim}_{\beta \to 0} \frac{1}{\pi} \frac{1}{\sqrt[4]{4s}} \int_{-\infty}^{\infty} \epsilon^{-\beta|\alpha|} H_i(\alpha) d\alpha \int_0^{\infty} \epsilon^{-(m^4/4)} \cos m\xi \, dm,$$

where $\xi = (\alpha - \eta)/\sqrt[4]{4s}$.

It is easily verified that a solution of the equation $(\partial H/\partial s) + (\partial^4 H/\partial \eta^4) = 0$ can be written in the form

$$(9) \qquad H = \frac{1}{\sqrt[4]{4s}} F\left(\frac{\eta}{\sqrt[4]{4s}}\right),$$

where the differential equation for $F$ is

$$(10) \qquad F''' = \xi F,$$

and where $\xi = (\eta/\sqrt[4]{4s})$. It is likewise easily verified that the infinite integral $\int_0^{\infty} \epsilon^{-(m^4/4)} \cos m\xi d\xi$ is a solution of (10) and it will therefore be denoted by $F(\xi)$. Then since $(\alpha - \eta)/\sqrt[4]{4s} = \xi$, $\alpha = \eta + \xi\sqrt[4]{4s}$, $d\alpha = \sqrt[4]{4s}\, d\xi$ and we have from (8) that

$$H = \operatorname{Lim}_{\beta \to 0} \int_{-\infty}^{\infty} \epsilon^{-\beta|\eta|} H_i(\eta) F(\xi) d\xi,$$

or

$$(11) \qquad H = \operatorname{Lim}_{\beta \to 0} \epsilon^{-\beta|\eta|} H_i(\eta) \int_{-\infty}^{\infty} F(\xi) d\xi = \frac{H_i(\eta)}{\pi} \int_{-\infty}^{\infty} F(\xi) d\xi.$$

We now introduce the initial pressure conditions consistent with the assumptions of a current initially in the form of a fluid sheet. Hence,

$$H_i = H_0 + \frac{\Delta s}{2} \quad \text{for} \quad \alpha < 0; \quad \text{i.e.} \quad -\infty < \xi < \frac{-\eta}{\sqrt[4]{4s}},$$

$$H_i = H_0 - \frac{\Delta s}{2} \quad \text{for} \quad \alpha > 0; \quad \text{i.e.} \quad \frac{-\eta}{\sqrt[4]{4s}} < \xi < \infty.$$

The solution therefore becomes

$$H = \left(H_0 - \frac{\Delta s}{2}\right)\frac{1}{\pi}\int_{\frac{-\eta}{\sqrt[4]{4s}}}^{\infty} F(\xi)d\xi + \left(H_0 + \frac{\Delta s}{2}\right)\frac{1}{\pi}\int_{-\infty}^{\frac{-\eta}{\sqrt[4]{4s}}} F(\xi)d\xi.$$

We now let

$$\Phi = \int_0^{\xi} F(\xi)d\xi,$$

and after a few reductions we have that

$$\frac{H - H_0}{\Delta s} = -\frac{1}{\pi}\Phi(\xi), \tag{12}$$

which is the expression found by Rossby for the elevation profiles. It will be noted that the nature of the differential equation (4) is such that it is possible to combine the time and distance variables into a single variable $\xi$. The velocity profiles are easily obtained from (12) by means of the gradient wind relation.

## APPENDIX 2.

### SOLUTION FOR THE SINGLE LAYER WHEN THE INITIAL CURRENT IS OF FINITE WIDTH.

The solution for the diffusion in a single, homogeneous, incompressible layer can be made more general by treating the case in which the current is initially of finite width. The equation of motion will be the same as (4) but it will be more convenient to use this equation in the form

$$\frac{\partial u}{\partial s} + \frac{\partial^4 u}{\partial \eta^4} = 0, \tag{29}$$

which is easily obtained by differentiating equation (4) with respect to $\eta$ and then using the gradient wind relation. The solution of (29) is of exactly the same form as that for (4) and is

$$u = \int_0^{\infty} \epsilon^{-\sigma^4 s}(A \cos \sigma\eta + B \sin \sigma\eta)d\sigma. \tag{30}$$

For the initial condition on $u$ we shall assume a uniform current of finite width, the velocity everywhere outside the current being zero.

If $u_i$ denote the initial distribution of velocity, (30) can be written in the form

$$u = \frac{1}{\pi}\int_{-\infty}^{\infty} u_i(\alpha)d\alpha \int_0^{\infty} \epsilon^{-\sigma^4 s} \cos \sigma(\alpha - \eta)d\sigma. \tag{31}$$

With the same substitutions as before, namely $\sigma^4 s = (m^4/4)$, and

$(\alpha - \eta)/\sqrt[4]{4s} = \xi$, (31) becomes

$$u = \frac{1}{\pi}\int_{-\infty}^{\infty} u_i(\eta + \xi\sqrt[4]{4s})F(\xi)d\xi, \tag{32}$$

where as before

$$F(\xi) = \int_0^\infty \epsilon^{-m^4/4}\cos m\xi dm.$$

Introducing now the initial velocity distribution consisting of a current of uniform velocity $u_i$ over a distance $2a$ and zero elsewhere, we have $u = u_i$ for $a < \alpha < -a$, $u = 0$ for $|\alpha| > a$.

Equation (32) then becomes

$$u = \frac{u_i}{\pi}\int_{\frac{-(a+\eta)}{\sqrt[4]{4s}}}^{\frac{a-\eta}{\sqrt[4]{4s}}} F(\xi)d\xi,$$

or

$$u = \frac{u_i}{\pi}\left[\Phi\left(\frac{a-\eta}{\sqrt[4]{4s}}\right) - \Phi\left(\frac{-a-\eta}{\sqrt[4]{4s}}\right)\right] = \frac{u_i}{\pi}\left[\Phi\left(\frac{a-\eta}{\sqrt[4]{4s}}\right) + \Phi\left(\frac{a+\eta}{\sqrt[4]{4s}}\right)\right], \tag{33}$$

since $\Phi$ is an odd function. This is the solution of (29) for the velocity profiles.

The elevation profiles are obtained from the gradient wind relation:

$$u = -\frac{1}{\rho f}\frac{\partial p}{\partial y} = \frac{-g}{f}\frac{\partial H}{\partial y} = \frac{-g}{f\lambda}\frac{\partial H}{\partial \eta} = \frac{-g}{f\lambda}\frac{1}{\sqrt[4]{4s}}\frac{\partial H}{\partial \xi}.$$

Since $u_i = (\Delta_s/2a)(g/f\lambda)$, where $\Delta_s$ is the increase in depth of the fluid from north to south across the current, it follows that

$$\frac{\partial H}{\partial \xi} = \frac{-\sqrt[4]{4s}}{\pi}\frac{\Delta_s}{2a}\left[\Phi\left(\frac{a-\eta}{\sqrt[4]{4s}}\right) + \Phi\left(\frac{a+\eta}{\sqrt[4]{4s}}\right)\right].$$

By integration we have

$$\int_0^\xi \frac{\partial H}{\partial \xi}d\xi = H - H_0 = -\sqrt[4]{\frac{4s}{a^4}}\frac{\Delta_s}{2\pi}\int_0^\xi\left[\Phi\left(\frac{a}{\sqrt[4]{4s}} - \xi\right) + \Phi\left(\frac{a}{\sqrt[4]{4s}} + \xi\right)\right]d\xi$$

and

$$\frac{H - H_0}{\Delta_s} = \frac{\sqrt[4]{4s}}{2\pi a}\left[\psi\left(\frac{a-\eta}{\sqrt[4]{4s}}\right) - \psi\left(\frac{a+\eta}{\sqrt[4]{4s}}\right)\right], \tag{34}$$

where $H_0$ is the height of the free surface at the center of the current

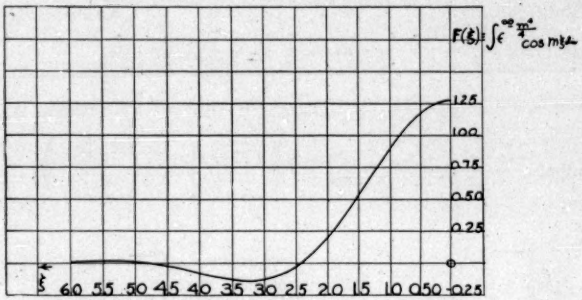


FIG. 10. Curve for the function $F(\xi) \equiv \int_0^\infty \epsilon^{-(m^4/4)} \cos m\xi dm$.

which is assumed constant. $\psi$ denotes the integral function of $\Phi$ and is an even function.

It is convenient to introduce a new distance variable $\zeta$ referring distance to the initial half width of the current. Let

$$\zeta = \frac{\eta}{a} = \frac{y/\lambda}{b/\lambda} = \frac{y}{b},$$

where $b$ denotes the actual half width of the current in linear measure. The non-dimensional equation for the elevation profiles then becomes

$$\frac{H - H_0}{\Delta_s} = \frac{1}{2\pi}\sqrt[4]{\frac{4s}{a^4}}\left[\psi\left(\frac{1-\zeta}{\sqrt[4]{\frac{4s}{a^4}}}\right) - \psi\left(\frac{1+\zeta}{\sqrt[4]{\frac{4s}{a^4}}}\right)\right]. \tag{35}$$

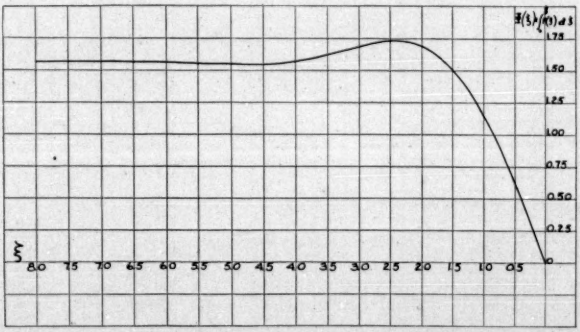


FIG. 11. Curve for the function $\Phi(\xi) \equiv \int_0^\xi F(\xi)d\xi$.

Since

$$u_i = \frac{\Delta_s}{2a}\frac{g}{f\lambda} = \frac{\Delta_s}{2a}\sqrt{\frac{g}{H_0}},$$

the non-dimensional equation for the velocity profiles is

$$\frac{1}{\Delta_s}\sqrt{\frac{H_0}{g}}\,u = \frac{1}{2\pi a}\left[\Phi\left(\frac{1-\zeta}{\sqrt[4]{\frac{4s}{a^4}}}\right) + \Phi\left(\frac{1+\zeta}{\sqrt[4]{\frac{4s}{a^4}}}\right)\right]. \tag{36}$$

## APPENDIX 3.

## THE MATHEMATICAL FUNCTIONS.

The fundamental partial differential equation upon which the developments for rectilinear flow depend is of the form

$$\frac{\partial H}{\partial s} + \frac{\partial^4 H}{\partial \eta^4} = 0.^3$$

This equation has apparently not been treated in the literature of mathematical physics, and it has been shown in Appendix 1 that the

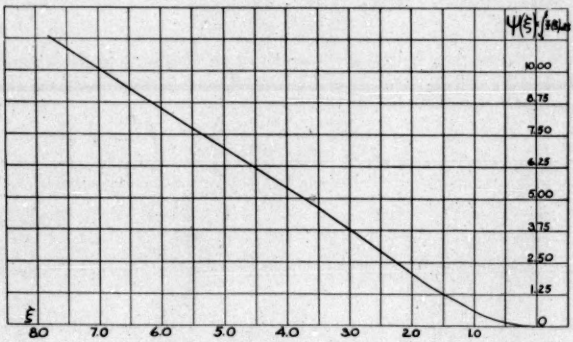


FIG. 12. Curve for the function $\Psi(\xi)$.

solution can be expressed in the form

$$H(\eta, s) = \frac{H_i(\eta)}{\pi}\int_{-\infty}^{\infty} F(\xi)d\xi,$$

where $H_i(\eta)$ is the initial distribution of $H$. Since $F(\xi)$ is an even

[3] The solution of this equation has been considered more recently by H. Ertel and Jeaujang Jaw in *Met. Zeit*, Band 56, Heft 3, 1939.

function, this becomes

$$H(\eta, s) = \frac{2}{\pi} H_i(\eta) \int_0^\infty F(\xi) d\xi,$$

where $F(\xi)$ is defined by the infinite integral

$$\int_0^\infty \epsilon^{-(m^4/4)} \cos m\xi dm,$$

and where

$$\xi = \frac{\eta}{\sqrt[4]{4s}}.$$

The function

$$F(\xi) \equiv \int_0^\infty \epsilon^{-(m^4/4)} \cos m\xi dm$$

for different values of $\xi$ is shown graphically in Fig. 10. The integral

TABLE 2.

*Tabular Values of the Functions, $F(\xi)$, $\Phi(\xi)$, and $\Psi(\xi)$.*

| $\xi$ | $F(\xi)$ | $\Phi(\xi)$ | $\Psi(\xi)$ | $\xi$ | $F(\xi)$ | $\Phi(\xi)$ | $\Psi(\xi)$ | $\xi$ | $F(\xi)$ | $\Phi(\xi)$ | $\Psi(\xi)$ |
|---|---|---|---|---|---|---|---|---|---|---|---|
| 0.000 | 1.282 | 0.000 | 0.000 | 0.900 | .964 | 1.055 | 0.498 | 1.800 | .332 | 1.639 | 1.755 |
| 0.025 | 1.282 | .032 | | 0.925 | .948 | 1.079 | | 1.825 | .315 | 1.647 | |
| 0.050 | 1.281 | .064 | 0.0016 | 0.950 | .932 | 1.102 | 0.553 | 1.850 | .299 | 1.655 | 1.837 |
| 0.075 | 1.279 | .096 | | 0.975 | .915 | 1.125 | | 1.875 | .284 | 1.662 | |
| 0.100 | 1.277 | .128 | 0.0064 | 1.000 | .898 | 1.148 | 0.609 | 1.900 | .268 | 1.669 | 1.920 |
| 0.125 | 1.275 | .160 | | 1.025 | .881 | 1.170 | | 1.925 | .253 | 1.676 | |
| 0.150 | 1.271 | .192 | 0.0143 | 1.050 | .864 | 1.192 | 0.668 | 1.950 | .238 | 1.682 | 2.004 |
| 0.175 | 1.269 | .224 | | 1.075 | .847 | 1.214 | | 1.975 | .223 | 1.688 | |
| 0.200 | 1.265 | .255 | 0.0254 | 1.100 | .830 | 1.235 | 0.728 | 2.000 | .208 | 1.693 | 2.088 |
| 0.225 | 1.260 | .287 | | 1.125 | .812 | 1.255 | | 2.025 | .194 | 1.698 | |
| 0.250 | 1.255 | .318 | 0.0397 | 1.150 | .794 | 1.275 | 0.791 | 2.050 | .180 | 1.703 | 2.173 |
| 0.275 | 1.249 | .350 | | 1.175 | .776 | 1.295 | | 2.075 | .166 | 1.707 | |
| 0.300 | 1.243 | .381 | 0.0572 | 1.200 | .758 | 1.314 | 0.856 | 2.100 | .153 | 1.711 | 2.258 |
| 0.325 | 1.237 | .412 | | 1.225 | .740 | 1.333 | | 2.125 | .139 | 1.715 | |
| 0.350 | 1.230 | .443 | 0.0778 | 1.250 | .722 | 1.351 | 0.923 | 2.150 | .126 | 1.718 | 2.344 |
| 0.375 | 1.222 | .473 | | 1.275 | .704 | 1.369 | | 2.175 | .114 | 1.721 | |
| 0.400 | 1.214 | .504 | 0.102 | 1.300 | .686 | 1.386 | 0.991 | 2.200 | .102 | 1.724 | 2.430 |
| 0.425 | 1.205 | .534 | | 1.325 | .668 | 1.403 | | 2.225 | .090 | 1.726 | |
| 0.450 | 1.196 | .564 | 0.128 | 1.350 | .649 | 1.420 | 1.061 | 2.250 | .078 | 1.728 | 2.516 |
| 0.475 | 1.187 | .594 | | 1.375 | .634 | 1.436 | | 2.275 | .067 | 1.730 | |
| 0.500 | 1.177 | .624 | 0.158 | 1.400 | .613 | 1.451 | | 2.300 | .056 | 1.732 | 2.602 |
| 0.525 | 1.166 | .653 | | 1.425 | .594 | 1.466 | | 2.325 | .045 | 1.733 | |
| 0.550 | 1.156 | .682 | 0.191 | 1.450 | .576 | 1.481 | 1.207 | 2.350 | .035 | 1.734 | 2.689 |
| 0.575 | 1.144 | .711 | | 1.475 | .558 | 1.495 | | 2.375 | .025 | 1.735 | |
| 0.600 | 1.133 | .739 | 0.226 | 1.500 | .540 | 1.509 | 1.281 | 2.400 | .015 | 1.735 | 2.775 |
| 0.625 | 1.121 | .767 | | 1.525 | .522 | 1.523 | | 2.425 | .006 | 1.735 | |
| 0.650 | 1.108 | .795 | 0.265 | 1.550 | .504 | 1.535 | 1.356 | 2.435 | .000 | 1.736 | |
| 0.675 | 1.095 | .823 | | 1.575 | .486 | 1.547 | | 2.450 | −.006 | 1.735 | 2.862 |
| 0.700 | 1.082 | .850 | 0.306 | 1.600 | .468 | 1.559 | 1.435 | 2.500 | −.024 | 1.735 | 2.949 |
| 0.725 | 1.068 | .877 | | 1.625 | .451 | 1.571 | | 2.550 | −.039 | 1.733 | 3.035 |
| 0.750 | 1.054 | .903 | 0.350 | 1.650 | .433 | 1.582 | 1.513 | 2.600 | −.053 | 1.731 | 3.122 |
| 0.775 | 1.040 | .930 | | 1.675 | .416 | 1.593 | | 2.650 | −.065 | 1.728 | 3.208 |
| 0.800 | 1.025 | .955 | 0.397 | 1.700 | .398 | 1.603 | 1.593 | 2.700 | −.076 | 1.723 | 3.295 |
| 0.825 | 1.011 | .981 | | 1.725 | .382 | 1.613 | | 2.750 | −.086 | 1.720 | 3.381 |
| 0.850 | 0.995 | 1.006 | 0.446 | 1.750 | .365 | 1.622 | 1.673 | 2.800 | −.095 | 1.715 | 3.466 |
| 0.875 | .980 | 1.031 | | 1.775 | .348 | 1.631 | | 2.850 | −.104 | 1.710 | 3.552 |

TABLE 2—(*Continued*).

| $\xi$ | $F(\xi)$ | $\Phi(\xi)$ | $\Psi(\xi)$ | $\xi$ | $F(\xi)$ | $\Phi(\xi)$ | $\Psi(\xi)$ | $\xi$ | $F(\xi)$ | $\Phi(\xi)$ | $\Psi(\xi)$ |
|---|---|---|---|---|---|---|---|---|---|---|---|
| 2.900 | −.111 | 1.706 | 3.637 | 4.700 | −.005 | 1.549 | 6.524 | 6.450 | .0030 | 1.573 | 9.254 |
| 2.950 | −.118 | 1.700 | 3.722 | 4.750 | −.002 | 1.549 | 6.602 | 6.500 | .0020 | 1.574 | 9.333 |
| 3.000 | −.124 | 1.692 | 3.807 | 4.778 | 0.000 | 1.550 | 6.645 | 6.540 | .0010 | 1.574 | 9.396 |
| 3.050 | −.128 | 1.687 | 3.891 | 4.800 | .001 | 1.550 | 6.679 | 6.550 | .0000 | 1.5740 | 9.412 |
| 3.100 | −.132 | 1.680 | 3.975 | 4.850 | .005 | 1.550 | 6.757 | 6.600 | −.0010 | 1.5739 | 0.490 |
| 3.150 | −.134 | 1.674 | 4.059 | 4.900 | .007 | 1.550 | 6.834 | 6.650 | −.0019 | 1.5738 | 9.569 |
| 3.200 | −.136 | 1.667 | 4.142 | 4.950 | .009 | 1.551 | 6.912 | 6.700 | −.0028 | 1.5737 | 9.648 |
| 3.250 | −.135 | 1.659 | 4.225 | 5.000 | .012 | 1.551 | 6.989 | 6.750 | −.0038 | 1.5736 | 9.726 |
| 3.300 | −.134 | 1.651 | 4.308 | 5.050 | .013 | 1.552 | 7.067 | 6.800 | −.0047 | 1.5734 | 9.805 |
| 3.350 | −.132 | 1.644 | 4.390 | 5.100 | .014 | 1.553 | 7.144 | 6.850 | −.0055 | 1.5733 | 9.883 |
| 3.400 | −.129 | 1.638 | 4.472 | 5.150 | .015 | 1.554 | 7.222 | 6.900 | −.0063 | 1.5732 | 9.962 |
| 3.450 | −.127 | 1.632 | 4.554 | 5.200 | .016 | 1.554 | 7.300 | 6.950 | −.0071 | 1.5731 | 10.041 |
| 3.500 | −.124 | 1.626 | 4.635 | 5.250 | .017 | 1.555 | 7.377 | 7.000 | −.0079 | 1.5730 | 10.119 |
| 3.550 | −.120 | 1.618 | 4.717 | 5.300 | .018 | 1.556 | 7.455 | 7.050 | −.0076 | 1.5729 | 10.198 |
| 3.600 | −.117 | 1.613 | 4.797 | 5.350 | .019 | 1.557 | 7.533 | 7.100 | −.0072 | 1.5728 | 10.276 |
| 3.650 | −.112 | 1.607 | 4.878 | 5.400 | .0200 | 1.558 | 7.610 | 7.150 | −.0069 | 1.5727 | 10.355 |
| 3.700 | −.108 | 1.602 | 4.958 | 5.450 | .0195 | 1.559 | 7.689 | 7.200 | −.0065 | 1.5726 | 10.433 |
| 3.750 | −.103 | 1.597 | 5.038 | 5.500 | .0190 | 1.560 | 7.766 | 7.250 | −.0062 | 1.5725 | 10.512 |
| 3.800 | −.098 | 1.592 | 5.118 | 5.550 | .0185 | 1.561 | 7.844 | 7.300 | −.0060 | 1.5723 | 10.590 |
| 3.850 | −.092 | 1.588 | 5.197 | 5.600 | .0180 | 1.562 | 7.922 | 7.350 | −.0058 | 1.5722 | 10.669 |
| 3.900 | −.086 | 1.583 | 5.277 | 5.650 | .0172 | 1.563 | 8.000 | 7.400 | −.0055 | 1.5721 | 10.747 |
| 3.950 | −.081 | 1.579 | 5.356 | 5.700 | .0165 | 1.564 | 8.078 | 7.450 | −.0049 | 1.5720 | 10.824 |
| 4.000 | −.075 | 1.576 | 5.434 | 5.750 | .0158 | 1.565 | 8.156 | 7.500 | −.0044 | 1.5719 | 10.904 |
| 4.050 | −.070 | 1.571 | 5.513 | 5.800 | .0150 | 1.565 | 8.235 | 7.550 | −.0038 | 1.5718 | 10.982 |
| 4.100 | −.065 | 1.567 | 5.592 | 5.850 | .0142 | 1.566 | 8.313 | 7.600 | −.0032 | 1.5717 | 11.061 |
| 4.150 | −.059 | 1.563 | 5.670 | 5.900 | .0135 | 1.567 | 8.391 | 7.650 | −.0029 | 1.5716 | 11.139 |
| 4.200 | −.054 | 1.561 | 5.748 | 5.950 | .0128 | 1.568 | 8.469 | 7.700 | −.0026 | 1.5715 | 11.217 |
| 4.250 | −.048 | 1.558 | 5.826 | 6.000 | .0120 | 1.569 | 8.548 | 7.750 | −.0023 | 1.5714 | 11.296 |
| 4.300 | −.043 | 1.556 | 5.904 | 6.050 | .0108 | 1.569 | 8.626 | 7.800 | −.0020 | 1.5712 | 11.374 |
| 4.350 | −.038 | 1.555 | 5.982 | 6.100 | .0095 | 1.570 | 8.705 | 7.850 | −.0018 | 1.5711 | 11.452 |
| 4.400 | −.032 | 1.554 | 6.059 | 6.150 | .0082 | 1.571 | 8.783 | 7.900 | −.0015 | 1.5710 | |
| 4.450 | −.027 | 1.553 | 6.137 | 6.200 | .0070 | 1.571 | 8.862 | 7.950 | −.0012 | 1.5709 | |
| 4.500 | −.023 | 1.552 | 6.214 | 6.250 | .0062 | 1.572 | 8.940 | 8.000 | −.0010 | 1.5708 | |
| 4.550 | −.017 | 1.552 | 6.292 | 6.300 | .0055 | 1.572 | 9.019 | | | | |
| 4.600 | −.013 | 1.551 | 6.369 | 6.350 | .0048 | 1.572 | 9.097 | | | | |
| 4.650 | −.009 | 1.550 | 6.447 | 6.400 | .0040 | 1.573 | 9.176 | ∞ | 0.000 | 1.5708 | ∞ |

function of $F(\xi)$ is an odd function and is defined by

$$\Phi(\xi) \equiv \int_0^{\xi} F(\xi)d\xi;$$

this is shown in Fig. 11. By continuing the process of integration, we obtain the following functions defined by

$$\psi(\xi) \equiv \int_0^{\xi} \Phi(\xi)d\xi,$$

an even function, and

$$R(\xi) \equiv \int_0^{\xi} \psi(\xi)d\xi,$$

an odd function. The function $\psi(\xi)$ is shown in Fig. 12.

Tabular values of the 3 functions $F(\xi)$, $\Phi(\xi)$, and $\psi(\xi)$ are given in Table 2. The function $F(\xi)$ was evaluated with the aid of the differential analyzer belonging to the Electrical Engineering Department of

the Massachusetts Institute of Technology, while the remaining functions were all evaluated by mechanical integration.

LITERATURE.

(1) ROSSBY, C. G., "On the Mutual Adjustment of Pressure and Velocity Distributions in Certain Simple Current Systems," *Journal of Marine Research*, Vol. 1, No. 1, 1937, pp. 15–28.

(2) PARR, A. E., "On the Probable Relationship Between Vertical Stability and Lateral Mixing Processes," *Journal du Conseil*, Vol. XI, No. 3, 1936.

(3) GRIMMINGER, G., "The Intensity of Lateral Mixing in the Atmosphere as Determined from Isentropic Charts," *Bulletin American Meteorological Society*, May, 1941, p. 227.

(*To be continued in December issue*)

## CURRENT TOPICS.

**Refrigerated Cargo Planes Foreseen by York Corporation.**—(*Refrigerating Engineering*, Vol. 46, No. 2.) Fleets of giant cargo planes which will bring the world's produce to the American dinner table hours instead of days after it has been gathered may be one of the early results of wartime advances in refrigeration and air conditioning, according to S. E. Lauer, president of the York Corporation.

Super-refrigerated air freighters are possible even now because of the higher efficiency of refrigerants and decrease in size of the equipment, a development brought on by military needs, Mr. Lauer said. Such new equipment, he added, will play a major role in solving the nation's food problem through greater production of quick-frozen and dehydrated foods and storage facilities for preserving produce for indefinite periods.

R. H. O.

### ARMY AND NAVY NOTES.

**Testing of Sights on Garand Rifles is Speeded With New Device.**—Both ammunition and manpower formerly used in testing the sights of Garand automatic rifles for the U. S. Army are saved with a new device that has been developed in the General Engineering Laboratory of the General Electric Co. Speaking recently before the South Bend Section of the American Institute of Electrical Engineers, Everett S. Lee, engineer in charge of the laboratory, described the apparatus.

V.2
194

Formerly, he said, the accuracy of the sights was tested at the Springfield Arsenal by actual firing of the rifles. With the new apparatus, however, a plug holding a mirror is inserted into the end of the barrel of the gun, which is held in a special stand. The mirror reflects an image of an illuminated cross to a screen. Images of the front and rear sights are also reflected to nearby screens, and in that way their accuracy is checked, he stated.

He also revealed that the photoelectric spectrophotometer, an electronic device so sensitive that it can measure the light thrown on the palm of the hand by a candle a mile away, is now being used by the U. S. Army in the standardization of camouflage colors. It can distinguish between 2,000,000 different colors, including some that are invisible. A recent improvement in the spectrophotometer, he stated, makes it possible to measure the glare from glossy surfaces, such as shiny paper.

Delicate measuring instruments, such as those used before the war for such peaceful uses as the determination of the thickness of enamel on electric refrigerators, are finding important war uses, he declared.

"Measuring instruments, as well as shells and guns, are essential war equipment," said Mr. Lee. "Such instruments are vital both for the manufacture and for the successful operations of every plane, tank and ship."

R. H. O.

# THE ADAPTATION OF MAGNETIC SUPPORT TO AIR-DRIVEN ULTRACENTRIFUGES.

BY

THOMAS J. DIETZ AND TERREL V. KISHBAUGH.

From the Biochemical Research Foundation, Newark, Delaware.

The routine operation of ultracentrifuges equipped with pneumatic support is restricted by the necessity for critical adjustment of supporting air pressure. The magnetic support was developed by Beams and his coworkers [1,2] for use with the electrically driven ultracentrifuge.

The magnetic lifting device consists of a solenoid, the armature of which is mounted on the drive shaft of the rotor. During the operation of the centrifuge, the solenoid is energized with sufficient direct current to relieve the pressure on the thrust-bearing upon which the rotor is supported when at rest. Thrust-bearing friction is thus reduced to a negligible quantity, and contact between the rotating system and the thrust-bearing is maintained only for the purpose of vertical stabilization.

One of the principal aims of a contemporary development, the "turret drive" of Pickels,[3] was to increase the stability of the pneumatic support by compensating for pressure fluctuations. However, in this as in other pneumatically supported units, failure of the supporting air pressure during operation results in excessive retarding torque being applied to the drive shaft. This objection has been obviated in the electrically driven unit [2] by the use of a lubricated thrust-bearing which could support the entire weight of the rotating system in case of failure of the D.C. supply. From the work of Skarstrom and Beams,[2] it appeared that the stability of the magnetically supported rotor was an improvement over that of the pneumatically supported rotor and the idea evolved that the magnetic support could be used to advantage on the air-driven ultracentrifuge. The results of the investigation are presented here.

## DESIGN.

The first unit to be converted in this laboratory to magnetic support was a Beams quantity ultracentrifuge;[4] the rough dimensions for the magnetic solenoid were arbitrarily taken from the electrically driven ultracentrifuge.[2] Figure 1 is a drawing of the converted assembly, a portion of which is cut away to show the main details of the driving system. The iron-sheathed solenoid *A*, consisting of 7,000 turns, random wound, of No. 32 SCC copper wire, and having a resistance of 87 ohms, operates on direct current. The gap between the stop *D* and the armature *E* of the solenoid is of the order of 0.020" when the thrust of the armature is against the upper bearing *F*. The stop of the solenoid is designed to accommodate the upper bearing and yet provides

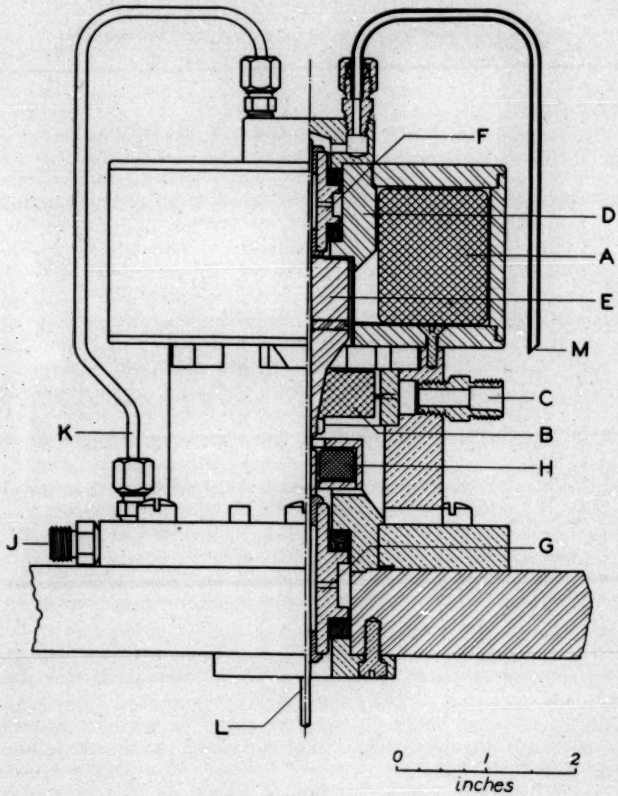


FIG. 1. Drawing of the driving head of the magnetically supported, air-driven, quantity ultracentrifuge showing:

*A*—iron sheathed supporting solenoid
*B*—duralumin turbine
*C*—air supply
*D*—iron stop
*E*—iron armature
*F*—upper bearing, brass with babbitt inserts
*G*—main bearing, brass with babbitt inserts
*H*—iron sheathed pick-up coil
*J*—lubricating oil supply
*K*—oil line to upper bearing
*L*—main shaft
*M*—oil overflow from upper bearing.

sufficient iron to maintain the cross-sectional area of the magnetic circuit. Because of the shape of the stop, there is a tendency toward slide-pull of the armature when the magnetizing current is increased beyond that necessary to balance gravitational forces.

The driving air pressure is supplied through *C* connected to the controlled pressure line by a short length of 1/4" copper tubing. The driving turbine *B* is mounted on the armature with a tapered fit and secured with a threaded thrust collar. The turbine buckets and the air jets are of standard design.[4] Only advancing jets are provided in this unit, and when a run is complete, the rotor must coast to rest. Since 3½ to 4 hours are required for the 8" duralumin rotor to come to rest from 500 r.p.s., a set of retarding jets is a desirable addition.

Below the turbine the armature is turned down to 3/16" diameter to act as armature for the speed pick-up coil *H*. The pick-up coil is energized by stray flux from the supporting solenoid.

The coil consists of approximately 9,000 turns of No. 40 enamelled magnet wire encased in a soft iron sheath; its resistance is 1,800 ohms. A 1/4" hole is drilled in the center of each face of the iron sheath to admit the co-axial armature. A semi-circular enlargement of the upper opening is made to correspond with a "flat" made on the armature as shown in Fig. 1. The output of the pick-up coil is fed into a frequency meter [5] which indicates the rotational speed of the ultracentrifuge in r.p.s. A minimum of 3 volts input is required by the frequency indicator, making it necessary to step up the output voltage of the pick-up coil with a 10 : 1 audio transformer.[6] Since the output of the pick-up coil is partially dependent upon the air gap between its armature and the soft iron sheath, any tendency of the armature to whirl is accompanied by an increase in output voltage. By measuring this voltage with a v.t. voltmeter, one can note any critical instability tending to deform the drive shaft.

TABLE I.

*Comparison of Operating Characteristics of Air-Driven Vacuum Type Ultracentrifuge Equipped with Pneumatic Support and with Magnetic Support.*

| | Pneumatic Support. | Magnetic Support. |
|---|---|---|
| Air pressure, accelerating, lbs./in.$^2$ | 80 | 81 |
| Angular acceleration at 250 r.p.s., rad./sec.$^2$ | 3.20 | 3.0 |
| Air pressure, idling at 500 r.p.s. | 17 | 13.5 |
| Air pressure, decelerating, lbs./in.$^2$ | 50 | — |
| Angular deceleration at 250 r.p.s., rad./sec.$^2$ | 1.78 | — |
| Air pressure, decelerating, lbs./in.$^2$ | 0 | 0 |
| Angular deceleration at 250 r.p.s., rad./sec.$^2$ | 0.37 | 0.17 |
| Pneumatic support, lbs./in.$^2$ | 12.5 | — |
| Magnetic support, ampere-turns | — | 2380 |

Rotor—duralumin, diam.—8", wt.—14.5 lbs.
Turbine—duralumin, diam.—1½".
Driving jets—eight, size—No. 54 drill.

OPERATION.

Data on the operating characteristics of the ultracentrifuge are presented in Table I which is a comparison of operating characteristics of the unit both before and after conversion to the magnetic support. This comparison is intended to indicate only that the magnetically supported system compares favorably in efficiency with the pneumatically supported system. The power input required by this type of

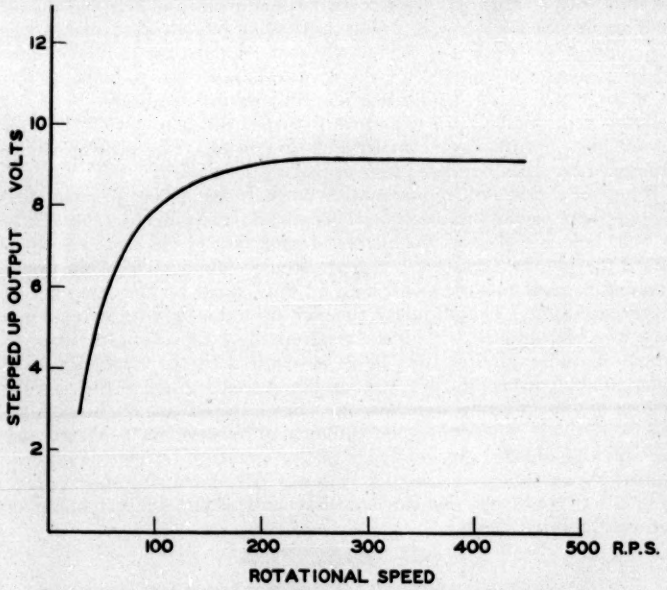


FIG. 2. Variation of the voltage output of the pick-up coil with rotational speed as measured across the secondary of the 10 : 1 transformer.

ultracentrifuge, in general, appears to be greater than that of some others, e.g., the "turret drive" unit.[3]

Figure 2 is a voltage-speed curve for the stepped-up output of the pick-up coil. The frequency characteristic of the transformer is not constant below 150 c.p.s. The output voltage, however, rises quickly to a value which is constant for the remainder of the acceleration period. Because of the relative stiffness of the armature, i.e., the section of the drive shaft between bearings *F* and *G*, and the flexibility of the shaft *L* below the main bearing *G* from which the rotor is suspended, no critical frequency of the system is detected by the pick-up coil.[7] The funda-

mental mode of deformation of the section of shaft $L$ below the main bearing $G$ weighted with the supported rotor occurs at too low a speed to be troublesome during acceleration. At the same time, the armature $E$ tends to stiffen the section of shaft between the bearings $F$ and $G$ sufficiently to raise its first critical frequency to a value which is above the normal operating range of the unit. In cases where critical speeds of the drive shaft have been encountered,[8] the output voltage rises rapidly to a peak, the maximum being reached at a rotational speed equal to the critical frequency of the armature.

The pick-up coil operates equally well when mounted so that the drive shaft of music wire alone acts as the armature. Filing of a "flat" on the shaft where it passes through the sheath of the pick-up coil is unnecessary. Variation in air gap during each revolution results from the unavoidable, slight dynamic unbalance which causes perceptible whirl of the shaft. When the shaft thus becomes the armature of the pick-up coil, the coil must be energized by means of an additional D.C. winding within the iron sheath. The design of the quantity ultracentrifuge in Fig. 1 probably could be improved by the use of such a pick-up coil placed about the rotor suspension directly below the main bearing. Then the present coil $C$ and the section of armature extending below the turbine could be discarded and the distance between the bearings $F$ and $G$ shortened.

The use of the magnetic support as a means of reducing thrust-bearing friction in the air-driven ultracentrifuge has been found to be practical in routine operation. Little attention is required for replacement of thrust-bearings. At the end of 165 hours, running time, the thrust-bearing surfaces of the unit described showed slight wear, suggesting that the life of the bearings tentatively be fixed at 150 hours. Additional information on the operation of this unit is to be included in another paper describing details of a semi-automatic control system utilizing standard industrial equipment.

#### REFERENCES

1. J. W. BEAMS AND S. A. BLACK, *Rev. Sci. Inst.*, 10: 59, 1939.
2. C. SKARSTROM AND J. W. BEAMS, *Rev. Sci. Inst.*, 11: 398, 1940.
3. E. G. PICKELS, *Rev. Sci. Inst.*, 9: 358, 1938.
4. J. W. BEAMS, F. W. LINKE, AND P. SOMMER, *Rev. Sci. Inst.*, 9: 248, 1938.
5. Electronic Frequency Meter, Type No. 854-B, General Radio Co.
6. Type 0–15, pri. imp. 8,000–15,000 ohms sec. imp. 1 meg., United Transformer Co.
7. Experimental work on the adaptation of the magnetic support to the Beams, tubular type, ultracentrifuge, to date, has shown the most serious obstacle to be the control of deformation of the weighted drive shaft at critical speeds.
8. An incomplete study of the modes of vibration of the tubular type ultracentrifuge indicates that the supporting armature on which the turbine is mounted (see Fig. 1) reaches its fundamental mode of deformation at approximately 1,000 r.p.s. Any improvement in design tending to shorten the distance between bearings will decrease the risk of failure at higher speeds.

## ARMY AND NAVY NOTES.

**Abrasive Blasts Save Time on Production Front.**—(*Compressed Air Magazine*, Vol. 48, No. 9.) War production is finding many new applications for sand-, grit-, and shot-blasting with the aid of compressed air. One of the most unusual of these is the shot-peening of airplane and automotive engine parts and other pieces of machinery to relieve fatigue-inducing stresses that cause failure. This work is done by projecting $\frac{1}{16}$ gram steel shot with air at from 80 to 100 pounds pressure against the surfaces of the metal, which has previously been heat-treated. Among the machine parts that are given such treatment are automobile- and airplane-engine valve springs, with the result that their service life, according to one manufacturer, is increased approximately eight times. Automobile clutch discs are similarly subjected to shot-peening, and flexing tests have shown that they possess far greater endurance than the ordinary type.

In making a survey of the many uses to which blast cleaning is put in industrial establishments, the Compressed Air Institute has found that many factories consider this method of cleaning metal parts, for example, more economical and easier to control than pickling. Fumes from the baths are hard to confine so that they will not cause damage to roof structures and other parts of buildings through corrosion. On the other hand, in the case of blast cleaning, the shot, grit, or sand is easily recovered in collectors that prevent their scattering and permit repeated re-use.

Today, the choice of an abrasive is not haphazard; it is selected with care for the job to be done. Steel grit is generally preferred for cleaning iron and steel, while sand and carborundum grit are generally utilized for non-ferrous metals. But steel grit has its advantages. As compared with sand it can be applied with from 10 to 12 per cent. less compressed air, and, besides, sand wears out blasting nozzles much faster than do steel particles.

In descaling forgings by blasting, it has been the practice to remove first the forging scale and then the annealing scale. Now time is saved by eliminating one of these operations—by descaling only once after annealing, which tends to soften the scale and makes it easier to blast away. Today, forgings are being made to close clearances so there is little metal to be cut away after blasting. This applies especially to shells, and helps to speed output.

R. H. O.

# A RECORDING AND CONTROLLING SYSTEM FOR AIR-DRIVEN ULTRACENTRIFUGES.

BY

THOMAS J. DIETZ.

From the Biochemical Research Foundation, Newark, Delaware.

The advantages of automatic speed control of oil- and air-driven ultracentrifuges have been amply reviewed in the literature.[1-7] It is the purpose of this paper to show that commercial equipment may be used successfully in recording and controlling the important variables in the operation of the air-driven ultracentrifuge. The automatic record of results not only aids in reducing personal error but also fixes any of the several major causes for failure of the equipment.

Various types of pneumatic support have been devised to relieve thrust-bearing friction on the rotor assembly of the air-driven ultracentrifuge.[8, 9, 10 and 11] Recently the magnetic support[4, 6] has been adapted by us to the air-drive.[12] Because of greater stability over long periods of operation, the magnetic support was found to be more serviceable than the air-support previously used. Therefore the control system, the details of which are presented here, was designed primarily for the operation with the magnetically supported, air-driven ultracentrifuge.

## CONTROL PANEL.

The positions of the various instruments on the assembled control panel are shown in Fig. 1. The principal units on the panel are: a 0–30 lbs. pressure gage *A* to indicate the driving pressure of air used in maintaining constant speed; a clock *B*; a 0–100 lbs. pressure gage *C* to indicate the driving pressure of air used for acceleration; a pressure-temperature recording unit *D* (0–100 lbs. and 0–100° C.) to supply a permanent record of pressure and temperature of the driving air supply; a recording millivoltmeter *E* (0–7.5 millivolts) to record speed and control driving air pressure; [13] and an electronic speed indicator *F* calibrated in revolutions per second.

An 11 ohm wire-wound resistor is placed in series with the milliammeter of the electronic speed indicator by means of connections provided in the rear of the panel and the voltage drop across this resistor is used to activate the speed recorder. The voltage drop across the resistor is proportional to the frequency of the e.m.f. input to the speed indicator which in turn is equal to the rotational speed in r.p.s.

A central area of the panel is cut out to receive an insert for auxiliary equipment, which includes: a filament milliammeter (0–50 ma.) *G*, a

microvoltmeter (calibrated 200–0 microns) *H*, a filament rheostat *I*, and a filament switch *J* all for a thermocouple vacuum gage; a D.C. ammeter (0–1.0 amp.) *K*, a field rheostat *L*, and a starting switch *M*, for the motor-generator set (32 volts D.C.) which supplies the power for the magnetic supporting solenoid; a lubricating oil pressure gage (0–30 lbs.) *N*, and thermal overload switches *O* and *P* for lubricating oil and vacuum pumps respectively. Other controls on the front of the panel are: an air switch *Q* in the air supply line to the panel; a switch *R* in the 120 volt A.C. line to the panel; a manual-automatic air switch *S* which in con-

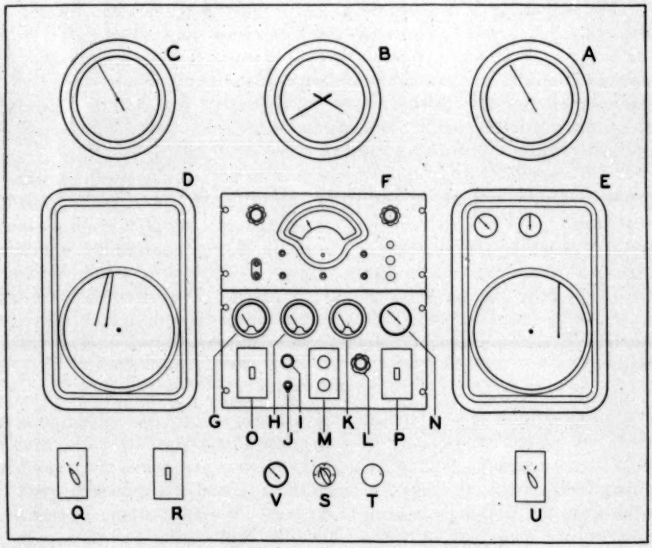


FIG. 1. Front view of ultracentrifuge control panel.

junction with the throttling valve *T* adjusts the air pressure required to maintain uniform speed; and an air switch *U* also coupled to the throttling valve for adjustment of the accelerating air pressure. Gage *V* (0–30 lbs.) indicates air pressure activating the diaphragm valves. An air filter and pressure reducer *W* are inserted in the air supply to the panel.

### AIR SUPPLY SYSTEM.

A schematic piping diagram of the control system is shown in Fig. 2. The compressed air is supplied by a 15 H.P. compressor at a pressure of

125 lbs./in.². A spiral heat exchanger of 6 sq. ft. cooling surface is placed in the supply line but it has not been found necessary. The temperature of the air in the line remains constant within 1° C. and slightly below the ambient temperature for operating periods as long

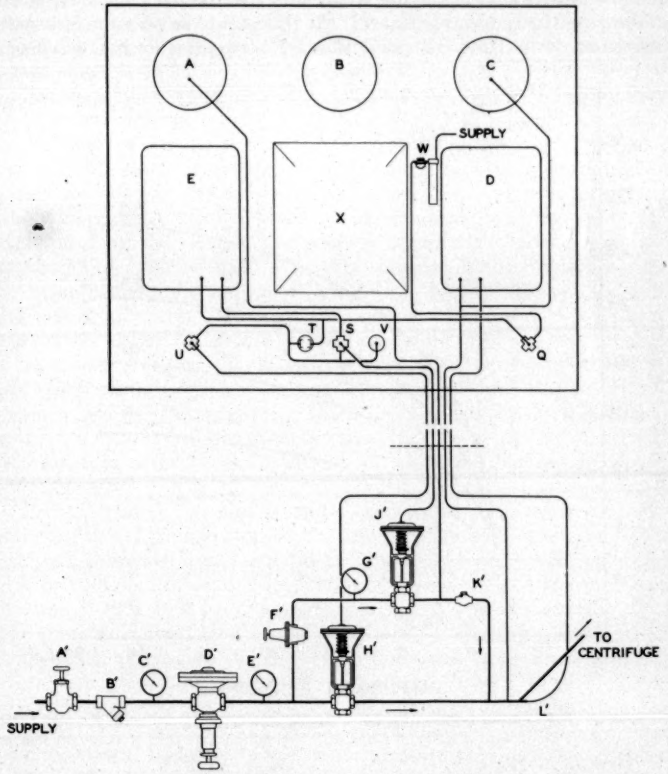


FIG. 2. Rear view of ultracentrifuge control panel as a schematic diagram of piping and valves of the driving air control system.

as 24 hours. The system is divided into two sections, a high pressure section having air at 75–100 lbs./in.² available, and a low pressure line carrying 15–30 lbs./in.².

The air supply line is $2\frac{1}{4}''$ galvanized iron pipe to the cooling unit; it is then reduced to 1″ and a gate valve $A'$ is placed in the line; $B'$ is a

fine mesh standard strainer and $C'$ is a 0–300 lbs. gage to indicate the line pressure. All of the piping between valve $A'$ and the centrifuge is copper with sweated fittings except in a few cases where couplings are more serviceable for connection to soft copper tubing. A pressure reducer is placed next in the line at $D'$ with a 0–100 lbs. gage $E'$ adjacent to indicate the reduced pressure. At this point the pressure is usually carried at 90 lbs./in.$^2$. Beyond $E'$ a 1/2″ low pressure line carrying a

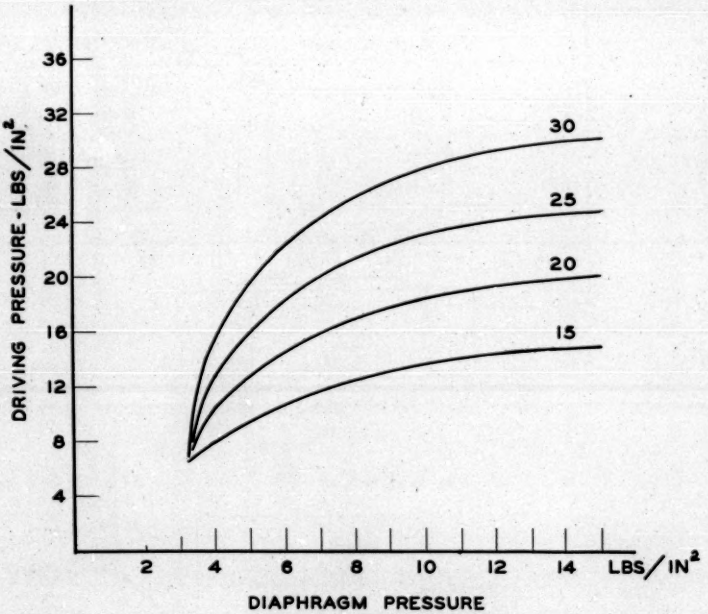


FIG. 3. The relation between dynamic driving pressure in the branch line and static pressure on the diaphragm of valve $J'$ for branch line reduced pressures of 15, 20, 25 and 30 lbs./in.$^2$ respectively.

reducer $F'$ branches from the main line. $F'$ reduces the branch line pressure to approximately 24 lbs./in.$^2$ as indicated by the 0–30 lbs. gage $G'$.

The diaphragm valves $H'$ and $J'$ control the air flow in the high and low pressure lines respectively. $H'$ was originally specified as a 1″, single seated, reverse action, V-port valve. It was of the open-shut type and its purpose was only to facilitate the opening and closing of the

high pressure line for the acceleration of the ultracentrifuge rotor. It was found from experience to be an improvement to make the air pressure for accelerating the rotor adjustable from zero to maximum. To accomplish this, the V-port plug was replaced with a special ratio plug having an effective taper of 0.015 in./in. and a maximum O.D. which would nearly close the orifice in the valve seat. Complete closure was effected by a rubber gasket which was retained from the discarded V-port plug.

The diaphragm valve $J'$ in the low pressure line, in a preliminary specification, was one having a 1/4 in. orifice, and a single seat ratio plug capable of passing 20 cu. ft./min. at 20 lbs./in.$^2$ with a pressure drop of 10 lbs./in.$^2$. The effective taper on the ratio plug was found to be excessive and it was consequently replaced by a special ratio plug having an effective taper of 0.0075 in./in. to obtain finer control of the quantity of air delivered. The relation between the pressure on the diaphragm of valve $J'$ and the driving pressure in the branch line for various adjustments of reducer $F'$ is shown in Fig. 3. These data were obtained by adjusting the reduced pressure to 15, 20, 25 and 30 lbs./in.$^2$ respectively as read on the low pressure gage $A$ on the panel, and for each of these pressures, the diaphragm pressure of valve $J'$ was raised by small increments from zero to maximum and the increase in driving pressure recorded from gage $A$. From these curves it can be seen that for a given pressure, the diaphragm valve gives a more delicate control of air pressure near the "open" position, i.e., when the diaphragm pressure is a maximum.

Referring again to Figs. 1 and 2, controlled pressure at the diaphragm valve $J'$ is indicated by the low pressure gage $A$ on the panel. Gage $A$ is protected from main line back pressure by the check valve $K'$. The low and high pressure lines then join to supply the ultracentrifuge. Pressure is indicated for either line by gage $C$ and recorded by $D$; a thermometer is also inserted in the line at $L'$ to permit a record of air temperature to be made at $D$. The system will not operate properly when both diaphragm valves, $H'$ and $J'$, are open. If they are inadvertently opened simultaneously, the high pressure in the main line will force the check valve to remain closed and the pressure indicated by gage $A$ will build up to the static pressure permitted by pressure reducer $F'$. This will not be harmful to gage $A$ unless $F'$ has been adjusted to maintain a reduced pressure greater than 30 lbs./in.$^2$.

From the data in Fig. 3 and from information on the relation of speed recorder pen movement to diaphragm pressure, the alteration in driving pressure with deviation of recorder pen from mean position may be obtained. Figure 4 shows such a relationship under normal operating conditions for a quantity ultracentrifuge, i.e., 460 r.p.s. with 14 lbs./in.$^2$ driving pressure. The driving pressure—recorder pen

deviation curve I applies when the maximum available pressure in the branch line as indicated on the panel gage *A* is 15 lbs./in.². Curve II represents conditions when the maximum available pressure in the branch line is raised to 20 lbs./in.². As will be explained in detail in later paragraphs, the automatic control system maintains the speed of the rotor constant to 0.2 per cent. average deviation under routine

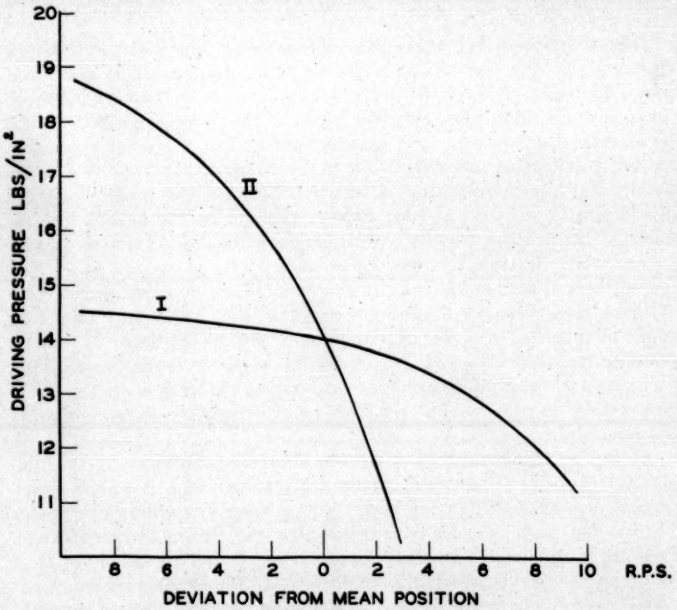


FIG. 4. The relation between speed recorder pen movement and controlled dynamic driving pressure in the branch line, graphically computed.

I—available pressure 15 lbs./in.².
II—available pressure 20 lbs./in.².

The abscissæ of the two curves have been adjusted to coincide at 14 lbs./in.² (the normal driving pressure required to maintain the ultracentrifuge at approximately 500 r.p.s.).

operating conditions. Thus from curve I the average variation in driving pressure is of the order of 0.2 lbs./in.². It can be seen from Curve II that if the ultracentrifuge were operated on a branch line pressure which was substantially greater than the demand, the variation in driving pressure resulting from a given deviation in speed would be excessive and "hunting" of the automatic control system would occur.

### OPERATION OF UNIT.

After the ultracentrifuge rotor has been loaded, the entire unit is assembled according to standard technique. Next, the charts of the pressure-temperature recorder and the speed recorder-controller are adjusted to read the time which will be correct when the run is started, and the recorder pens are lowered into contact. The line switch of the electronic speed indicator and the standardizing current switch of the speed recorder-controller are turned on to permit the units to warm up. Next, the lubricating oil pump, the vacuum pump, and the D.C. generator are turned on. The D.C. voltage is adjusted by means of the field rheostat on the panel to energize the magnetic lifting solenoid sufficiently to support the rotor with slight thrust against the upper bearing of the driving system. A current which is just insufficient to lift the rotor free from thrust on the lower bearing may also be used. As soon as the pressure in the rotor chamber has been reduced to 50 microns or less, zero adjustments are made on the charts, the standardizing current of the recording millivoltmeter is corrected, and preparation for the run is complete.

At the start of the run the A.C. line supply to the panel is turned on and the diaphragm valve in the accelerating pressure line is opened by means of its air switch. The accelerating pressure is then manually adjusted to a standard value by means of the throttling valve. Once the rotor has reached the speed chosen for the run, the accelerating pressure is cut to zero, and the manual-automatic air switch which controls the diaphragm valve in the low pressure line is turned to "automatic" and the recording millivoltmeter takes over the control of the driving air pressure to maintain a constant speed of rotation for the duration of the run.

When the run at maximum speed is complete, it is only necessary to cut the driving pressure to zero by turning off the manual-automatic air switch and permit the rotor to coast to a stop. While it is desirable to increase the deceleration by means of reverse driving jets, the use of additional retarding torque has been avoided in order to have successive records of deceleration available for a study of bearing friction. When the rotor has come to rest, all of the switches on the panel are to be turned off.

### ACCURACY OF CONTROL.

To obtain a measure of the accuracy of automatic control, a special clock was driven from the output of the speed pick-up coil; the clock reading was then referred to a time standard, the alternating current lighting supply. A 25 watt P.A. amplifier was used as the source of power, and the field coil of the test clock (impulse type) was replaced by approximately 500 turns of No. 32 DCC magnet wire having a D.C. resistance of 8.0 ohms.

The accuracy of the test clock was checked on a frequency of 480 c.p.s. obtained with a small laboratory-built alternator driven by a 3/8 H.P. synchronous motor (1800 r.p.m., 120 volts, 60 cycles, A.C.). The output of the alternator was amplified to drive the test clock, and photographic comparison with another clock, a secondary time standard,[14] was made. Exposures of 1/40 sec. were made of the two clocks at 0.0, 1.5, 3.0, and 4.5 hours. The instant of exposure was chosen to record the sweep hand of the standard clock in the "nine o'clock" position so as to reduce error caused by backlash in the standard clock. Comparison photographs of the two clocks showed that the test clock was capable of following the multiple of the 60 cycle line frequency with an error of not more than $\pm 0.001$ per cent.

To test the over-all accuracy of the automatic control of constant ultracentrifuge rotor speed, the test clock was driven from the amplified output of the speed pick-up coil of the ultracentrifuge. The rotor was accelerated to 462 r.p.s. as read from the electronic speed indicator and then switched to automatic control. Approximately 20 min. were allowed for the control unit to reach equilibrium before the first photograph of the two clocks was taken. Photographs were taken at twenty-minute intervals for an 8 hour period under conditions similar to those mentioned in the previous paragraph. The results of the speed test showed that the mean speed of the rotor for the 8 hour period was 458 r.p.s. The average deviation from the mean of actual rotor speed as integrated over a twenty-minute interval was calculated to be $\pm 0.2$ per cent.

The accuracy of speed control obtained with the standard equipment used in this assembly is in reasonable agreement with the accuracy obtained with the electrically driven ultracentrifuge control unit,[6] and that of the laboratory-built electronic controls for the air-driven ultracentrifuge [1, 2, and 7] and for the oil-driven ultracentrifuge.[5]

This control equipment is classed as semi-automatic because the ultracentrifuge rotor is accelerated under manual control and is converted to automatic control when optimum speed is reached. When the run is complete, the driving air pressure must be shut off manually to permit deceleration of the rotor. If desired, the control panel can be made fully automatic by the addition of time schedule control equipment of standard design.

## DISCUSSION.

In analyzing operation records, a reasonable approximation of the acceleration-time curve may be expressed by the following equation:[5]

$$Id\omega/dt = kP - f\omega, \qquad \text{I}$$

where $I$ is the moment of inertia of the rotating system, $\omega$ is the angular velocity of the rotor, $P$ is the pressure of the driving air, $k$ is a constant,

and $f$ is a number having the dimensions of a frictional constant. Upon integration, equation (I) becomes

$$\omega = k/f[P - (P - P_0)e^{-ft/I}] \qquad \text{II}$$

and

$$d\omega/dt = k/I(P - P_0)e^{-ft/I}, \qquad \text{III}$$

in which $(P - P_0)\ k$ is obtained as the constant of integration.

The limitations in the usefulness of equations (II) and (III) are more apparent when $d\omega/dt$ is small. In practice, retarding forces in addition to those included in equation (I) are exerted probably as the result of varying amounts of dynamic unbalance in parts of the rotating system. The effect of these forces could be considered by the introduction of a term, $-f'\omega^2$, into the right side of equation (I), $f'$ being a frictional constant different from $f$. However, the integration of such an equation yields an expression for $\omega$ which is more difficult to apply to actual speed-time curves than equation (II).

## CONCLUSION.

The facts acquired in the use of the control equipment herein described, indicate that standard industrial control apparatus, particularly of the pneumatic type, can be applied advantageously to the operation of air-driven ultracentrifuges.

## REFERENCES.


1. DAVIS, T., *Rev. Sci. Inst.*, **7**: 96, 1936.
2. BEAMS, J. W., AND SNODDY, L. B., *Science*, **85**: 185, 1937.
3. KAHLER, H., *Rev. Sci. Inst.*, **9**: 257, 1938.
4. BEAMS, J. W., AND BLACK, S. A., *Rev. Sci. Inst.*, **10**: 59, 1939.
5. BJÖRNSTÅHL, Y., *Rev. Sci. Inst.*, **10**: 258, 1939.
6. SKARSTROM, C., AND BEAMS, J. W., *Rev. Sci. Inst.*, **11**: 398, 1940.
7. ROTHEN, A., *Rev. Sci. Inst.*, **12**: 355, 1941.
8. BEAMS, J. W., AND PICKELS, E. G., *Rev. Sci. Inst.*, **6**: 299, 1935.
9. PICKELS, E. G., AND BEAMS, J. W., *Science*, **81**: 342, 1935.
10. BEAMS, J. W., AND LINKE, F., *Rev. Sci. Inst.*, **8**: 160, 1937.
11. PICKELS, E. G., *Rev. Sci. Inst.*, **9**: 354, 1938.
12. DIETZ, T. J., AND KISHBAUGH, T. V., *J. Frank. Inst.* (current issue).
13. With the exception of the panel insert carrying auxiliary equipment and the electronic speed indicator, the complete panel was supplied by The Bristol Co., Waterbury, Conn. The electronic speed indicator is the 834 B frequency meter of General Radio Co., Cambridge, Mass. The panel insert was assembled in the laboratory from standard items including a thermocouple vacuum gage supplied by General Electric Co., Schenectady, N. Y.
14. Information on the accuracy of the 60 cycle, A.C. line voltage used as a secondary time standard was received from the power company. The error in frequency was $\pm 0.2$ cycles with a maximum cumulative error of less than 2.0 seconds.

## ARMY AND NAVY NOTES.

**Air Conditioning Aids in Artillery Optical Equipment Manufacture.**—(*Heating and Ventilating*, Vol. 40, No. 8.) The third installation of air conditioning equipment in the binocular assembly room of Bausch & Lomb, optical manufacturers of Rochester, N. Y., was recently made. Air conditioned rooms are required for the preparation of optical parts of binoculars because dirt cuts the light-gathering properties of the prisms and lenses. In cementing the lens element, the room air must be scrupulously clean in order that the Canada balsam shall not be contaminated. Also, the temperature must be held within close limits both for applying the balsam and for drying.

Air conditioning is also being called on at Bausch & Lomb to aid in high precision work in the manufacture of range finders, essential components of modern warfare. In space where these products are manufactured, assembled and tested, air conditioning equipment reduces heat that is generated by motors and people, eliminating danger of expansion or contraction of delicate metal parts by maintaining constant temperature. Likewise it controls humidity to prevent corrosion caused by perspiration on the fingers of workmen.

In the assembly of lenses in microscopes, air conditioning is used to dehumidify the air between the assembled lenses so that they will not fog up under the varying temperature conditions of field use. Absolute dust control is required because a speck of dust on a range finder, for example, might look like a distant airplane to the observer.

Polishing lenses is another delicate operation which calls upon air conditioning to help insure perfection. For the polishing process, lenses are mounted on wax and any change in the wax, either softening or hardening, might cause inaccuracies. Consequently, it is important that the wax mountings remain the same during polishing, and air conditioning insures against the possibility of changes.

R. H. O.

## II. ON A NEW METHOD OF MEASURING THE MEAN HEIGHT OF THE OZONE IN THE ATMOSPHERE.

BY

**K. WATANABE,**

Astrophysical Observatory,
California Institute of Technology.

The purpose of this paper is to present the results obtained by applying a new method [1] of measuring the "mean height" of the atmospheric ozone. Part I by John Strong [2] treats the background and the theory of the method, and describes the apparatus and some of the results obtained. Here, his paper will be designated JS-I.

Briefly, the method requires three sets of determinations; namely, measurements of the total thickness of ozone in the atmosphere between the observer and the sun, of the total thickness of water vapor between the sun and the observer, and of the atmospheric absorption of solar radiation in the 9.6 $\mu$ ozone band. All three measurements are involved directly in the computation of the mean height of ozone in such a way that the accuracies of all must be emphasized. The essential feature of the method is the measurement of the 9.6 $\mu$ ozone band by a residual ray apparatus [3] which yields the pressure effect [1(b),2] on the absorption band. From the "average" total pressure under which the ozone exists one may deduce the average height of the atmospheric ozone. The effect of pressure on the 9.6 $\mu$ ozone band has been determined in the laboratory over a sufficient range to furnish a calibration for the absorption of atmospheric ozone—covering the range of total thickness of ozone and of the total pressure. Of course, the ozone concentration and temperature are different for the case of the laboratory measurements.

Numerous individual measurements are desirable to obtain curves of these measurements in order to study the changes in ozone height throughout the day; accordingly, it has been our purpose to simplify the manipulation of the instruments and also the computation whenever conveniently possible.

### DETERMINATION OF $x_0$ AND VARIATION OF log $R_0$.

The amount of ozone overhead, $x_0$ (in cm. at N.T.P.), was obtained by measuring the ratio, $R$, of the intensities of solar radiation at 3110 and 3050 Å with a Hilger-Müller double-quartz monochromator and

[1] (*a*) John Strong, *Phys. Rev.*, **55**, 1114 (1939). (*b*) John Strong and Kenichi Watanabe, *Phys. Rev.*, **57**, 1049 (1940).

[2] John Strong, JOUR. OF FRANKLIN INSTITUTE, **231**, 121 (1941).

[3] John Strong, *J. O. S. A.*, **29**, 520 (1939).

by employing the following equation (refer to p. 135, JS-I):

$$\log R - \log R_0 = (\alpha' - \alpha)x_0 \sec \zeta + (\beta' - \beta) \sec z \qquad (1)$$

or for our case,

$$\log R - \log R_0 = 1.40x_0 \sec \zeta + 0.03 \sec z. \qquad (1a)$$

It was necessary to check frequently the settings on the drum-scale of the monochromator, since the positions of the wave-lengths with respect to the scale varied gradually during the day due apparently to changes

TABLE I.

| Date. | Location. | Log $R_0$. | Sunspot groups. | Spot counts. |
|---|---|---|---|---|
| June 27, 1939 | Pasadena | .115 | 13 | 172 |
| 28 | " | .160 | 16 | 226 |
| 30 | " | .130 | 12 | 73 |
| Oct. 4 | " | .135 | 10 | 83 |
| 5 | " | .165 | 9 | 80 |
| 9 | " | .175 | 7 | 73 |
| 10 | " | .165 | 8 | 78 |
| 11 | " | .160 | 6 | 114 |
| 12 | " | .145 | 10 | 99 |
| 13 | " | .175 | 9 | 150 |
| 14 | " | .160 | 5 | 81 |
| Nov. 20 | " | .225 | 5 | 41 |
| 21 | " | .260 | 4 | 70 |
| 22 | " | .280 | 5 | 39 |
| 29 | " | .210 | 5 | 43 |
| 30 | " | .225 | 3 | 43 |
| June 5, 1940 | Palomar | .200 | 6 | 56 |
| 6 | " | .185 | 10 | 77 |
| 11 | " | .170 | 12 | 80 |
| 13 | " | .200 | 10 | 120 |
| 14 | " | .215 | 10 | 77 |
| 15 | " | .245 | 10 | 102 |
| July 2 | " | .285 | 6 | 22 |
| 3 | " | .285 | 9 | 30 |
| 4 | " | .295 | 9 | 20 |
| 5 | " | .330 | 9 | 28 |
| 23 | " | .320 | 6 | 58 |
| 29 | " | .295 | 7 | 39 |
| 30 | " | .275 | 6 | 45 |
| 31 | " | .285 | 8 | 64 |

in temperature of the instruments. The wave-lengths transmitted by the monochromator were usually kept within about 2 Å of the assigned wave-lengths. This 2 Å introduces an error of about 2 per cent. in the value of $R$. It was also necessary to correct $R$ from a calibration curve for the non-linearity of the galvanometer deflections. A value of 1.40 was taken as the "best value" for the difference in the absorption coefficients $(\alpha' - \alpha)$, and it is to be noted from equation (1) that the inaccuracy in this value [4] affects all values of $x_0$ in the same way.

[4] C. Fabry and H. Buisson, *J. de Phys.*, **5**, 196 (1913); *Compte Rendu*, **192**, 457 (1931). J. Dutheil and M. Dutheil, *J. de Phys.*, **7**, 414 (1926). Ny-Tsi-Ze and Choon-Shin-Piaw, *Chinese J. Phys.*, **1**, 1 (1933).

Log $R_0$ was determined graphically for "steady" days by extrapolation (see, for example, p. 137, JS-I); * however, the determined value of log $R_0$ was not constant over an extended period as is shown in Table I.

The same Table also shows some correlation between the values of log $R_0$ and the sunspot activity—the sunspot data being taken from the *Monthly Weather Review*. Although an attempt was made to correlate the value of log $R_0$ with solar activity,† our data are insufficient to make a careful analysis of the correlation indicated by Table I owing to the error involved in one day's value of log $R_0$.

During the period, summer of 1939 to summer of 1940, the maximum variation of log $R_0$ is about 0.2 which seems to show that the intensity of solar emission at the shorter wave-length (3050 Å) varied about 50 per cent. more than at the other (3110 Å). This non-constancy of log $R_0$ presents an uncertainty in our value of $x$; since our measure-

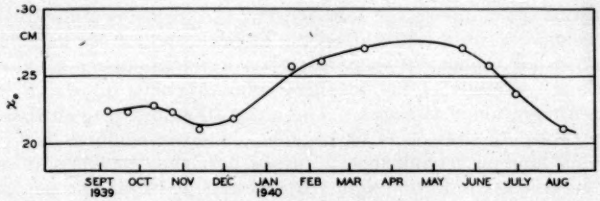


FIG. 1.

ments are not accurate enough to differentiate real changes in log $R_0$ from errors involved in extrapolation. However, over a period of several days or even a month log $R_0$ was fairly constant as seen in Table I. For our present work log $R_0$ is assumed to change gradually and values of log $R_0$ used were values averaged over a period of several "steady" days when the curve of log $R$ vs. sec $\zeta$ is essentially linear for the morning and afternoon values. Log $R_0$ is determined under the assumption that there is no diurnal variation of the amount of ozone. It is evident that it is not possible from our measurements alone to differentiate sudden changes in the amount of ozone (ozone holes or clouds) from the effect of sudden changes in the relative solar emissions at 3050 and 3110 Å. A further study of the suggested variation in the intensities of the ultraviolet solar radiation would seem to be indicated.

Figure 1 shows the annual variation of ozone at Pasadena (latitude 34° 08′) and on Palomar Mtn. (33° 22′) over a period of a year. The

* Note: the values of log $R_0$ should be positive in Table III of the reference cited.

† Dr. Seth B. Nicholson of Mount Wilson Observatory favored the author with a helpful discussion on solar activities.

annual variation shown in Fig. 1 is in general agreement with the results of the extensive survey of Dobson.[5] The existence or absence of a regular diurnal variation of the amount of ozone cannot be settled by our data owing to the uncertainty in the value of log $R_0$.

### MEASUREMENT OF $\tau_0$.

The amount of water vapor overhead, $\tau_0$, is measured with the help of the Φ-band as described on p. 136 JS-I. About 30 readings of the galvanometer deflection are taken in covering the band contour, particular care being taken to determine precisely the solar emission in the band wings and the "zero" galvanometer readings. Numerous tests show that the result, the absorption by the Φ-band, is independent of the width of the slit and that, by widening the slit over the value giving good resolution of the band, it was possible to decrease the time of measurement of the band from 7 to about 4 minutes. This shorter time and the increased deflections increased the accuracy of the $\tau_0$ determination; also, during the shorter time, the coelostat holds the sun's image relatively more constant on the monochromator slit and there is less chance for changes of solar intensity or galvanometer background deflections. Moreover, the resulting smooth curve allows of a less tedious integration of the area. The integration and the calculation of the percentage of absorption are obtained from the readings by a calculating machine with sufficient accuracy. $\tau$, the thickness of water vapor in the solar radiation light path, is obtained from the percentage absorption using Fowle's data.[6] For small amounts of water vapor we used an empirical equation, $\tau = cA_\Phi^2$, derived from Fowle's data. Sample curves of Φ-band are shown on pp. 138 and 140 in JS-I. The variation we found of the amount of water vapor overhead during the day is presented graphically, with the curves of the ozone height, in that reference and in one of the following figures.

At Pasadena (altitude c. 800 ft.) the measurements of $\tau_0$ were not very regular. Later measurements carried on at Palomar Mtn. (altitude c. 5600 ft.) were much more consistent. Furthermore, the smaller amount of water vapor at the higher altitude requires a smaller correction factor in determining the ozone absorption at 9.6 $\mu$ and thus reduces error. $\tau_0$ on Palomar was usually about 1 cm. and its value fluctuated less than in Pasadena, presumably because at Pasadena the atmosphere is more affected by irregular ocean and land air masses.

### MEASUREMENT OF $W'$.

The residual ray apparatus measured the atmospheric absorption in the neighborhood of 9.66 $\mu$ and its response to solar radiation was

[5] G. M. B. Dobson, *Proc. Roy. Soc.*, A129, 416 (1930).
[6] F. E. Fowle, *Smithsonian Misc. Coll.*, 68, No. 8 (1917).

calibrated from time to time against a constant temperature globar (refer to the response curve on p. 141 JS-I). This repeated calibration was essential not only to compute the solar energy but to take into account the variation of sensitivity of the apparatus. Due apparently to the change in room temperature, the sensitivity of the instrument drops rapidly between 11 A.M. and 3 P.M., as much as 10 per cent.; thus a daily sensitivity curve is essential for interrelation of the solar deflection.

TABLE II.

Date: June 11, 1940.
Location: Palomar Observatory.

| Φ band measurement. | | | Ozone measurement. | | | |
|---|---|---|---|---|---|---|
| $t$. | $A$. | $\tau$. | $t$. | sec $\zeta$. | $R$. | $x$. |
| −3:28 | .0198 | 0.970 cm. | −3:23½ | 1.420 | 5.52 | .373 cm. |
| −2:59 | .0244 | 1.244 | −2:53½ | 1.293 | 4.95 | .342 |
| −2:41 | .0190 | 0.931 | −0:12½ | 1.020 | 3.83 | .268 |
| −0:23 | .0230 | 1.126 | 1:08 | 1.057 | 3.99 | .280 |
| 0:02 | .0201 | 0.972 | 2:17 | 1.180 | 4.51 | .316 |
| 1:03 | .0193 | 0.945 | 3:25 | 1.430 | 5.58 | .377 |
| 1:50 | .0198 | 0.970 | 4:25 | 1.885 | 8.72 | .505 |
| 2:22 | .0219 | 1.073 | 5:02½ | 2.18 | 14.33 | .653 |
| 2:57 | .0270 | 1.350 | | | | |
| 3:31 | .0263 | 1.315 | | | | |
| 3:58 | .0287 | 1.435 | | | | |
| 4:19 | .0320 | 1.600 | | $\log R_0 = .180$ | | |
| 4:36 | .0383 | 1.915 | | mean $x_0 = .264$ cm. | | |
| 4:50 | .0390 | 1.950 | | | | |
| 5:47½ | .0545 | 2.80 | | | | |

| Globar measurement. | | | 9.6μ band measurement. | | | | |
|---|---|---|---|---|---|---|---|
| $t$. | $d_G$. | $\theta$. | $t$. | $d_\odot$ | $(10x)^{\frac{1}{2}}$. | $W'/C$. | $h$. |
| −3:05½ | 1.648 | 1282° | −3:07 | 4.360 | 1.887 | 1.392 | 22.3 km. |
| −2:34 | 1.639 | 1282° | −2:48½ | 4.451 | 1.844 | 1.411 | 22.2 |
| −0:05 | 1.640 | 1296° | −0:09½ | 4.870 | 1.631 | 1.570 | 22.0 |
| 1:58 | 1.510 | 1279° | 1:20 | 4.562 | 1.682 | 1.537 | 22.2 |
| 3:52 | 1.553 | 1296° | 2:39 | 4.160 | 1.822 | 1.431 | 22.2 |
| 4:57½ | 1.523 | 1293° | 3:20 | 3.865 | 1.929 | 1.360 | 22.3 |
| | | | 4:05 | 3.387 | 2.126 | 1.213 | 21.8 |
| | | | 4:25½ | 3.143 | 2.245 | 1.158 | 22.2 |
| | | | 4:42 | 2.903 | 2.377 | 1.112 | 22.6 |
| | | | 5:07 | 2.405 | 2.575 | 0.988 | 22.4 |
| | | | | | | mean | 22.2 |

The solar energy received by the instrument, $W$, may be expressed as follows:

$$W = C\left(\frac{1}{e^{14330/9.66\theta} - 1}\right)\frac{d_\odot}{d_G}, \qquad (2)$$

where $\theta$ is the temperature of the globar as obtained from an optical pyrometer, $d_\odot$ and $d_G$ are respectively the deflections produced by the sun and the globar. Let $W'$ be the solar energy after correcting for

the absorption of water vapor; then we have,

$$W'/C = \frac{d_\odot}{d_G}\frac{10^{0.052\tau}}{2.144} \qquad \text{for} \qquad \theta = 1296^\circ \text{ K.}, \tag{3}$$

where $\tau$ is the actual thickness of water vapor expressed in cm. of precipitable water. For our ozone height measurements, the temperature of the globar, which was measured periodically with an optical pyrometer, was usually within the range, 1296° K. ± 7°. Thus the value of the reciprocal of the quantity in the parenthesis of equation (2) was usually within the range, 2.144 ∓ 0.021. If the globar was at a temperature 1296° ± 7°, the value 2.144 was used; otherwise the value of the reciprocal of the parenthesis was recalculated.

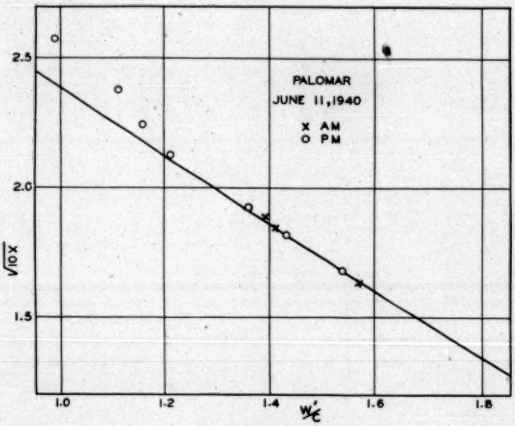


FIG. 2.

The deflections, $d_\odot$ and $d_G$, were determined with the images of the sun and of the globar source alternately covering the entrance aperture of the residual ray instrument. Several deflections were averaged in such a way as to eliminate the effect of galvanometer drifts.

The value of $W'$ is thus determined in terms of $C$ for different hour angles, $t$. The values for June 11, 1940 are tabulated at the lower right of Table II together with corresponding interpolated values of the square root of the ozone thickness.

### CALCULATION OF THE MEAN HEIGHT OF OZONE.

To illustrate the process of calculating the "mean height," $h$, of ozone, in kilometers, we consider the summary of one day's measurement, Table II. The summary consists of a series of Φ-band measure-

ments, a series of ozone thickness measurements, a series for the globar measurements and a series of the $\pi$ band measurements as shown in Table II.

All the values of $\tau$, $x$, and $d_G$ taken in one day are plotted on a graph with the hour angle as abscissa. From the smooth curves drawn through these points, the values of $\tau$, $x$, and $d_G$ are interpolated for hour angles corresponding to the $\pi$ band measurement, $d_\odot$. Values of

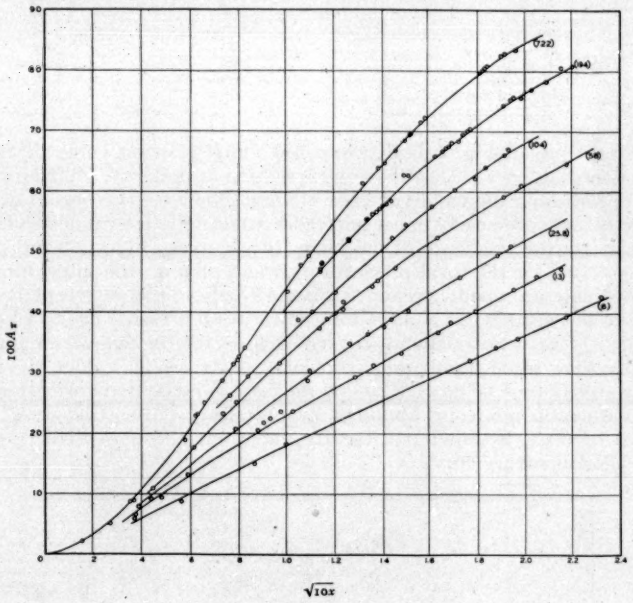


FIG. 3.

$W'/C$ are then computed from equation (3), and these values are plotted against the corresponding values of $\sqrt{10x}$ as illustrated in Fig. 2.

The laboratory calibration of the $\pi$ band is essential for the determination of the ozone height. The curves of $A_\tau$ (absorption of the $\Phi$-band) versus $\sqrt{10x}$, at different total pressures is reproduced [1b,2] in Fig. 3. It is to be noted in this graph that the range of total pressures of interest here is values from 100 mm. to 10 mm. and from 1.5 to 2.5 in the values of $\sqrt{10x}$. The above pressure limits correspond roughly to heights of 15 and 30 km., the region of the greatest concentration of atmospheric ozone.

TABLE III.

| Date. | $W_0/C$. | $W_0/C$ (estimated). |
|---|---|---|
| June 6, 1940 | 2.67 | 2.92 |
| 11 | 2.83 | 3.12 |
| 14 | 3.08 | 3.39 |
| 15 | 2.93 | 3.22 |
| 25 | 2.85 | 3.12 |
| 26 | 2.77 | 3.03 |
| July 2 | 2.94 | 3.22 |
| 3 | 3.05 | 3.36 |
| 4, 5, 6 | 3.06 | 3.38 |
| 29 | 2.91 | 3.19 |
| 30 | 2.81 | 3.07 |
| Aug. 1, 2, 3 | 3.07 | 3.39 |
| 11, 12, 13 | 3.03 | 3.35 |
| Weighted mean | 2.95 | 3.22 |

The curve in Fig. 2 is extrapolated for $W_0/C$, the value of $W'/C$ corresponding to $x = 0$. This extrapolation is done by utilizing only points for which the values of $\sqrt{10x}$ are less than 2.0—this region of the curve being more nearly linear and more accurately determined. If we extrapolate the segments of the laboratory curves (Fig. 3) from $\sqrt{10x} = 1.5$ to 2.0 for the total pressures 25.8 and 58 mm. the intercepts on the ordinate are about .06 and .12 respectively. The intercept is less if we take a segment of a curve for a lower total pressure or for a lower range of $\sqrt{10x}$. Solar energy curves such as the one shown in Fig. 2 usually show some curvature particularly at the higher values of $\sqrt{10x}$. One determines a value of $W_0/C$ by making an estimated correction to the values of intercept obtained graphically. Table III gives the values of $W_0/C$ extrapolated linearly and the same ones "corrected" with the laboratory curve.

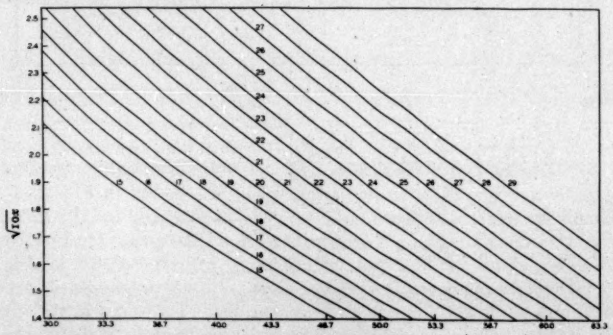


FIG. 4.

The value $W_0/C$ may be assumed to be a constant, for the sun is presumably a constant radiation source at 9.66 $\mu$. The measured value of $W_0$ is necessary to determine the absorption $A_r$ from the equation $A_r = (W_0 - W')/W_0$ and consequently in order that Fig. 3 may be applied. We have taken $W_0/C = 3.0$. Figure 4 is reconstructed from the data of Fig. 3 in terms of height rather than of total pressure, in order to facilitate the reduction of the measurement. Scales of Fig. 2

TABLE IV.

| Date. | Daily mean of $h$. | Daily mean of $x_0$. | Daily mean of $r_0$. |
|---|---|---|---|
| May 23, 1940 | 22.3 km. | 0.264 cm. | 2.26 cm. |
| 24 | 21.2 | 0.266 | 2.39 |
| June 4 | 21.3 | 0.251 | 1.29 |
| 5 | 20.4 | 0.271 | 1.02 |
| 6 | 20.7 | 0.266 | 0.90 |
| 11 | 22.2 | 0.264 | 0.91 |
| 12 | 21.4 | 0.258 | 1.02 |
| 13 | 23.2 | 0.264 | 1.09 |
| 14 | 22.7 | 0.255 | 0.70 |
| 15 | 21.9 | 0.236 | 0.54 |
| 19 | 22.2 | 0.236 | 0.96 |
| 20 | 23.1 | 0.254 | 0.84 |
| 25 | 23.6 | 0.253 | 1.31 |
| 26 | 21.6 | 0.257 | 0.71 |
| July 2 | 23.4 | 0.227 | 1.10 |
| 3 | 22.7 | 0.228 | 0.61 |
| 4 | 22.1 | 0.228 | 0.30 |
| 5 | 21.6 | 0.224 | 0.25 |
| 6 | 21.9 | 0.209 | 0.70 |
| 23 | 24.7 | 0.215 | 2.64 |
| 28 | 23.7 | 0.208 | 1.16 |
| 29 | 21.1 | 0.212 | 0.73 |
| 30 | 23.0 | 0.215 | 1.03 |
| 31 | 21.8 | 0.209 | 1.20 |
| Aug. 1 | 22.1 | 0.201 | 0.78 |
| 2 | 22.4 | 0.211 | 0.84 |
| 3 | 22.5 | 0.215 | 1.33 |
| 11 | 21.8 | 0.219 | 1.88 |
| 12 | 22.5 | 0.209 | 1.74 |
| 13 | 21.5 | 0.207 | 1.37 |
| Mean | 22.2 | 0.234 | 1.13 |

*Note:* Measurements in May were made in Pasadena; the others, at Palomar. We take $W_0/C = 3.0$.

and 4 are made identical so that heights can be read off by superposing the curves.

## RESULTS.

From the value of $W_0/C$ the temperature of the sun may be estimated. The values 3.0 and 3.2 give respectively 5100° and 5500° K. as the temperature of the sun.

In Table IV daily mean values of the ozone thickness overhead, of the thickness of water vapor overhead, and of the mean height of ozone

are summarized. Several daily observations are shown in Fig. 5 in terms of the hour angle. The ordinates of this figure are to be multiplied by $10^{-2}$ cm. for $x_0$, by $10^{-1}$ cm. for $\tau_0$, and 1 km. for $h$. Comparison of the result shown in Fig. 5 for July 23 with the preliminary result for the same date (Fig. 16, JS-I) shows how the correction of $\log R_0$ influenced the values of $h$ and $x_0$.

The seasonal mean value of the heights in Table IV would be about 2 km. lower if we had used $W_0/C = 3.2$ instead of $W_0/C = 3.0$; thus giving 20 km. as the mean height of atmospheric ozone. The "mean height" of our measurement is not exactly the height of the centroid

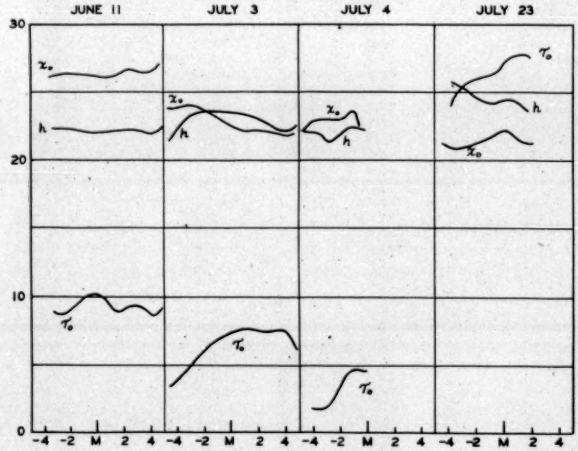


FIG. 5.

of the masses of ozone molecules in the atmosphere; we measure the height of the centroid of the $\pi$ band absorption. The height we obtain is, approximately,

$$h_{\text{mean}} = \frac{\int kP^{\frac{1}{2}}hd\sqrt{x}}{\int kP^{\frac{1}{2}}d\sqrt{x}}, \tag{4}$$

where $P$ is the total pressure at a given height and $x$ is the amount of ozone penetrated by the solar beam at the height $h$. Actually, our "mean height," as defined by Eq. 4, deviates but little from the heights observed by other methods—the magnitude depending on the ozone distribution.

## CONCLUSIONS.

There are several sources of errors and uncertainties in the new method of measuring the mean height of the atmospheric ozone. Several of these uncertainties, which are involved in the extrapolation of laboratory data to atmospheric conditions, have been noted;[2] and they are rather difficult to resolve. The errors in the observation itself, such as the measurement of $R$, $d_G$, $d\odot$, $\theta$, and $A_\Phi$ are estimated to amount to a combined error of less than 5 per cent. in the value of $h$. Uncertainties in the values of $\log R_0$, $W_0$, and $(\alpha' - \alpha)$ and the extrapolation necessary in using the data of Fig. 3 would influence the absolute value of $h$ to a much greater degree. The relative values of $h$ are probably quite reliable. The error in the value of $W_0$ affects the various values of $h$ approximately by the same amount.

The value of $W_0$ may possibly be as high as $3.2C$. We conclude this on the basis of a comparison of the curvature of our laboratory calibration curves with the definite curvature occurring almost invariably in the curves obtained from the atmospheric data. This higher value of $W_0$ yields 20 km. as the mean height of ozone for the summer of 1940 at Palomar. The uncertainty in $W_0$ may be avoided by measuring the contour of the $\pi$ band to determine $A_\pi$ directly as we obtain $A_\Phi$ from the contour of the $\Phi$ band.

The distinct advantage of the new method is that one height measurement can be made per half hour over the greater part of a day. By providing recording instruments, one person could manipulate the instruments and compute the height. Since our measurements of ozone height extend over a period of only three months in one locality, we are unfortunately not now in a position to correlate the mean height of atmospheric ozone with various meteorological factors; however, a more extensive survey may prove to be a worthwhile undertaking.

Here, I wish to express my gratitude to Dr. John Strong for his patient guidance and the privilege to collaborate with him in developing this method.

## ARMY AND NAVY NOTES.

**Ethyl Cellulose Production Doubled to Meet War Needs.**—(*Manufacturers Record*, Vol. 112, No. 9.) Production of ethyl cellulose, one of the newest and most important in the family of cellulose derivatives, has been doubled at the Hopewell, Va., plant where it is made in the world's largest chemical cotton plant. Because of its special properties, it has found wide application in war uses, with a postwar future that seems equally bright.

A rapidly developing and very important use for ethyl cellulose, due to high impact resistance, is in hot-melt plastics for making dies and jigs for forming tools for shaping aluminum. This process is very economical because the plastic is light in weight and can be remelted and recast in different molds. This saves time in change-over on design and also saves machining operations.

It is also used for coating insulating wires of airplane engines because, in addition to excellent electrical properties, it will not snap under frigid conditions of sub-zero stratosphere cold and quick temperature change. Extruded ethyl cellulose plastic is also being used in cable cores.

In addition, brightly colored squares of cloth used to identify Army ground equipment and prevent American planes from attacking their own troops are coated with ethyl cellulose. These patches of cloth, some of them only a few feet square, can be seen two miles up by fighter planes going at top speed.

The present uses for ethyl cellulose are strictly in line with its inherent properties. Where performance specifications have been set up for a thermoplastic material to meet the rigors of field operations in both freezing and tropic conditions, such as the Signal Corps flashlight and the QMC canteen, ethyl cellulose has out-performed the other materials submitted and has been used.

It has exceptional dimensional stability under troublesome weathering conditions, such as heat and humidity. It can resist the lowest freezing temperatures better than any known plastic and yet be formulated to stand temperatures as high as 175° F., and, in addition, it possesses remarkable impact strength.

These important properties are supplemented by other factors of almost equal importance. It has the lowest density of any of the cellulose products, meaning lighter weight and more pieces per pound. It has a wide range of compatibility with chemical plasticizers, vegetable and mineral oils, waxes and resins; this offers a multitude of combinations. These many modifiers can be selected for best heat stability, water insolubility, stability to light, hardness, flow, and other properties.

R. H. O.

# THEORY OF THE HALFTONE PROCESS. III. DOT SIZE AND HALFTONE DENSITY.

BY

J. A. C. YULE.

Communication No. 953 from the Kodak Research Laboratories.

SUMMARY.

The theoretical and experimental quantitative relationships between the dot diameter, dot area, and density of a halftone are given. Experimental results do not agree exactly with the theoretical relationships except for screen negatives and positives with sharp dots. For accurate rendering, highlight dots in a reproduction must increase extremely rapidly in size for small density increments in the highlights of an original. A "semi-dark-field" densitometer is described which eliminates the effect of dot fringe in measuring densities of screen positives. The relationship between density of screen positive and density of proof is briefly discussed.

---

## INTRODUCTION.

Although Part II of this series,[1] which deals with the diffraction of light behind a halftone screen, leaves much to be said on the subject of diffraction, the concluding section on diffraction requires experimental work which has been set aside for the present. Its publication must therefore be postponed until after the present paper, which is an extension, both theoretical and experimental, of Murray's [2] work on the relationship between dot diameter, dot area, density, ink spreading, and etching.

Since this paper was prepared, an article on the same subject by Dorst [3] has appeared. Although there is some duplication of Dorst's paper, with which we are in complete agreement, the present paper is believed to contain sufficient additional material to justify its publication.

The density of a uniform area of a halftone depends upon the density, area, and sharpness of the dots. The relationship between these factors, and also the influence of the shape of the dots, are important factors in investigations of the halftone process. A further study of this problem was also necessary as a preliminary to a paper on dot sharpness, which will be presented later in this series.

### HISTORICAL.

The relationship between halftone negative and positive and the ideal shape of the sensitometric curve for halftone negatives were described by Ives [4] and elaborated by Tritton and Wilson,[5] who emphasized the basic difference between this relationship and that of continuous-tone negatives and positives. Whereas with continuous-tone negatives and positives a logarithmic brightness relationship exists, a linear relationship is found in halftones.

In connection with contact screens, the ideal dot sizes for correct tone reproduction were described by Bekk,[6] Deville,[7] Tritton and Wilson,[8] and Ludlam.[9] Most of this work was restricted to square dots, and in all cases the use of a printing ink with infinite density was assumed. In some of these papers, the dot size calculations were combined with conclusions drawn from the penumbra theory of dot formation, which has since been shown to be untenable.[1]

For cases where the ink density is not infinite (that is, in all practical work), the relationship of dot area to integrated density was given by Davies [2] in the following formula:

$$D = \log \frac{1}{1 - a(1 - r)}, \qquad (1)$$

where $D$ = the integrated density,* $a$ = the fractional area occupied by the black dot, and $r$ = the reflecting power of the ink. This formula is strictly true only when the density is uniform throughout the dot area and zero in the remaining area. In the case of a screen negative with sharp, dense dots, where $r$ can be taken as zero, the formula reduces to:

$$D = \log \frac{1}{1 - a}. \qquad (2)$$

As pointed out by Davies, not only the contrast, but also the shape, of the tone-reproduction curve, depends on the ink density. A low ink density reduces the contrast in the shadows much more than in the highlights.

### DOT DIAMETER AND DOT AREA.

In examining a halftone with a magnifier, it is difficult to estimate directly the area of the dots. The obvious geometrical characteristics of a dot are its shape and diameter. First, it is necessary to clarify the relationship between dot diameter, area, and density.

It is possible to calculate the area of a rounded dot in terms of the average of the maximum and minimum diameters. However, this leads

* The term "integrated density," referring to the density of a halftone measured with the dots out of focus, is a convenient term, although rather misleading, since it is the reflectance rather than the density which is integrated.

to errors up to 11 per cent. in the area as the form of the dots approaches a square. Another method would be to work out a table giving areas in terms of maximum and minimum diameters. This method, although quite accurate, would not lend itself to graphical representation. The most practical method is to measure the dot diameter at 45 degrees to the screen ruling, express this as a fraction of the maximum possible diameter, and allow for departures from the normal dot shape in computing the area. The "diameter" of a square dot measured in this way is determined by the length of its sides, not its diagonal. Figure 1 illustrates the method of expressing dot diameter. According to this method, the diameter is always expressed as that of the black dot,

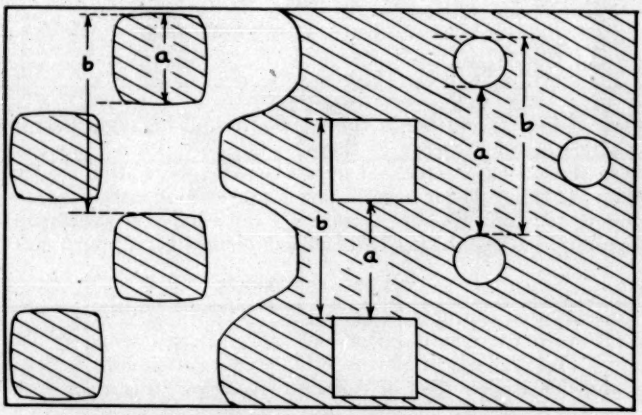


FIG. 1. Definition of dot diameter. Expressed as a fraction, the diameter is $a/b$, or expressed as a percentage, 100 $a/b$.

being equal to 1.0 minus that of the clear dot. The diameter and the area may be expressed either as a fraction or as a percentage, a checkerboard pattern having a dot diameter of 0.5 or 50 per cent.

The next step is to work out the relationship between dot diameter and dot area. The theoretical curves are given in Fig. 2 and Table 1 for dots of various shapes, ranging from round black dots (Curve *B*) through square dots (Curve *A*) to round clear openings (Curve *C*). Intermediate between these extremes lies Curve *D* ("standard" dot shape) which is a representative form of dot selected for use in the present calculations from the wide variety of shapes to be found in commercial halftones. The "standard" dot shapes are illustrated at

TABLE 1.

*Relationship of Dot Radius to Dot Area.*

| Relative Dot Diameter, per cent. | Dot Area, per cent. | | | |
|---|---|---|---|---|
| | Square Dots, per cent. | Round Black Dots, per cent. | Round Clear Dots, per cent. | Standard Dots, per cent. |
| 0 | 0 | 0 | 0 | 0 |
| 10 | 2.0 | 1.57 | — | 1.57 |
| 20 | 8.0 | 6.28 | — | 6.34 |
| 30 | 18.0 | 14.2 | 23.0 | 14.8 |
| 40 | 32.0 | 25.2 | 43.2 | 29.0 |
| 50 | 50.0 | 39.3 | 60.7 | 50.0 |
| 60 | 68.0 | 56.8 | 74.8 | 71.0 |
| 70 | 82.0 | 77.0 | 85.8 | 85.2 |
| 80 | 92.0 | — | 93.72 | 93.66 |
| 85 | 95.5 | — | 96.46 | 96.45 |
| 90 | 98.0 | — | 98.43 | 98.43 |
| 95 | 99.5 | — | 99.61 | 99.61 |
| 100 | 100 | — | 100 | 100 |

the top of Fig. 2, and are in the form of round highlight and shadow dots which become squarer as they get larger, to form a checkerboard pattern at 0.5 dot diameter. It should be remembered that this diagram represents a uniform increase of dot *diameter* (not integrated density) from left to right. This "standard" dot shape is satisfactory for lithography, but should not be regarded as ideal for all purposes.

### DOT AREA AND DENSITY.

The dot area can now be converted to density by means of Equation (1), with the results given in Figs. 3, 4, and 5 and in Table 2. Figure 3 and Table 2 show the calculated relationships between dot area and density for inks of different densities. Figure 4 shows the

TABLE 2.

*Relationship of Dot Diameter to Integrated Density.*

| Relative Dot Diameter, per cent. | Dot Area, per cent. | Integrated Density. | | | | |
|---|---|---|---|---|---|---|
| | | Max. = ∞, per cent. | Max. = 1.6, per cent. | Max. = 1.3, per cent. | Max. = 1.0, per cent. | Max. = 0.7, per cent. |
| 0 | 0 | 0 | 0 | 0 | 0 | 0 |
| 10 | 1.57 | .007 | .007 | .007 | .006 | .005 |
| 20 | 6.34 | .029 | .029 | .028 | .026 | .022 |
| 30 | 14.8 | .070 | .069 | .067 | .063 | .056 |
| 40 | 29.0 | .15 | .15 | .14 | .13 | .11 |
| 50 | 50.0 | .30 | .29 | .28 | .25 | .21 |
| 60 | 71.0 | .54 | .51 | .49 | .44 | .36 |
| 70 | 85.2 | .83 | .77 | .72 | .63 | .50 |
| 80 | 93.66 | 1.20 | 1.06 | .96 | .80 | .60 |
| 85 | 96.45 | 1.45 | 1.22 | 1.08 | .88 | .64 |
| 90 | 98.43 | 1.80 | 1.39 | 1.19 | .94 | .67 |
| 95 | 99.61 | 2.41 | 1.53 | 1.27 | .98 | .69 |
| 100 | 100 | ∞ | 1.6 | 1.3 | 1.0 | .7 |

same relationship, plotted in a different way. The solid ink density is joined to the upper left-hand corner of the chart by a straight line. The reflectance corresponding to a given dot area may then be read off at the left side of the chart, or the density along the right side. For instance, with an ink density of 1.3, a dot area of 84 per cent. should

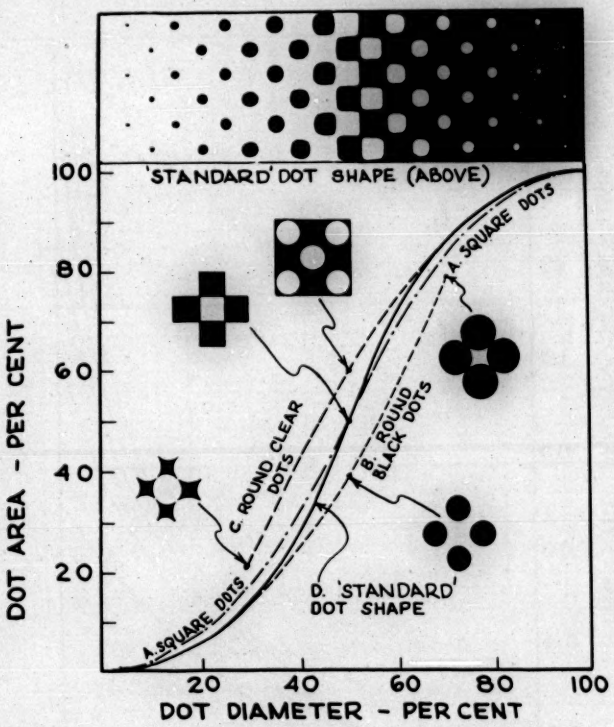


FIG. 2. Relationship of dot diameter to dot area, for dots of different shapes.

give a reflectance of 20 per cent. or a density of 0.7. With the "standard" dot shape, this dot area is seen, from Fig. 2, Curve *D*, to correspond to a dot diameter of 69 per cent. For the "standard" dot shape, Figs. 2 and 3 can be combined to give the relationship between dot diameter and density shown in Fig. 5*A*. If a scale of the density of the original were substituted for the dot diameter scale, the shape

of the curves in Fig. 5*A* would also represent the tone-reproduction curve that would be obtained if the dots increased uniformly, although such tone-reproduction curves are usually plotted the other way up, i.e., with the densities of the original as abscissas. These curves show

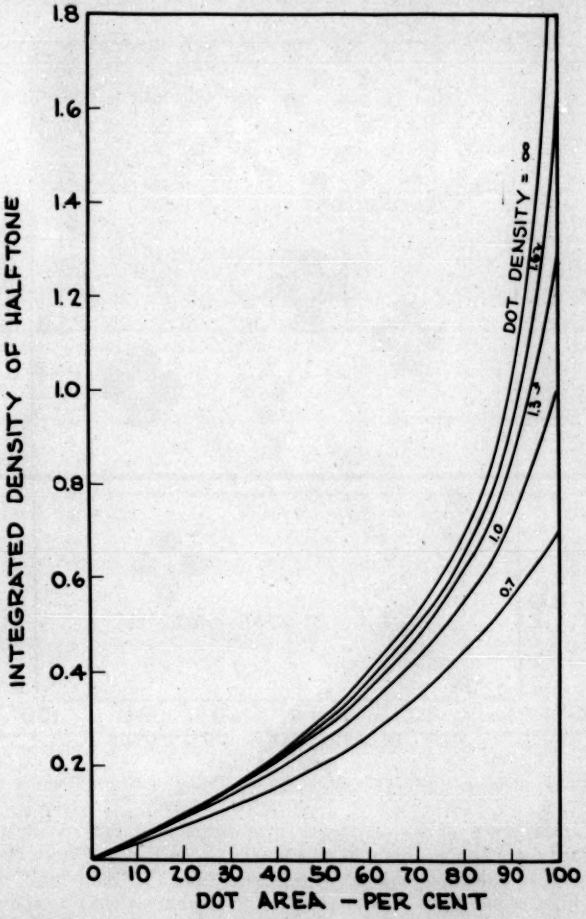


FIG. 3. Calculated relationship between dot area and integrated density with standard dot shape.

that if the dots increased in diameter by the same amount for each density step in the original, there would be an extreme flattening of the highlights, while the shadow contrast would depend on the dot density. This flattening of the highlights is seen by looking at the halftone scale at the top of Fig. 2, at such a distance that the individual dots are not clearly visible.

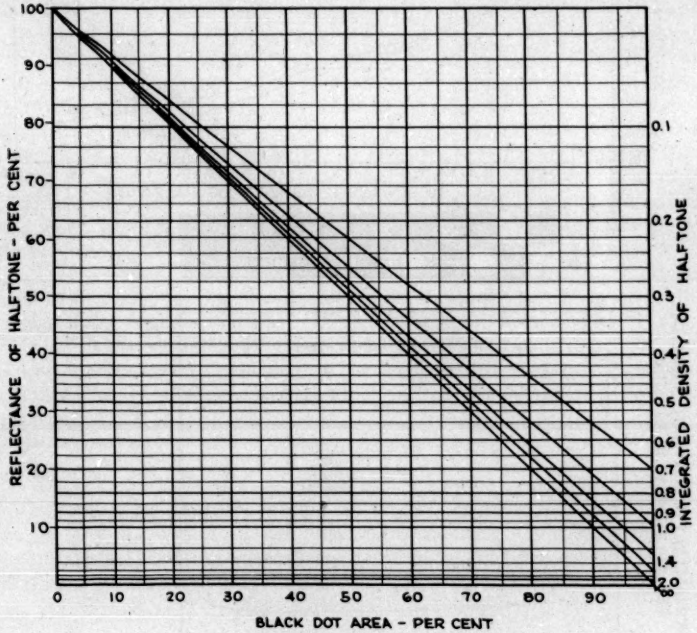


FIG. 4. Calculated relationship between dot area and integrated density and linear brightness scale.

Another feature which can be deduced from these curves is the dot structure which would be necessary to give straight-line density rendering. The dots themselves are represented in Fig. 5*B*, and the rate at which dot diameter should increase with equal density increments is given in Fig. 5*C*. It will be seen that for densities between 0.2 and 1.2, the density increases almost uniformly with dot diameter, but the small shadow dots and, to a still greater extent, the highlight dots, must increase much more rapidly to give the same density increment.

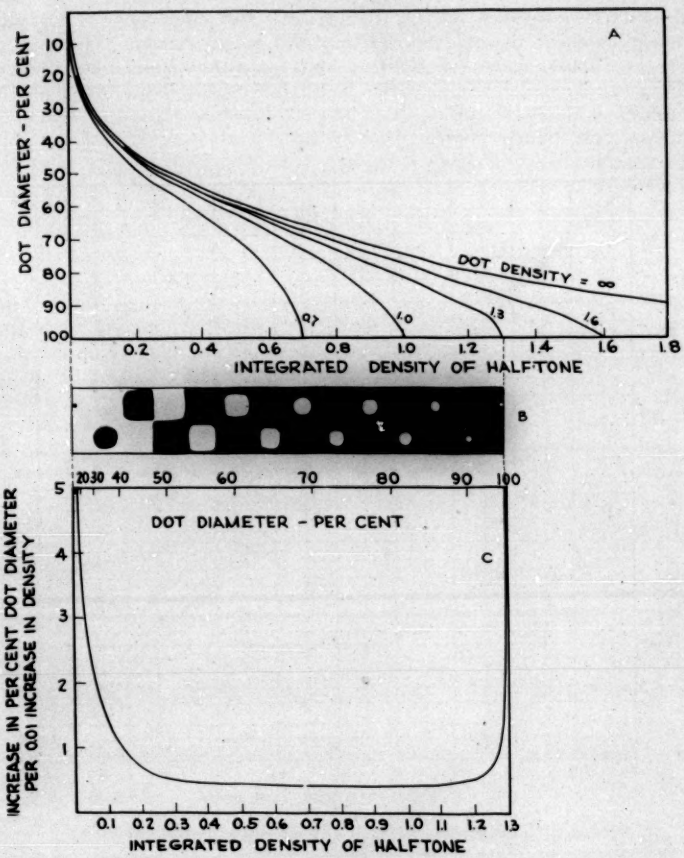


FIG. 5. *A*, calculated relationship of halftone density to dot diameter, with standard dot shape; *B*, dot structure required to give uniform increase of density, with ink density of 1.3; *C*, rate of increase of dot diameter with uniformly increasing density, with ink density of 1.3.

A dot diameter of 37 per cent. only gives a density of 0.1, and this is the reason for the well-known loss of contrast which usually occurs in the extreme highlights of halftones.

These curves have a very important bearing upon the practical knowledge of halftone work, and operators will therefore be well repaid

by a careful study of Fig. 5. It is easy to understand that a checkerboard pattern contains a fifty-fifty proportion of black to white, and it is easy and perfectly correct to deduce from this that such a formation is halfway up the scale of light absorption between white and black, so that it will reflect about half as much light as a clear undotted area. At the same time it is too easy to conclude incorrectly—and the reader or student is too often left to make the tacit assumption—that this so-called 50 per cent. dot, checkerboard dot, or "halftone" is the middle point in a uniform scale of values of gray. It is necessary to remember that a fifty per cent. absorption is far from being half as "dark" as a black ink. The key to this discrepancy lies, of course, in the fact that the visual impression of "darkness" or "value" corresponds approximately to the optical density, which is a logarithmic function of the per cent. reflection or absorption. Figure 4 shows that the 50 per cent. or the checkerboard dot is indeed halfway up the scale of absorption, but Fig. 3 or Fig. 5*A* shows that, with a black ink which has a density of 1.3, it is only about *one-fifth* of the way up the scale of density.

These curves are not included here to encourage the halftone operator to try to compute density from estimates or even measurements of dot area or diameter. It is usually much easier and more accurate to read the densities directly on a halftone-integrating densitometer. These curves are drawn merely to explain the causes of various peculiarities of tone rendering which are observed in the halftone process.

### EXPERIMENTAL RELATIONSHIP BETWEEN AREA AND DENSITY.

The relationships just discussed are entirely theoretical, being derived from Equation (1) which, as stated, is based on assumptions which are not usually strictly true in practice. The experimental relationships were determined by measuring the dot diameters and densities in halftone gray scales. The measurements were made at

TABLE 3.

*Comparison of Calculated and Observed Densities in Halftone Positive with Very Sharp, Dense Dots.*

| Dot Area, per cent. | Observed Density. | Density Calculated from Dot Area. | Error. |
|---|---|---|---|
| 12 | 0.05 | 0.06 | +.01 |
| 27.6 | 0.11 | 0.14 | +.03 |
| 48.4 | 0.19 | 0.21 | +.02 |
| 53.7 | 0.30 | 0.33 | +.03 |
| 69.9 | 0.53 | 0.52 | −.01 |
| 80.5 | 0.73 | 0.71 | −.02 |
| 88.6 | 0.93 | 0.94 | +.01 |
| 93.8 | 1.21 | 1.21 | 0 |
| 98.3 | 1.75 | 1.77 | +.02 |

100x magnification with a micrometer eyepiece, the average of four dots being taken except in the case of extremely small dots, whose dot size was very variable. In this case, the root-mean-square diameter of about 20 dots was determined.

Dot sizes were then converted to areas by means of Fig. 2. The actual observed dot shapes were used in this conversion, since in a few cases density errors up to 0.05 would have been introduced by the assumption that dot shape was standard. In a screen positive having extremely sharp dense dots, the densities calculated from the dot areas

TABLE 4.

*Reduction of Densities of Screen Positives to Maximum of 1.3.*

Example: Density of 1.73 in positive would be only 1.16 if dot density were 1.3.

| | 0 | .01 | .02 | .03 | .04 | .05 | .06 | .07 | .08 | .09 |
|---|---|---|---|---|---|---|---|---|---|---|
| 0.0 | 0 | .01 | .02 | .03 | .04 | .05 | .06 | .06 | .07 | .08 |
| 0.1 | .09 | .10 | .11 | .12 | .13 | .14 | .15 | .16 | .17 | .18 |
| 0.2 | .18 | .19 | .20 | .21 | .22 | .23 | .24 | .25 | .26 | .27 |
| 0.3 | .28 | .29 | .30 | .30 | .31 | .32 | .33 | .34 | .35 | .36 |
| 0.4 | .36 | .37 | .38 | .39 | .40 | .41 | .42 | .43 | .44 | .44 |
| 0.5 | .45 | .46 | .47 | .48 | .49 | .49 | .50 | .51 | .52 | .53 |
| 0.6 | .54 | .55 | .55 | .56 | .57 | .58 | .59 | .59 | .60 | .61 |
| 0.7 | .62 | .62 | .63 | .64 | .65 | .66 | .67 | .67 | .68 | .69 |
| 0.8 | .70 | .70 | .71 | .72 | .73 | .73 | .74 | .75 | .76 | .77 |
| 0.9 | .77 | .78 | .78 | .79 | .80 | .81 | .82 | .82 | .82 | .83 |
| 1.0 | .84 | .84 | .85 | .85 | .86 | .86 | .87 | .88 | .88 | .89 |
| 1.1 | .90 | .90 | .91 | .92 | .92 | .93 | .93 | .94 | .94 | .95 |
| 1.2 | .95 | .96 | .97 | .97 | .97 | .98 | .99 | .99 | 1.00 | 1.00 |
| 1.3 | 1.01 | 1.01 | 1.02 | 1.02 | 1.02 | 1.03 | 1.03 | 1.04 | 1.04 | 1.05 |
| 1.4 | 1.05 | 1.06 | 1.06 | 1.07 | 1.07 | 1.08 | 1.08 | 1.08 | 1.09 | 1.09 |
| 1.5 | 1.09 | 1.10 | 1.10 | 1.10 | 1.11 | 1.11 | 1.11 | 1.12 | 1.12 | 1.12 |
| 1.6 | 1.13 | 1.13 | 1.13 | 1.13 | 1.14 | 1.15 | 1.15 | 1.15 | 1.15 | 1.16 |
| 1.7 | 1.16 | 1.16 | 1.16 | 1.16 | 1.17 | 1.17 | 1.17 | 1.17 | 1.18 | 1.18 |
| 1.8 | 1.18 | 1.19 | 1.19 | 1.19 | 1.20 | 1.20 | 1.20 | 1.21 | 1.21 | 1.21 |
| 1.9 | 1.21 | 1.21 | 1.22 | 1.22 | 1.22 | 1.22 | 1.22 | 1.22 | 1.22 | 1.23 |
| 2.0 | 1.23 | 1.23 | 1.23 | 1.23 | 1.23 | 1.23 | 1.23 | 1.24 | 1.24 | 1.24 |
| 2.1 | 1.24 | 1.25 | 1.25 | 1.25 | 1.25 | 1.25 | 1.25 | 1.25 | 1.25 | 1.25 |
| 2.2 | 1.26 | 1.26 | 1.26 | 1.26 | 1.26 | 1.26 | 1.26 | 1.26 | 1.26 | 1.26 |
| 2.3 | 1.26 | 1.26 | 1.26 | 1.26 | 1.26 | 1.27 | 1.27 | 1.27 | 1.27 | 1.27 |
| 2.4 | 1.27 | 1.27 | 1.27 | 1.27 | 1.27 | 1.27 | 1.28 | 1.28 | 1.28 | 1.28 |
| 2.5 | 1.28 | 1.28 | 1.28 | 1.28 | 1.28 | 1.28 | 1.28 | 1.28 | 1.28 | 1.28 |
| 2.6 | 1.29 | 1.29 | 1.29 | 1.29 | 1.29 | 1.29 | 1.29 | 1.29 | 1.29 | 1.29 |
| 2.7 | 1.29 | 1.29 | 1.29 | 1.29 | 1.29 | 1.29 | 1.29 | 1.29 | 1.29 | 1.29 |
| 2.8 | 1.29 | 1.29 | 1.29 | 1.29 | 1.30 | 1.30 | 1.30 | 1.30 | 1.30 | 1.30 |
| 2.9 | 1.30 | | | | | | | | | |

agreed well (see Table 3) with the observed densities. However, in the case of proofs on paper (Fig. 6), the measured density was appreciably higher than the calculated value in the low and medium densities, the difference amounting to 0.11 in one case. This cannot be caused by variations in the ink density, since, in several cases, the densities were higher than should be produced even if the ink density were infinite—for instance, a checkerboard pattern gave a density higher than 0.3. This can only be accounted for by assuming that the density of the white paper is higher in the neighborhood of the printed dots.

Possibly the vehicle spreads, or the dots cause a slight shadow within the paper.

Another discrepancy is noted in the high densities. Where the printing plate has small shadow dots which fill up in printing owing to ink spreading, the density is often lower than where the printing plate

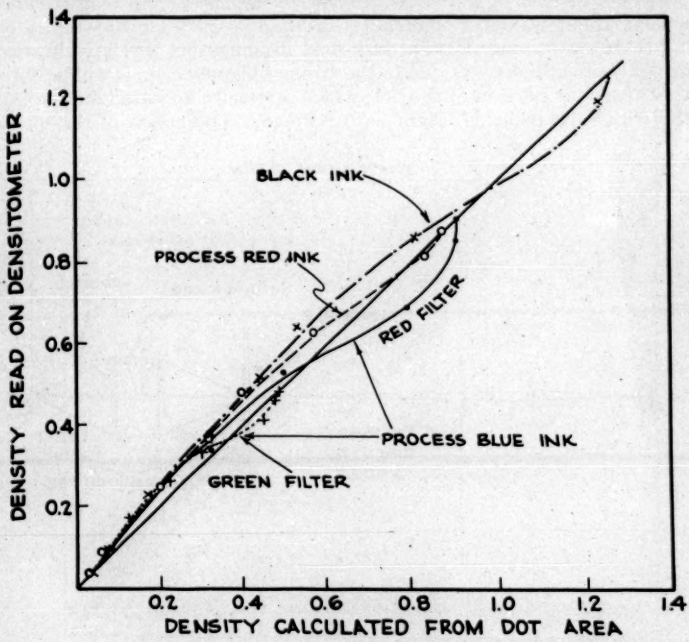


FIG. 6. Calculated *vs.* observed densities, in proofs on coated paper.

is solid, i.e., devoid of dots. The explanation of this peculiar effect, which is bound up with the physics of ink transfer, is not clear.

### EFFECT OF "FRINGE" ON THE DOTS.

These density measurements on screen positives were made on a screen positive whose dots were extremely sharp, without any obvious low-density fringe. The effect of this fringe in increasing the density beyond that corresponding to the effective size of the dot has been shown by Tritton.[5] In inspecting the dots of a screen negative with a hand magnifier, it is common practice to use both bright- and dark-

field illumination. The latter shows the dot fringe as a white ring surrounding the black core of the dot. This is caused by the fact that, in this type of illumination, the light-scattering power of the silver grains predominates over the absorbing power. It is now possible to extend this method to actual measurements of the densities of screen positives, instead of mere examination, by means of what may be called a semi-dark-field densitometer.

If, in examining dots in dark-field illumination, a relatively weak direct beam of light is added to the strong oblique beam, it will be noted that the clear portion of the dot, which originally appeared darker than the fringe, becomes as bright as the fringe. The action of the special

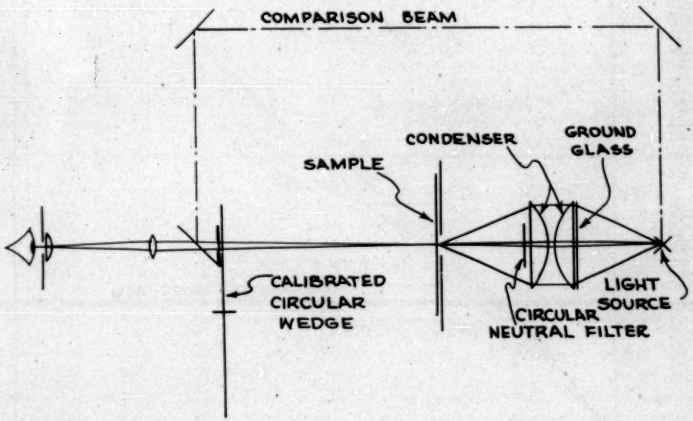


FIG. 7. Optical system of semi-dark-field densitometer.

densitometer may perhaps be more readily understood by proceeding in the opposite direction. In bright-field illumination, the dot fringe appears darker than the clear openings. If strong oblique (dark-field) illumination is added, the dot fringe becomes lighter until it equals the openings in brightness. A densitometer was constructed with this form of illumination (Fig. 7), and it was found that with this instrument the density readings are not affected by the useless fringe of the dot and correspond to actual effective dot sizes except perhaps in the extreme shadows.

As in the Eastman T. and R. densitometer, the light from a small area of the sample is integrated by imaging it on the pupil of the eye (see Fig. 7). In order to see the photometric comparison field clearly, the latter is imaged on the retina of the eye. The illumination system

consists of a light source imaged on the sample by means of a condenser, the central rays being partially cut off by a circular neutral gray filter. Since the photometric wedge is specularly illuminated, it must be calibrated for this type of illumination.

Results obtained with this type of densitometer are shown in Fig. 8. A screen positive whose dots were only moderately sharp was used, and a duplicate positive on high-contrast film was made from this by

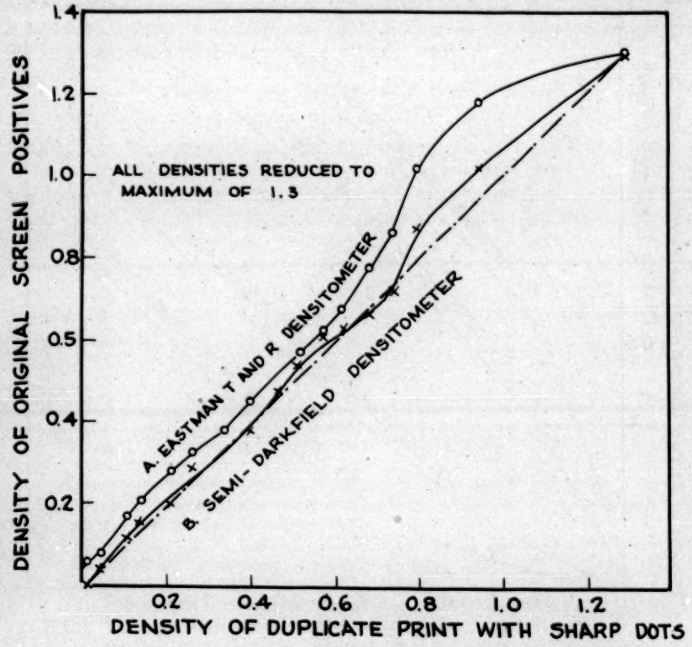


FIG. 8. Halftone densities measured with semi-dark-field densitometer.

contact printing. As regards printing down onto metal, the effective sizes of the dots in the original and in the duplicate were identical. However, on an ordinary densitometer (Curve *A*, Fig. 8), the original had higher densities than the duplicate, owing to the fringe on the dots. The densities of the original were also read on the semi-dark-field densitometer; they checked fairly well with the duplicate, representing a great improvement over the ordinary densitometer readings. For example, the first step consisted of dots too low in density to be recorded

in a printing down onto metal. With the ordinary integrating densitometer, this step read 0.06; with semi-dark-field illumination, however, these dots disappeared, giving a reading of zero. The densities were all corrected to a maximum dot density of 1.3, as explained later, to avoid exaggeration of errors at high densities, and the fog density was subtracted from all readings. The greater spread of the semi-dark-field

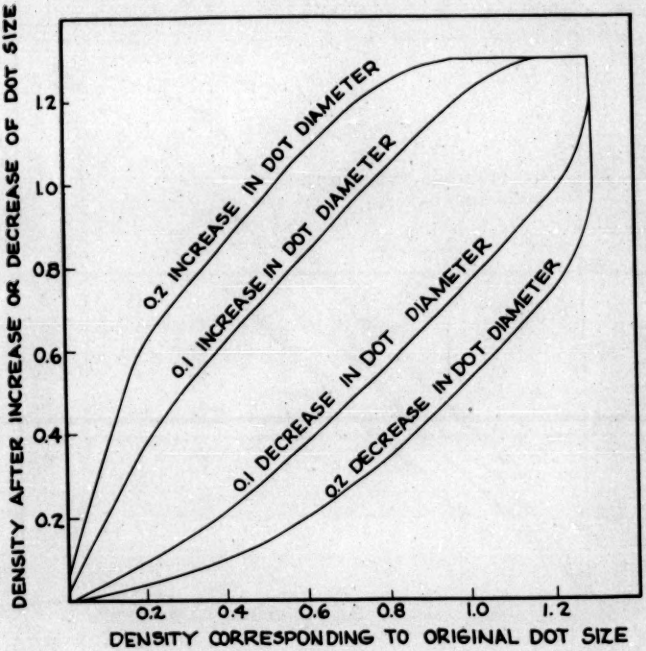


FIG. 9. Theoretical effect of a uniform increase or decrease of dot diameter caused by etching or ink spreading.

readings is probably caused by the use of a crude temporary apparatus which did not give as high precision as the T. and R. densitometer.

Such an instrument would only be of value for screen positives and the highlights of screen negatives. In the shadows of screen negatives, the smallest measurable density difference represents such a large density difference in the final proof that the results are too inaccurate to be of practical significance.

V.2
194

### CORRECTION FOR MAXIMUM INK DENSITY.

Density readings made on screen positives (and even on screen negatives, except in the shadows) with this type of densitometer are of more value than ordinary density measurements. However, there are two more factors to be considered. The first is the fact that printing inks have lower densities than screen positive dots. To allow for this, a conversion table (Table 4) has been worked out from Equation (1) which gives the density which a proof in ink of density 1.30 should have if its dots duplicate the size of the dots in the screen positive, whose density may be taken as infinity without serious error.

### DISTORTION OF VALUES IN THE PRINTING PROCESS.

The second factor is the distortion of tone reproduction, caused mainly by a change in dot size, that occurs in plate-making and proving. Dots are reduced in size by etching and increased in size by ink spreading,[2] and not necessarily uniformly over the entire scale. The calculated effect of uniform increase or decrease of dot size throughout the scale is shown in Fig. 9. The actual relationship between density of screen positive and density of proof will be the subject of a subsequent paper, but it may be stated here that the curves of Fig. 9 are quite similar to the actual effects of etching in photoengraving and of ink spreading in lithography.

### REFERENCES.

1. J. A. C. YULE. "The Theory of the Halftone Process," Parts 1 and 2. J. FRANKLIN INST., 231, 23–28 (1941); 235, 483–498 (1943).
2. A. MURRAY. "Monochrome Reproduction in Photoengraving." J. FRANKLIN INST., 221, 721–744 (June, 1936).
3. P. W. DORST. "Halftone Densities." *J. Opt. Soc. Am.*, 33, 436–439 (August, 1943).
4. H. E. IVES. "Tone Reproduction in the 'Halftone' Photo-Engraving Process." *J. Opt. Soc. Am.*, 13, 536–552 (November, 1926).
5. F. J. TRITTON AND E. T. WILSON. "Tone Rendering by Transparent Screen Negatives and Positives." *Phot. J.*, 79, 396–405 (June, 1939).
6. J. BEKK. "Der gegenwärtige Stand der Rasterphotographie." *Ber. VIII Intern. Kongress wiss. Photographie*, Dresden, pp. 320–334 (1931). *Deutscher Drucker*, 37, 605–606, 677–679 (August and September, 1931).
7. E. E. DEVILLE. "The Theory of the Screen in the Photomechanical Process." *Trans. Roy. Soc. Canada, Sect. 3*, 29–61 (1895). *Practical Process Worker & Photomechanical Printer*, I, 38, 45–49 (July, 1896).
8. F. J. TRITTON AND E. T. WILSON. "Tone Rendering by Vignetted or Contact Screens." *Phot. J.*, 80, 65–71 (March, 1940).
9. E. M. LUDLAM. "Basic Factors in Reproduction of Tone Values." *Modern Lithography*, 9, 23–26 (August, 1941).

## ARMY AND NAVY NOTES.

**New Amphibious Truck is the Army's Most Versatile Vehicle.**—(*Engineering News Record*, Vol. 131, No. 9.) Amphibious action is playing an ever increasing part in World War II and the 2½ ton amphibian truck, now in volume production at General Motors truck and coach factories, is giving American armies a growing advantage over the Axis. In the water, it has all the qualities of a large landing boat, plus the ability to keep going when it reaches shoals and shore line. On land, it performs like an army truck, plus the ability to swim lakes and streams.

Carrying cargoes from ocean freighters to inland supply depots; establishing beachheads and bridgeheads; unloading ships where no harbor facilities are available; aiding in reconnaisance work where no roads or bridges exist; carrying or pulling cannon and howitzers; transporting scores of troops or tons of equipment—these are all in a day's work for this sturdy, seagoing truck.

Christened "The Duck" by the workmen on the assembly line it has the same qualities on or off the road that distinguish military trucks, while in addition it has the ability to run in and out of water of any depth. True to its name, it is as much at home on water as on land.

Military regulations prevent the disclosure of many of "The Duck's" detailed specifications, but it can be revealed that the boat-like body is mounted on the standard 6 wheel drive chassis, about the same as is furnished the Army for the basic 2½ ton military transport vehicle.

A water-tight steel hull encases the truck frame assembly, below which are mounted the springs, spring brackets, and wheels, thus making the unit a motorized boat on wheels.

On land the unit can be driven through all six wheels. In the water, it is driven by a rear-mounted water propeller. The axle and water propeller shafts pierce the hull through sealed tubes. The steering gear is connected to the rudder, so that the steering wheel guides the vehicle in water. The water propeller thrust is augmented, when desired, by the driving wheels. Thus, the driver can shift control to provide a land or water drive as needed.

The amphibian can readily surmount ordinary difficulties without loss in speed or maneuverability. Where bridgeheads must be forced, the amphibian truck enables a foothold to be established and the waterway to be bridged for the transporting of troops, material and the usual cargo of an invading force. It can also be used in transporting troops and equipment quickly across marshes or rivers.

R. H. O.

## NOTES FROM THE NATIONAL BUREAU OF STANDARDS.*

### REHABILITATION PROGRAM OF HOROLOGICAL INSTITUTE.

A meeting was held at the Chamber of Commerce of the State of New York, 65 Liberty St., New York, on August 26 to discuss the rehabilitation of war veterans in the field of watchmaking. This was a preliminary meeting looking toward the adoption of a definite program of coöperation between the Horological Institute of America, the horological schools, the State educational boards, the manufacturers of watches, and the Veterans Administration.

Edward H. Hufnagel, Mt. Vernon, N. Y., treasurer of the Horological Institute, served as chairman of the meeting. The Bureau was represented by Ralph E. Gould, chief of the time section, and secretary of the Institute.

The meeting was opened by Mr. Hufnagel who reviewed the conditions leading to the foundation of the Institute in 1921 by the National Research Council and described its objects and the progress it has made. Mr. Gould told of the coöperation existing between the Institute and the Bureau, explained the plan of certifying watchmakers which has been in operation for 22 years, and described the procedure followed in conducting these examinations.

The work of the Institute's educational committee was discussed by the committee's chairman, John J. Bowman, director of the Bowman Technical School. Howard L. Beehler, president of the Institute, outlined the rehabilitation program and explained in considerable detail a proposed course of instruction which would give disabled soldiers, interested in watch repairing, the necessary technical education.

Following these statements by Institute members, William A. Gilchrist of the Veterans Administration described the needs and plans of the Administration in selecting and placing men in various approved schools. While no funds are available for preliminary development, he said that the schools which met the standards would receive tuition payment for each man placed. He stated, as his opinion, that it would be about two years before actual placement started, as the men first would have to be rehabilitated physically.

John W. Iseman, of the New York State Education Department, told of the course already established at Morrisville and the proposed introduction of a horological course in the National Technical Institute in New York City.

Discussion of ways and means for financing the project led to offers of assistance from American watch manufacturers, provided that

* Communicated by the Director.

jewelers and watchmakers would likewise help. This would lead to the establishment of a fund in the Horological Institute for the prepration of a text book and educational material to be used in the proposed instruction courses.

The need for more trained watch repairers is very great, the present supply and the annual number of graduates from the horological schools being far short of the demand. Many men trained as watch repairers have gone into instrument repair work and other mechanical occupations, or are serving in the armed forces, thus still further reducing the number of available trained men to care for the public's watches. It is hoped that through the coöperation of the various groups and an adequate program of instruction the number of trained men will be substantially increased, and that many partially disabled veterans will be furnished a means of earning a living at an honorable trade.

---

### RAILWAY TRACK SCALE TESTING SERVICE TO BE CURTAILED.

A major change has been made in the scope of the Bureau's railway track scale testing service. A number of considerations, some legalistic, others fiscal, were responsible for this decision, which has resulted in a curtailment of the field work. On September 1, when the itinerary of Testing Equipment No. 2 was completed, this equipment was laid up at the Master Scale Depot in Chicago. Equipment No. 1 alone is being operated under a plan the details of which have been worked out with the Association of American Railroads. This is based primarily upon a continuance by the Bureau of its fundamental service of calibrating master railway track scales. Mr. David V. Smith is carrying on this work with Equipment No. 1. Mr. H. Haig Russell, who has had charge of the equipment for many years, has been assigned to duty in the Weights and Measures Division of the Bureau at Washington.

V.2
194

---

### LUMINOUS EFFICIENCY OF RADIANT ENERGY FROM THE SKY.

In order to supply information requested, the Bureau has reduced and compared available data in the literature on the luminous efficiency of radiant energy from the blue sky. The best estimate which can be made is 100 lumens per watt. This estimate is based upon Moon's compilation of radiometric data for the sun (Parry Moon, "Proposed Standard Solar-Radiation Curves for Engineering Use," *J. Franklin Inst.*, **230**, 583; 1940) combined with the Rayleigh law of scattering which has been shown by Fowle (F. E. Fowle, "The Atmospheric Scattering of Light," *Smithsonian Misc. Coll.*, **69**, No. 3; 1918) to apply to scattering of radiant energy by dry, dust-free air. From this law the luminous efficiency of the radiant energy scattered in the upper atmosphere is found to be 90.2 lumens per watt.

By penetration to the earth's surface this energy is changed in spectral distribution so as to be more efficient in yielding light. The amount of this change is estimated by comparison with results computed by Moon for the unscattered solar energy (Tables IV and V) which indicate the following luminous efficiencies:

| Air mass. | Luminous efficiency of sunlight. Lumens per watt. |
|---|---|
| 0 | 93.3 |
| 1 | 106 |
| 2 | 106 |
| 3 | 103 |
| 4 | 98.4 |
| 5 | 93.1 |

It is seen that as the sun's energy penetrates the atmosphere its luminous efficiency increases. Similarly it is to be expected that the luminous efficiency of scattered radiant energy would increase from this cause and would vary between 90 and 106 lumens per watt depending upon the dust and water-vapor content of the atmosphere. The round number, 100 lumens per watt, may well be representative of a typical cloud-free sky.

These estimates are fairly consistent with 138 measurements made by Kimball (*Monthly Weather Rev.*, **52**, 479; 1934) in Washington during the spring and summer of 1924 which indicate the following luminous efficiencies of radiant energy from the sun and from the sun and sky incident on a horizontal surface:

| Air mass. | Luminous efficiency. Sun. Lumens per watt. | Sun plus Sky. Lumens per watt. |
|---|---|---|
| 1.1 | 109 | 108 |
| 1.5 | 106 | 104 |
| 2.0 | 104 | 100 |
| 2.5 | 103 | 98 |
| 3.0 | 102 | 97 |
| 3.5 | 101 | 96 |
| 4.0 | 100 | 96 |
| 4.5 | 99 | 96 |
| 5.0 | 98 | 96 |

## ADHESIVENESS OF GUMMED PAPER TAPE.

The Technical Association of the Pulp and Paper Industry has adopted a method for testing the adhesiveness of gummed paper tape used for sealing fiber containers, in which the Harnden-McLaurin machine is specified as the standard testing apparatus.

Investigation at the Bureau, in coöperation with a technical committee of the Gummed Industries Association, showed that if the apparatus complied with the TAPPI specification, it would serve the purpose satisfactorily.

The testing machine has two pivoted tables placed side by side with the adjacent parallel edges free to move in an arc when the force of a heavy pendulum is applied. The action of the tables simulates that of the closed flaps of a fiber-board shipping case after the pressure on them has been removed, allowing them to spring back to a partially open position. In making a test, a piece of kraft paper is fastened over the tables and is slit above the space between them. A piece of the gummed tape is fed from a roll over a moistening device, cut to the proper size, pressed over the slit in the kraft paper, and the tables are then tilted apart by releasing the pendulum. The resistance of the gum of the tape to the swing of the pendulum is indicated on a suitable scale. The method was described in the June 17, 1943, issue of *Paper Trade Journal.*

---

### FRICTION METER FOR FABRICS.

The consumer of fabrics is interested in their smoothness, "sheen," "creep," and wear—characteristics that are associated with a fabric's frictional properties. New fibers and improved finishing agents developed for the production of fabrics more acceptable to the consumer require adequate means for evaluating their effectiveness. Accordingly, the American Society for Testing Materials and the Bureau, with the support of the textile industry, undertook to develop quantitative test methods and instruments for evaluating fabric finishes. One of these instruments, designed by Edwin C. Dreby, research associate of the ASTM, is a friction meter for evaluating the coefficient of friction, a characteristic important in the "feel" of fabrics.

The coefficient of friction between the surfaces of two fabrics is a measure of resistance to slippage, a characteristic that is readily appreciated with the hands.

The friction meter combines ruggedness, sensitivity, and ease of operation—requirements which must be met by any instrument intended for routine textile testing. It can be used to determine the coefficients of friction of a wide variety of fabrics, to evaluate finishing agents, and to control processing with respect to the frictional characteristics of fabrics. A detailed description will be published in the October *Journal of Research.*

---

### STRUCTURE OF THE WOOL FIBER AS REVEALED BY THE ELECTRON MICROSCOPE.

Wool fibers are not simple homogeneous structures but are made up of various parts and layers which become apparent under suitable conditions of observation. Thus, a growing wool hair is found to consist of a bulbous root situated below the surface of the skin, and a

filamentous shaft which extends above the skin surface. The shaft, in turn, is made up of dead cellular units which are arranged in three layers—an outer layer of scales (cuticle), a middle region called the cortex, and a central core or medulla. The medulla, which in the finest grades of wool is either very narrow or absent altogether, is not believed to contribute appreciably to the mechanical properties on which the usefulness of wool depends. Accordingly, attention has been directed largely to an understanding of the structure of the scale and cortical cells. The former are restricted to a thin layer which constitutes the outer surface of the fiber, whereas the latter, either in the form of a hollow or solid cylinder, depending on medullation, make up the bulk of the fiber.

The principal chemical constituent of wool is keratin, a protein consisting essentially of long polypeptide chains connected laterally by disulfide cross-linkages. Although both the cuticle and cortex appear to belong to this same general class of proteins, there is, nevertheless, evidence from studies with the optical microscope, and from a consideration of the behavior of these layers in swelling media, in dyes, and in other reagents, that there are certain differences between them. Since the dissimilarities in chemical composition of the cuticle and cortex are slight, it seems probable that the differences in behavior of these two regions may depend more on physical than on chemical properties. Accordingly, an investigation was undertaken by Charles W. Hock and Howard F. McMurdie to see whether differences in structure between the cuticle and cortex could be observed with the electron microscope—an instrument which, under suitable conditions, can resolve details of the order of magnitude of only one six millionth of an inch.

As reported in the October *Journal of Research* it was found that the cortical cells always showed a distinctly fibrous structure. Whereas with the optical microscope only fibrils were observed within the cortical cells, the higher resolving power of the electron microscope made possible the resolution of still finer microfibrils. The scale cells, on the other hand, showed little internal organization. This difference between the fibrous structure of the cortex and the non-fibrous or amorphous structure of the cuticle may be of fundamental importance in interpreting many of the properties of the fiber.

---

### PURIFICATION, ASSAYING, AND ULTRAVIOLET ABSORPTION SPECTRUM OF POTASSIUM *p*-PHENOLSULFONATE.

The test and control of the pH (acidity or alkalinity) of mildly alkaline solutions, such as boiler waters, require the use of chemicals called buffers or acidity regulators. At present, borates and secondary phosphates are used, but these do not cover completely the important

pH range, 7 to 10. Potassium *p*-phenolsulfonate is a good buffer for the pH range of 8.4 to 9.2, and for spectrophotometric pH work with certain indicators. Since the purified product is not commercially available and since quantitative tests for indicating its purity have not been reported, an investigation covering the purification, assaying, and ultraviolet absorption spectra of potassium *p*-phenolsulfonate was undertaken by Elizabeth E. Sager, Marjorie R. Schooley, and S. F. Acree at the Bureau. Several recrystallizations from water of a commercial product gave a pure compound. A quantitative method of analysis by bromometric titration was developed, and it was found that two molecules of bromine react quantitatively with one molecule of *p*-phenolsulfonate in molar hydrochloric acid at 0° C. within 5 minutes.

Ultraviolet absorption spectra were obtained for the impure compound and for the successive portions of the material subjected to six recrystallization steps. The spectrophotometric data agreed with the results of bromine analyses. The spectrophotometric curves obtained for the secondary salt of the *p*-phenolsulfonate are quite different from those for the primary salt. The absorption spectra of the compound in water and in diluted hydrochloric acid indicate that the sulfonate group is almost completely ionized.

The detailed report on this work will be published in the October *Journal of Research.*

V.2
194

---

### X-RAY PATTERNS OF HYDRATED CALCIUM SILICATES.

A paper entitled, "Formation of Hydrated Calcium Silicates at Elevated Temperatures and Pressures," by E. P. Flint, H. F. McMurdie, and L. S. Wells was published in *J. Research NBS*, **21**, 617 (1938), RP1147. In that study various hydrated calcium silicates were formed by hydrothermal action. These were identified by X-ray powder patterns. The patterns made at that time were not sharp and accurate enough to justify publishing the data from them.

The X-ray powder patterns have been remade by H. F. McMurdie and E. P. Flint on more modern equipment and the powder diffraction data on the following compounds are given in the October number of the *Journal of Research:* $CaO.2SiO_2.2H_2O$, $2CaO.3SiO_2.2H_2O$, $4CaO.5SiO_2.5H_2O$, $5CaO.5SiO_2.H_2O$, $CaO.SiO_2.H_2O$, $2CaO.2SiO_2.3H_2O$, $3CaO.2SiO_2.1.5H_2O$, $3CaO.2SiO_2.3H_2O$, $5CaO.3SiO_2.3H_2O$, $2CaO.SiO_2.H_2O$, $2CaO.SiO_2.H_2O$ (second crystalline form), $10CaO.5SiO_2.6H_2O$, $6CaO.3SiO_2.2H_2O$, $3CaO.SiO_2.2H_2O$.

These data may be useful to those working on boiler scale, sand-lime brick, and the hydration of portland cement.

# THE FRANKLIN INSTITUTE.

## STATED MONTHLY MEETING, OCTOBER 20, 1943.

The members of The Franklin Institute met after their summer recess at a stated monthly meeting in the Hall of the Institute at 8:15 P.M., Wednesday, October 20.

The meeting was called to order by the President, Mr. Charles S. Redding. All stood at attention during the playing of the National Anthem.

The Chairman announced that the minutes of the last meeting had been printed in full in the June issue of the JOURNAL of the Institute and that, unless objection were raised, they would be declared approved as printed. They were so approved.

The Secretary of the Institute, Dr. Henry Butler Allen, was then asked for his report.

He reported that increases in membership continue at a gratifying rate and stated that since the meeting in May nineteen new members in the Sustaining Membership category had been added, making a total of forty-nine; four hundred and ninety-three active, totaling three thousand and forty-seven; one hundred and seventy-seven Associates, totaling one thousand, seven hundred and thirty-two; and seventy-eight new Student members, making that total six hundred and twenty-four. These, together with forty-nine Honorary Members, make a grand total of five thousand, five hundred and one members to date.

He then asked the membership to vote upon the election to Honorary Membership of the following:

To—Colonel Philip Fox, U. S. A., Commanding Officer, Signal Corps Officers School, Cambridge, Massachusetts. (First Director, of first planetarium in this country—Adler in Chicago.)

"In recognition of his development of the possibilities of the planetarium instrument in a manner calculated to popularize the science of astronomy."

To—Samuel S. Fels, President, Fels and Company, member of the Board of Managers of The Franklin Institute, donor of the Fels Planetarium to the people of Philadelphia.

"In recognition of his deep abiding interest in his fellow man which caused him to visualize the importance of the planetarium as an instrument of instruction and recreation, and to order its importation to this country as a source of lasting benefit to the City of Philadelphia."

To—Mary Curtis Zimbalist: "patron of the arts and sciences, distinguished daughter of a distinguished father, who, by her devoted interest to The Franklin Institute, has coöperated in making live in the present the high aspirations for the name of Franklin which her father venerated in the past."

It was regularly moved, seconded and carried that the above named persons should be duly elected to Honorary Membership in The Franklin Institute.

Dr. Allen then explained that the occasion was the Tenth Anniversary of the opening of the new building and expressed a cordial invitation to all members to join in celebrating this interesting event. He stated that a special function for members would be held and that announcements would be sent out in due time.

Dr. Allen stressed the fact that the Celebration would be simple in character due to war times, and stated that the Institute continued to participate in war work through the activities of its staff. He announced that ten members of the official family are now in uniform in the armed forces.

At the conclusion of the Secretary's report the Chairman introduced the speaker of the evening, Dr. Robert R. Williams, Chairman, Cereal Committee, Food and Nutrition Board,

and cited that, among other honors, Dr. Williams had been the recipient of the Cresson Medal from the Institute for his researches on $B_1$.

Dr. Williams addressed the meeting on the subject of "The Applied Science of Nutrition." He explained the functions of the Food and Nutrition Board, formed in 1940 to give mass effect to our present revolutionary knowledge of nutrition and gave as its aims better cooking, better farming, better factory processing, scrutiny of army and civilian rations, and mass repair of faulty staples (bread and flour).

The meeting was dismissed with a rising vote of thanks to Dr. Williams for his very instructive talk.

HENRY BUTLER ALLEN,
*Secretary.*

October 22, 1943.

---

## LIBRARY NOTES.

The Committee on Library desires to add to the collections any technical works that members would wish to contribute. Contributions will be gratefully acknowledged and placed in the library. Duplicates received will be transferred to other libraries as gifts of the donor.

Photostat prints of any material in the collections can be supplied on request. The average cost for a print 9 × 14 inches is thirty-five cents.

The library and reading room are open on Mondays, Tuesdays, Fridays and Saturdays from nine o'clock A.M. until five o'clock P.M., Wednesdays and Thursdays from two until ten o'clock P.M.

### RECENT ADDITIONS.

#### AERONAUTICS.

CHANDLER, CHARLES DE FOREST, AND FRANK P. LAHM. How Our Army Grew Wings. 1943.
GREENWOOD, ERNEST J., AND JOSEPH R. SILVERMAN. Stress Analysis for Airplane Draftsmen. First Edition. 1943.
MATSON, RANDOLPH. Aircraft Electrical Engineering. First Edition. 1943.
NILES, ALFRED S., AND JOSEPH S. NEWELL. Airplane Structures. Third Edition. Two Volumes. 1943.

#### AGRICULTURE.

Welsh Journal of Agriculture. Volume XVII. 1943.

#### ARCHITECTURE AND BUILDING.

GAY, CHARLES MERRICK, AND HARRY PARKER. Materials and Methods of Architectural Construction. Second Edition. 1943.

#### AUTOMOTIVE ENGINEERING.

Motor's Truck Repair Manual. First Edition. 1943.
Society of Automotive Engineers. SAE Handbook. 1943.

#### CHEMISTRY AND CHEMICAL TECHNOLOGY.

BURK, R. E., AND OLIVER GRUMMITT, Editors. The Chemical Background for Engine Research. 1943.
CALDWELL, WILLIAM T. Organic Chemistry. 1943.

#### ELECTRICITY AND ELECTRIC ENGINEERING.

HECTOR, L. GRANT, HERBERT S. LEIN AND CLIFFORD E. SCOUTEN. Electronic Physics. 1943.
KERCHNER, RUSSELL M., AND GEORGE F. CORCORAN. Alternating-Current Circuits. Second Edition. 1943.

NILSON, ARTHUR R., AND J. L. HORNUNG. Practical Radio Communication. Second Edition. 1943.

RIDER, JOHN F. Perpetual Trouble Shooter's Manual. Volume 12. 1942.

SARBACHER, ROBERT I., AND WILLIAM A. EDSON. Hyper and Ultrahigh Frequency Engineering. 1943.

### ENGINEERING.

HOOL, GEORGE A., AND W. S. KINNE, Editors-in-Chief. Foundations, Abutments and Footings. Second Edition. 1943.

MORRIS, CLYDE T., AND SAMUEL T. CARPENTER. Structural Frameworks. 1943.

### GRAPHIC ARTS.

LAWSON, PHILIP J. Practical Perspective Drawing. First Edition. 1943.

ROGERS, BRUCE. Paragraphs on Printing Elicited from Bruce Rogers in Talks with James Hendrickson. 1943.

### MATHEMATICS.

HOF, HANS. Seven Place Full Natural Trigonometric Tables. Three Volumes. 1943.

U. S. Work Projects Administration for the City of New York. On the function $H(m, a, x) = \exp.(-ix)F(m+1-ia, 2m+2; ix)$. 1942.

U. S. Work Projects Administration for the City of New York. Table of the Zeros of the Legendre Polynomials of Order 1–16 and the Weight Coefficients for Gauss' Mechanical Quadrature Formula. 1942.

### MECHANICAL ENGINEERING.

HINMAN, C. W. Die Engineering Layouts and Formulas. 1943.

### METALLURGY AND FOUNDING.

BARRETT, CHARLES S. Structure of Metals. First Edition. 1943.

FREY, CHRIS J., AND STANLEY S. KOGUT. Metal Forming by Flexible Tools. 1943.

HARTLEY, LAWRENCE A., Editor. Elementary Foundry Technology. Third Edition. 1941.

HOYT, SAMUEL L. Metals and Alloys Data Book. 1943.

### METEOROLOGY.

CLAYTON, HENRY HELM. Solar Relations to Weather and Life. Two Volumes. 1943.

HUMPHREYS, W. J. Fogs, Clouds and Aviation. 1943.

### NAVAL ARCHITECTURE AND NAVIGATION.

COEN, MARTIN J. Ship Welding Handbook. 1943.

KELLS, LYMAN M., WILLIS F. KERN AND JAMES R. BLAND. Navigation. Part 1. First Edition. 1943.

NIEDERHOFF, AUGUST E. Blueprint Reading for the Shipbuilding Trades. First Edition. 1943.

SCULL, JOHN E. Ship Wiring. 1943.

### PHYSICS.

American Society for Testing Materials. Symposium on Radiography. 1943.

LEA, FREDERICK CHARLES. Hydraulics. Sixth Edition. 1942.

LINDSAY, ROBERT BRUCE. Students' Handbook of Elementary Physics. 1943.

MADELUNG, ERWIN. Die mathematischen Hilfsmittel des Physikers. Dritte vermehrte und verbesserte Auflage. 1943.

WAHLSTROM, ERNEST E. Optical Crystallography. 1943.

### RAILROAD ENGINEERING.

American Railway Engineering Association. Proceedings. Volume 44. 1943.

**SAFETY METHODS.**

BLAKE, ROLAND P., Editor. Industrial Safety by T. O. Armstrong and Others. 1943.

**SANITARY ENGINEERING.**

EHLERS, VICTOR M., AND ERNEST W. STEEL. Municipal and Rural Sanitation. Third Edition. 1943.

**SOCIOLOGY.**

WRISTON, HENRY M. Challenge to Freedom. 1943.

V.2
194

## NOTES FROM THE BIOCHEMICAL RESEARCH FOUNDATION.

**Paramecium caudatum as a Test Animal for Organic Arsenicals.**—HUGH E. POTTS. The evaluation of the therapeutic action of drugs has always been costly and time-consuming and has required the use of large numbers of laboratory animals. It was thought that perhaps some of these obstacles could be obviated by the use, as a test animal, of a simple organism such as paramecium. Paramecia have the advantages of being readily cultured in great numbers and of being large enough to see easily with the use of a low power magnification. Such visual changes as swelling, blistering, loss of motility, formation of large vacuoles and death can be used as criteria of the effect of drugs, and effects on respiration can also be measured. Of all these criteria, death is the simplest and most certain, and death alone is considered in this investigation.

Such drugs as quinine (Marie Feiler, *Archiv für Protistenkunde*, **59**: 562, 1927), $As_2O_3$ (E. W. Surber and O. L. Meehan, *Transactions of the American Fisheries Society*, **61**: 225, 1931) and some of the sulfa drugs (Ferguson, Holmes and Lavor, *Journal of the Elisha Mitchell Scientific Society*, **58**: 53, 1942) have been tested on paramecium but a search of the literature revealed no work on paramecium with organic arsenicals.

*Paramecium caudatum* was obtained from a nearby pond. The paramecia were cultured at first on a hay infusion consisting of 15 grams of hay to a liter of distilled water which had been boiled for fifteen minutes, filtered, diluted 1 to 1, and adjusted to pH 7.8. Cultures of *Aerobacter aerogenes* or *Serratia marcescens* were added to the hay infusion at the same time that the inoculation of 0.1 cc. of paramecia was made. This method produced fairly successful cultures and was used for the first 21 experiments, after which time a change was made. Instead of subculturing on hay infusions, a few flakes of rolled oats were added to the hay infusion cultures. This was done because the rolled oats gave much thicker cultures. Cultures originally inoculated with *Serratia marcescens* were used subsequently. These were maintained by adding a few flakes of rolled oats twice a week and making subcultures about once a month. The subcultures were made by pouring about one third of an old culture into a clean jar and adding distilled water, a few cc. per day, until the vessel was filled. Large amounts of distilled water added at one time killed the paramecia.

These cultures were obviously not pure in regard either to protozoa or to bacteria. A small percentage of flagellates and rotifers was present. The bacterial flora was not checked but *Serratia marcescens*

was probably the dominant group, since a pinkish color was noticeable in old cultures.

The pH of the oatmeal cultures was brought down to about 7.0 and maintained there by the addition of small amounts of NaOH or $NaHCO_3$.

All tests were done in No. 9850 watch glasses made by the A. H. Thomas Co., Philadelphia. The watch glasses used have a diameter of about 20 mm. They are grooved on the bottom and have bevelled ground glass rims, so that one can be stacked upon another, thus preventing any appreciable amount of evaporation. Used in this manner, the capacity of each glass was about one cc.

Into each watch glass was placed the desired number of drops of paramecium culture (between 10 and 20 drops). Then the drug was added, bringing the total up to 20 drops. Controls consisted of 20 drops of culture. The experimentals contained from 10 to 19 drops of culture and corresponding numbers of drops of drugs to make the total volumes up to 20 drops. In most cases matched pipettes were used for drug and for culture, but in some cases the same pipette was used for both. In the latter case the pipette was rinsed thoroughly with distilled water after every operation. All drugs were brought to pH 7.0 prior to use, through addition of the required amount of NaOH. A series of concentrations was used for each drug tested, such concentrations being chosen to cover a range in which it was hoped that the greater concentrations would be fatal to paramecia in 6 and in 24 hours and that the least concentration would have little or no effect.

The tests were run for at least 24 hours. Examinations were usually made every hour for the first 6 hours and finally after 24 hours. The pH was estimated roughly by use of bromothymol blue, either at or within a few hours of the beginning of a series of tests. Frequent checks on pH showed that there never was any appreciable change in pH, even after 24 hours.

All paramecia were examined under a dissecting microscope, using a magnification of 40× or 80×.

The arsenicals tested consisted of a number of benzene, pyridine and pyridone compounds, mostly synthesized by Binz and Räth and brought to this Laboratory by Dr. Binz in 1937.

Results of experiments are expressed in Table I below, in terms of the least concentrations tested which would kill all paramecia in 24 hours and in 6 hours, and the greatest concentrations tested which failed to kill all paramecia in 24 hours.

For convenience of analysis four groups can be recognized, i.e. group I, containing all arsenicals which failed to kill all paramecia in 24 hours in concentrations of 1:200 or less, group II, those drugs killing all paramecia in 24 hours or less, in concentrations of 1:200 to 1:1,000, group III, all drugs killing all paramecia in 24 hours or less in concentra-

TABLE I.

*Effect of Various Pyridine, Pyridone and Benzene Arsenicals on Paramecia.*

| Expt. No. | Chemical Structure. | Concentrations Tested. | Effect on *Paramecium caudatum.* | Group. |
|---|---|---|---|---|
| IV | 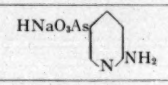 | 1:834 | Failed to kill all in 24 hours | I |
| VIII | 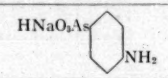 | 1:200<br>1:300 | Killed all in 6 hours<br>Failed to kill all in 24 hours | II |
| XVII | 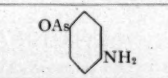 | 1:63,931<br>1:82,197<br>1:114,200 | Killed all in 6 hours<br>Killed all in 24 hours<br>Killed all in 24 hours | IV |
| VII | | 1:200<br>1:600 | Killed all in 24 hours<br>Failed to kill all in 24 hours | II |
| XXIX | 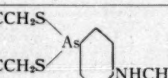 | 1:55,332<br>1:553,320 | Killed all in 6 hours<br>Failed to kill all in 24 hours | IV |
| I | 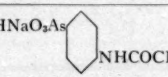 | 1:579<br>1:772 | Killed all in 6 hours<br>Failed to kill all in 24 hours | II |
| XXXII | 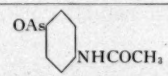 | 1:7,407<br>1:11,111 | Killed all in 6 hours<br>Failed to kill all in 24 hours | III |
| II | 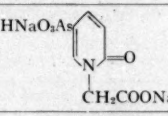 | 1:488 | Failed to kill all in 24 hours | I |
| LVII | 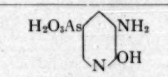 | 1:427 | Failed to kill all in 24 hours | I |
| LIX | 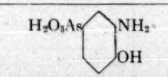 | 1:431 | Failed to kill all in 24 hours | I |
| XVI | 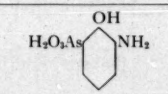 | 1:644 | Failed to kill all in 24 hours | I |

TABLE I (*Cont'd*).

| Expt. No. | Chemical Structure. | Concentrations Tested. | Effect on *Paramecium caudatum*. | Group. |
|---|---|---|---|---|
| XV | 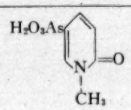 | 1:644 | Failed to kill in all 24 hours | I |
| LIII | 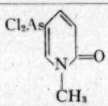 | 1:803<br>1:2,007<br>1:4,014 | Killed all in 24 hours<br>Killed all in 24 hours<br>Failed to kill all in 24 hours | III |
| LVIII | 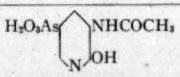 | 1:483<br>1:966<br>1:1,288 | Killed all in 24 hours<br>Killed all in 24 hours<br>Failed to kill all in 24 hours | II |
| III | 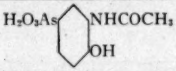 | 1:400<br>1:800 | Killed all in 24 hours<br>Failed to kill all in 24 hours | II |
| XXXIII | 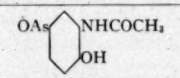 | 1:69,157<br>1:103,735<br>1:138,735 | Killed all in 6 hours<br>Killed all in 24 hours<br>Failed to kill all in 24 hours | IV |
| LXV | 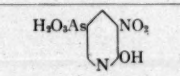 | 1:706 | Failed to kill all in 24 hours | I |
| LXVII | 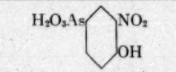 | 1:633 | Failed to kill all in 24 hours | I |
| LXI | 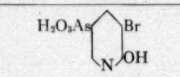 | 1:591 | Failed to kill all in 24 hours | I |
| XXIII | 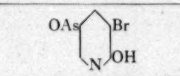 | 1:1,684<br>1:1,901<br>1:3,168<br>1:4,753 | Killed all in 6 hours<br>Killed all in 24 hours<br>Killed all in 24 hours<br>Failed to kill all in 24 hours | III |
| LXII | 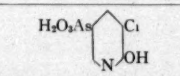 | 1:702 | Failed to kill all in 24 hours | I |
| XXIV | 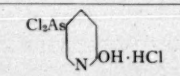 | 1:1,205<br>1:1,506 | Killed all in 24 hours<br>Failed to kill all in 24 hours | III |
| VI | 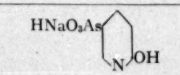 | 1:626 | Failed to kill all in 24 hours | I |

TABLE I (*Cont'd*).

| Expt. No. | Chemical Structure. | Concentrations Tested. | Effect on *Paramecium caudatum*. | Group. |
|---|---|---|---|---|
| LXIII | 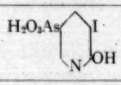 | 1:507 | Failed to kill all in 24 hours | I |
| XII | | 1:617<br>1:823 | Killed all in 24 hours<br>Failed to kill all in 24 hours | II |
| XIV | 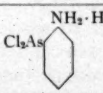 | 1:29,000<br>1:36,500<br>1:73,000 | Killed all in 6 hours<br>Killed all in 24 hours<br>Killed all in 24 hours | IV |
| V | 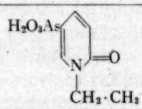 | 1:761 | Failed to kill all in 24 hours | I |
| LVI | 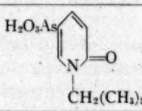 | 1:900 | Failed to kill all in 24 hours | I |
| LV | 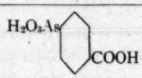 | 1:1,000 | Failed to kill all in 24 hours | I |
| XXV | 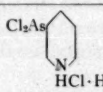 | 1:35,000<br>1:89,800<br>1:179,600 | Killed all in 6 hours<br>Killed all in 24 hours<br>Failed to kill all in 24 hours | IV |
| LIV | | 1:540<br>1:675<br>1:1,351<br>1:2,702 | Killed all in 6 hours<br>Killed all in 24 hours<br>Killed all in 24 hours<br>Failed to kill all in 24 hours | III |
| LX | 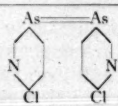 | 1:333,333<br>1:666,667<br>1:1,333,333 | Killed all in 6 hours<br>Killed all in 24 hours<br>Killed all in 24 hours | IV |
| IX | 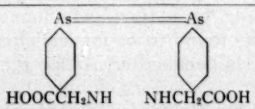 | 1:800<br>1:1,000<br>1:2,000<br>1:10,000 | Killed all in 6 hours<br>Killed all in 24 hours<br>Killed all in 24 hours<br>Failed to kill all in 24 hours | III |

tions of 1:1,001 to 1:10,000. Group IV contains the most active chemicals, killing all paramecia in 24 hours or less, in concentrations of 1:10,001 and less. All concentrations represent grams of arsenical per cc. of culture + drug. These groups are shown in the right-hand column of Table I.

On such a basis all the arsonic acid arsenicals, benzene, pyridine and pyridone, fall into the first two groups. One trivalent arsenical, No. XII, also falls into this group (group II). Groups III and IV consist of only trivalent arsenicals, oxides, dichlorides and arseno compounds.

It should also be mentioned here that No. LX, 2,2′-dichlor-5,5′-arsenopyridine may have had some material in suspension. It was only slightly soluble in water. It was made up in a $4 \times 10^{-5}$ M suspension and all large undissolved particles settled to the bottom. The samples tested were taken from the clear fluid near the surface.

It will be noticed that the number of paramecia per glass was not kept constant, but increased with dilution of the drug. The true effectiveness of the drug therefore will be minimized to some extent. Thus the activity of the drugs described is probably somewhat greater in the higher dilutions than shown here.

From the results shown in Table I above, it can be seen that the pentavalent arsenicals have practically no action on paramecia, whereas many of the trivalent arsenicals are active in concentrations of around 1:50,000 or less.

Pentavalent arsenicals have been shown also to have little effect *in vitro* on trypanosomes (Yorke and Murgatroyd, *Annals of Tropical Medicine and Parasitology*, **24**: 449, 1930). It is therefore interesting to note that the concentrations of atoxyl, arsacetin and tryparsamide which kill paramecia are approximately the same as those shown by Yorke and Murgatroyd to kill trypanosomes.

This relationship does not hold, however, for the triavlent arsenicals in the form of arsine oxides and arsine dichlorides, for roughly one thousand times the concentrations shown by Yorke and Murgatroyd to kill trypanosomes are needed to kill paramecia.

There is some disagreement concerning the action *in vitro* of arsenobenzene compounds. A 1:100 solution of arsenophenylglycine killed trypanosomes *in vitro* in one hour (Plimmer and Fry, *Proceedings of the Royal Society, series B*, **81**: 354, 1909). This was confirmed by Schilling (*Archiv für Schiffs- und Tropen-Hygiene*, **13**, 1, 1909), who found it even less effective. Salvarsan was likewise found to be far less effective on trypanosomes *in vitro* than *in vivo* (Halberstaedter, *Archiv für Schiffs- und Tropen-Hygiene*, **16**: 641, 1912).

A contrary finding was reported by Moldovan (*Zeitschrift für Immunitätsforschung und experimentelle Therapie*, **21**: 481, 1914) and by Kolmer, Schamberg and Raiziss (*Journal of Infectious Diseases*, **20**: 10,

1917), who showed that salvarsan was effective *in vitro*. Yorke and Murgatroyd showed that arsenophenylglycine in 1:400,000 would kill trypanosomes in 6 hours and that 1:3,200,000 would kill in 24 hours.

Only one arsenobenzene compound and one arsenopyridine were tested in this Laboratory. A 1:2,000 solution of arsenophenylglycine (No. IX) killed all paramecia in 24 hours. The arsenopyridine, 2,2′-dichlor-5,5′-arsenopyridine, was very active, killing all paramecia in 24 hours in a concentration of 1:1,333,333. In regard to the effect of arsenophenylglycine on paramecia, there appears to be little correlation between the effective concentration and its reported effect on trypanosomes.

As a whole, the trivalent benzene and pyridine arsenicals, in the form of oxides and dichlorides, were very active killing agents for paramecia. One trivalent pyridone (n-acetic acid-2-pyridone-3-arsenoxide) showed only slight activity, a concentration of 1:617 killing in 24 hours and 1:823 failing to kill. All the others killed in 24 hours in concentrations of less than 1:1,000 and usually less than 1:10,000. The pyridones as a whole seemed to show less activity than pyridines and benzenes.

Experiments made on the effects of various arsenicals on *Paramecium caudatum* showed:

1. The pentavalent arsenicals were only weakly active, killing only in concentrations of 1:1,000 or greater. Not all arsenicals were tested in concentrations as great as 1:200, but many in concentrations between 1:400 and 1:1,000 failed to kill.

2. Among the trivalent arsenicals, the pyridones were conspicuously inactive, as were also reduced arsacetin and arsenophenylglycine.

3. The most active compounds were the trivalent oxides and chlorides of benzene and pyridine. 2,2′-Dichlor-5,5′-arsenopyridine was particularly active.

4. The activity of arsacetin, atoxyl and tryparsamide on paramecium was of the same order as that of the same compounds tested by Yorke and Murgatroyd on *Trypanosoma rhodesiense in vitro*, but the reduced compounds did not show the same activity on both organisms. Roughly a thousand times greater concentration was required to kill paramecium than to kill *T. rhodesiense*.

5. Paramecium is sensitive to organic arsenicals and therefore can be used as a test animal.

## BOOK REVIEWS.

FLUID MECHANICS, by R. C. Binder, Ph.D. 307 pages, charts and diagrams, 16 × 23 cms. New York, Prentice-Hall, Inc., 1943. Price $3.75.

This is a subject, a knowledge of which is useful in almost every kind of engineering. It is rapidly becoming a "must" subject to the engineer. Modern fluid mechanics is based upon a healthy combination of physical analysis and experimental observations, which should be the background of every engineer. The general objective is to provide dependable practical results and a thorough understanding of fundamental flow features. The book at hand has for its aim the introduction to the fundamentals of fluid mechanics.

The work opens with a discussion of some fluid properties, a foundation upon which the rest is built. It is here that a definite distinction is made between force and mass, specific weight and density, which is maintained throughout. Statics is the first topic of the treatment proper. This is followed by kinematics and dynamics. That powerful, easily applied and useful tool of the engineer, the energy equation for the steady flow of any fluid, is discussed and indication is made of its generality and usefulness. Other tools, dimensional analysis and dynamic similarity, are explained.

An important and widely applicable part of the book is that on the flow of incompressible fluids in pipes and of like importance is the later treatment of flow in open channels. Likewise is the coverage on fluid measuring instruments, and the discussion of forces acting on a body completely immersed in a relatively large expanse of fluid. Under the heading of dynamics of compressible flow an introduction is made to compressibility effects of practical importance.

The latter chapters of the book deal with more or less specialized topics. They include lubrication, covering the mechanism for different types of bearings, properties of oils, and types of flow; fluid machinery, including the general features and performance characteristics of pumps, turbines, fluid couplings, and torque converters, and there is also a review of basic fluid power and control systems. The last chapter is devoted to a discussion in brief form of some of the fundamental relations useful in making a mathematical analysis of fluid motion.

The treatment is a practical one with a logical approach from the standpoint of the student. The presentation is one which involves work to follow but there is an indication of no insurmountable difficulties. At the end of each chapter is a list of selected references and a number of practical problems. A very important feature of this text is the list of answers to the problems to be found in the back. This inclusion widens the usefulness and value of the book to include its use not only as a text in the classroom, but for the home study student and practicing engineer as well.

R. H. OPPERMANN.

STRUCTURE OF METALS, by Charles S. Barrett, Ph.D. 567 pages, charts and illustrations, 15 × 23 cms. New York, McGraw-Hill Book Company, Inc., 1943. Price $6.00.

No mention need be made of the great importance of the knowledge of the structure of metals in modern industry. Its rapid application to widely diversified work speaks for itself. The results of this application can hardly be overlooked, particularly in those industries where safety as well as efficiency depends on the quality of metal employed in machinery. That progress is still being made in extending the knowledge of the structure of metals is indicated by the discoveries and developments of recent years. It can be said, therefore, that the subject is a live one with many interesting and promising possibilities.

This book is intended to serve both as a text and a reference work. It starts out with a discussion on the fundamentals of crystallography, stereographic projection for the analysis of markings appearing on polished grains, and a coverage in some detail of the nature and

methods of producing X-rays. In this latter the fundamental principles of radiography are discussed briefly but not the practical art. Later there is a brief survey of the principles and the several methods by which X-rays are employed to investigate the inner structure of metals which include simple sketches for each of the more common types of cameras and films.

The methods treated upon in the book include the Lane method, the rotating-crystal method and its modifications, and the powder method in which mention is made of the more important developments. The steps necessary in determining the structure of a crystal are laid out and each taken up in a simple, straightforward manner. With regard to the subject of pole figures and orientation determination, an entire chapter is devoted to a detailed explanation of methods. The plotting of pole figures which show preferred orientations in polycrystalline aggregates is covered first and is followed by a treatment of X-ray methods and etch-pit methods applicable to single crystals.

The author refers to the numerous summaries of crystal structures that have been published and confines his coverage to a correlation of the structures and an understanding of the principles underlying the structures of the metallic phases. After a treatment on the types, theory and order of superlattices, the electron theory of metals and alloys is taken up in the way of a summary of certain results of general interest with a minimum outline of the reasoning by which they were derived. Stress measurement by X-rays and plastic deformation of metals are given good explanations. The concern is first of the crystallography of slip, twinning, and fracture. Later there are taken up current theories of plastic flow, the structure of deformed metal, the nature and theories of preferred orientations generated by plastic flow, and directional properties resulting from preferred orientations.

The work is a good presentation in a simple style. The many good illustrations add greatly to understanding. Much effort has been put forth, both in logical sequence and the inclusion of basic and modern data, to make this book valuable to undergraduate as well as graduate students. It is of equal value as a reference work in practical situations.

R. H. OPPERMANN.

ALTERNATING CURRENT CIRCUITS, by Russell M. Kerchner, M.S., and George F. Corcoran, M.S. 553 pages, charts and diagrams, 14 × 22 cms. New York, John Wiley & Sons, Inc., 1943. Price $4.75.

A thorough knowledge of alternating current circuits is not only a necessity in the work of an electrical engineer, but it is a basic part of the subject which leads to a better understanding of all electrical engineering. Because alternating current circuits is a subject of paramount importance it must be presented with a familiarity with all the devices that make for clarity and impressiveness to students. The text book must measure up to all of the teaching requirements, in order to be of greatest effect.

The book at hand is in its second edition. It has been somewhat rearranged and revised to reflect the results of longer and larger experience in teaching the subject. For college grade students, it assumes a knowledge of differential and integral calculus, although there are only a few places in the text where a detailed workable knowledge of these is absolutely necessary for a good understanding. Trigonometry is of course necessary. There are sixteen chapters, the first eleven of which contain the principles. These start with general concepts and fundamental definitions, alternating current and power with applied sinusoidal voltage, effective current and power, a good treatment on vector algebra as applied to A.C. circuit analysis, sinusoidal single-phase circuit analysis, non-sinusoidal waves, coupled circuits, balanced polyphase circuits, unbalanced polyphase circuits, alternating current measurements and determination of circuit parameters. The rest of the book covers transmission line calculations, electric wave filters, symmetrical components, power system short circuit calculations and transient conditions.

There are a great number of illustrations throughout the work. These include diagrams, tables, curves and oscillograms. They are equally as valuable as the text. The general method of presentation is first theoretical discussions, then illustrative examples, worked out and well explained. Exercises appear at the ends of chapters.

A glance over the chapter headings reveals many that are difficult to present simply and successfully. Referring to these, the work itself shows a remarkable sympathy with the situation of the student and every effort is made to facilitate understanding.

R. H. OPPERMANN.

THE CHEMICAL BACKGROUND FOR ENGINE RESEARCH, by R. E. Burk and Oliver Grummitt. 297 pages, charts and diagrams, 15 × 23 cms. New York, Interscience Publishers, Inc., 1943. Price $3.50.

The Western Reserve University has been concerned with the problem of having their faculty kept up to date in knowledge, not only with regard to the various specialized subjects but in the broader fields. As a matter of fact this problem of keeping abreast of science is the concern of many individuals outside of the University in industry. To meet these difficulties, the University conceived the idea of inviting distinguished scientists in the field of chemistry and closely related fields to be professors for a day. Each of these men presents two lectures along lines of his work. This book contains lectures by six of these men. The coverage is along somewhat related fields.

The first, by E. F. Fiock of the National Bureau of Standards, presents a survey of combustion research and is confined to stationary flames and to that sort of burning or explosion occurring when homogeneous combustible mixtures in the gaseous state are traversed by flame. This is followed by a contribution by Frederick G. Rossini, also of the National Bureau of Standards. He gives a brief review of the fundamental principles of chemical thermodynamics of hydrocarbons which is followed by discussion of the definition and evaluation of the free energy, evaluation of entropies by means of the third law and by means of statistical calculations, evaluation of heats of formation, and calculation of free energies of formation, equilibrium constants and equilibrium concentrations.

Synthetic methods for hydrocarbons whose structures are known, and especially the paraffin hydrocarbons, is the subject by Frank C. Whitmore of Pennsylvania State College. After this there appears a progress report on the Kinetics of Flame and Combustion by Guenther von Elbe of Carnegie Institute of Technology. This furnishes facts on which hope of future success may be based. Bernard Lewis of the Bureau of Mines then gives a plain talk describing some of the more important tools employed in fundamental researches on combustion engines. This is very timely. And finally, O. Beeck of Shell Development Company acquaints the reader with a series of laboratory experiments which contribute to the understanding of the many complex factors in lubrication which engine research per se is not able to give us.

The work is commendable and should fulfill its purpose. Readers interested in the subject are urged to study these lectures.

R. H. OPPERMANN.

---

## PUBLICATIONS RECEIVED.

*Structure of Metals*, by Charles S. Barrett, Ph.D. 567 pages, charts and illustrations, 15 × 23 cms. New York, McGraw-Hill Book Company, Inc., 1943. Price $6.00.

*Biochemistry of the Fatty Acids*, by W. R. Bloor. 387 pages, 16 × 23 cms. New York, Reinhold Publishing Corp., 1943. Price $6.00.

*Encyclopedia of Substitutes and Synthetics*, by Morris D. Schoengold. 382 pages, 16 × 24 cms. New York, Philosophical Library, Inc., 1943. Price $10.00.

*Advanced Quantitative Analysis*, by Hobart H. Willard, Ph.D., and Harvey Diehl, Ph.D. 457 pages, charts and diagrams, 15 × 22 cms. New York, D. Van Nostrand Company, Inc., 1943. Price $4.75.

*Semimicro Qualitative Analysis*, by John F. Flagg, Ph.D., and Willard R. Line, Ph.D. 140 pages, charts and diagrams, 14 × 22 cms. New York, D. Van Nostrand Company, Inc., 1943. Price $1.50.

*Patent Law*, by Chester H. Biesterfeld, B.Ch.E., M.P.L. 225 pages, 14 × 22 cms. New York, John Wiley & Sons, Inc., 1943. Price $2.75.